2016-02-01

Determination of Fine Particulate Matter Composition and Development of the Organic Aerosol Monitor

Paul Michael Cropper
Brigham Young University - Provo

Determination of Fine Particulate Matter Composition and Development of the Organic Aerosol Monitor

Paul Michael Cropper

A dissertation submitted to the faculty of
Brigham Young University
in partial fulfillment of the requirements for the degree of

Doctor of Philosophy

Jaron C. Hansen, Chair
Milton L. Lee
Steven R. Goates
Roger G. Harrison
Steven L. Castle

Department of Chemistry and Biochemistry

Brigham Young University

February 2016

ABSTRACT

Determination of Fine Particulate Matter Composition and
Development of the Organic Aerosol Monitor

Paul Michael Cropper
Department of Chemistry and Biochemistry, BYU
Doctor of Philosophy

Tropospheric fine particulate matter (PM) poses serious health risks and has a significant impact on global climate change. The measurement of various aspects of PM is challenging due to its complex chemical nature. This dissertation addresses various aspects of PM, including composition, measurement, and visibility. The U.S. Environmental Protection Agency (EPA) proposed a new secondary standard based on visibility in urban areas using 24-h averaged measurements of either light scatter or PM concentration. However shorter averaging times may better represent human perception of visibility. Data from two studies conducted in Lindon, UT, 2012, and Rubidoux, CA, 2003, were used to compare different techniques to estimate visibility, particularly the effect of relative humidity on visibility estimations. Particle composition was measured in Salt Lake City during January-February of 2009. One-hour averaged concentrations of several gas phase and particle phase inorganic species were measured. The results indicate ammonium nitrate averages 40% of the total PM2.5 mass in the absence of inversions and up to 69% during strong inversions. Also, the formation of ammonium nitrate is nitric acid limited, while the formation of ozone appears to be oxidant and volatile organic carbon (VOC) limited. Reduction of NOx will reduce ammonium nitrate secondary particle formation, however, a decrease in NOx may increase ozone concentration.

Due to the complexity of PM it is poorly characterized. A large fraction of PM is composed of organic compounds, but these compounds are not regularly monitored due to limitations in current sampling techniques. The GC-MS Organic Aerosol Monitor (OAM) combines a collection device with thermal desorption, gas chromatography and mass spectrometry to quantitatively measure the carbonaceous components of PM on an hourly averaged basis. A compact GC and simple pre-concentrator were developed for the system to decouple separation from manual injection and enhance separation of environmentally-relevant polar organic compounds, such as levoglucosan. The GC-MS OAM is fully automated and has been successfully deployed in the field. It uses a chemically deactivated filter for collection followed by thermal desorption and GC-MS analysis. Laboratory tests show that detection limits range from 0.2 to 3 ng for many atmospherically relevant compounds. The GC-MS OAM was deployed in the field for semi-continuous measurement of the organic markers, levoglucosan, dehydroabietic acid, and several polycyclic aromatic hydrocarbons (PAHs) during winter (January to March), 2015 and 2016. Results illustrate the significance of this monitoring technique to more fully characterize the organic components of PM and identify sources of pollution.

Keywords: air pollution, fine particulate matter, $PM_{2.5}$, secondary organic aerosol, organic markers, levoglucosan, PMF

ACKNOWLEDGEMENTS

Funding was provided by Southern California Edison, Sunset Laboratory, the National Science Foundation, the National Institute of Health, and the Environmental Protection Agency.

Thank you Jaron Hansen for your adept mentorship and support.

Sarah Ann Cropper, thank you.

TABLE OF CONTENTS

LIST OF TABLES

LIST OF FIGURES

LIST OF ACRONYMS

AIM	ambient ion monitor
AMS	aerosol mass spectrometer
BC	black carbon
CM	carbonaceous material
CMB	chemical mass balance
DHA	dehydroabietic acid
DLEE	dry light extinction efficiency
DO OC-EC	dual oven organic carbon- elemental carbon
EPA	Environmental Protection Agency
FDMS	filter dynamics measurement system
FRM	federal reference method
FWHM	full-width half maximum
GC	gas chromatography
IC	ion chromatography
LOD	limit of detection
LOQ	limit of quantitation
MLEE	moist light extinction efficiency
NAAQS	national ambient air quality standards
NVOC	non-volatile organic carbon
NVOM	non-volatile organic material
OAM	Organic Aerosol Monitor
OC	organic compounds
OM	organic material
PAHs	polycyclic aromatic hydrocarbons
PCC	pre-column concentrator
PID	proportional integral derivative
PM	particulate matter
PMF	positive matrix factorization
RH	relative humidity
RIC	reconstructed ion chromatogram
RT	retention time
SCAQMD	South Coast Air Quality Management District
SCE	Southern California Edison
SD	standard deviation
SN	separation number
SOA	secondary organic aerosol
SVOC	semi-volatile organic compounds
SVOM	semi-volatile organic material
TEOM	tapered element oscillating microbalance
TIC	total ion chromatogram
UFP	ultra fine particles
VOC	volatile organic compounds
WRF	Weather Research and Forecasting

1 AIR POLLUTION IINTRODUCTION

1.1 Air Pollution Overview

The atmosphere is one of earth's primary resources, vital to life on earth. The lower layer of the atmosphere is called the troposphere, extending from the earth's surface to a height of 6-10 km. The chemistry of the troposphere is dynamic, due to both solar radiation and direct interaction with the biosphere including human life. Within the troposphere numerous chemical processes take place that are naturally kept in balance. However, while the troposphere and its chemical composition may be considered a renewable resource, it has become apparent that it can be disrupted and that it must be cared for and maintained.

Disruption and contamination of the atmosphere occurs due to air pollution, which is the introduction of harmful material into the atmosphere (primarily the troposphere). Air pollution causes diseases in humans and other living organisms, and can disrupt global and local ecosystems. For instance elevated ozone and sulfur dioxide levels cause visible damage to plant leaves affecting photosynthesis and crop yield.[1-2] Air pollution has both acute and chronic effects on human health, including increased morbidity and mortality rates.[3]

Air pollutants can be classified as particle phase or gas phase. Gas phase pollutants include NO, NO_2 , CO, SO_2, O_3, NH_3 and volatile organic compounds. Pure gas phase processes are relatively well understood; however, our knowledge of the particle phase is very fragmentary.[4] Particle phase air pollution is referred to as particulate matter (PM) and is a type of

aerosol. Primary emitted particles are those that are directly emitted from single sources such as ash from fires, and dust from roads and fields. Secondary particles are formed in the atmosphere as pollutants react, combine and condense with one another.

PM can further be characterized by particle size. Aerosol particles range from a few nanometers in diameter to up to 100 micrometers. Particles ranging from 2.5 μm to 10 μm are considered coarse particles, and particles larger than this are super coarse particles. Coarse particles are primarily formed mechanically due to grinding or wind erosion, and are usually composed of crustal material. Pollen, spores, and particles from sea spray are also considered primary coarse particles. Because these particles are large, they settle out of the air only minutes to hours after being emitted.

Fine particles are those with a diameter smaller than 2.5 μm, also referred to as $PM_{2.5}$. These particles can stay suspended in the air for days to weeks and travel long distances. They are also usually secondary in nature. Secondary particle formation can begin by the reaction of ammonia with nitrogen oxides (NO_x, including HNO_3) and/or sulfur dioxide to form ammonium nitrate and/or sulfate.[5] This then provides a backbone for other species to condense onto, such as water or organic species.[6-7] The condensation of water on particles depends upon the relative humidity (RH), thus RH has a significant impact on the measurement of fine PM (discussed in Chapter 2). Multiple studies performed in the Salt Lake Valley have shown that NH_4NO_3 is a major component of PM; Chapter 3 further discusses the composition of $PM_{2.5}$ and the limiting reagent for secondary particle formation in the Salt Lake Valley.

Fine PM that is composed of organic material is often referred to as secondary organic aerosol (SOA). SOA is particulate matter that is formed by the chemical and phase transformations of primary organic material. The reactions which lead to SOA are complex, and

are currently a major focus of laboratory-based aerosol studies. However, models formed by these studies often predict far less SOA than is observed in the atmosphere, which suggests the importance of additional unknown processes.[8-9] Fine PM, especially SOA, is among the most harmful pollutants to human health, and is very complex in nature because it is a conglomeration of hundreds or even thousands of different compounds. Elevated concentrations of fine PM have been shown to increase morbidity and mortality.[10-11] Fine PM is small enough to get lodged deep within the lungs and eventually enter the blood stream. For these and other reasons (e.g., visibility) the EPA has set the acceptable limit of $PM_{2.5}$ to 35μg/m^3, for an 8-h averaged time.[12] However, while the total mass of $PM_{2.5}$ is regularly monitored, individual organic compounds in $PM_{2.5}$ are not.

Individual compounds within $PM_{2.5}$ provide great insight into pollution sources because they act as signatures of their emission sources. For example, levoglucosan is a product of cellulose combustion and thus a marker for wood smoke.[13-14] Hopanes and polycyclic aromatic hydrocarbons (PAHs) are markers for motor-vehicle emissions.[15-16] PAH profiles have helped distinguish between gasoline and diesel vehicle sources in source apportionment studies. In order to further current understanding of fine particulate matter in terms of sources and health effects, it is necessary to more closely monitor SOA composition.

1.2 Current Organic Aerosol Composition Analysis Techniques

Currently most analysis of organic aerosol particles occurs in the laboratory using benchtop instrumentation and either solvent extraction or shotgun methods. Solvent extraction methods primarily involve manual processing (e.g., solvent extraction) of samples which are collected over a period of days to weeks. GC-MS analysis of these samples is the primary

accepted means of identification and quantification.[15] This method was illustrated by Chow et al.[17], who collected 5 to 6 h samples on Teflon filters, 4 times a day and obtained detailed organic marker information for $PM_{2.5}$. Collecting samples in this manner was only maintained for a total of 15 days. Detailed information concerning source contribution was obtained, but was likely limited by the 5-hour sampling period, and the relatively short duration of the campaign. Elsasser et al.[18] successfully collected hourly samples and analyzed them using a similar GC-MS based approach, but only maintained hourly collection for 5 days. These same temporal limitations are evident in similar studies.[19-20]

Shotgun methods are those which use no separation prior to MS analysis. Bruns et al. demonstrated one such method called atmospheric solids analysis probe mass spectrometry.[21] They loaded a probe with PM material, placed it in the ionization region of an atmospheric pressure, chemical ionization mass spectrometer, and used a heated stream of N_2 to thermally desorb the sample. Many large organic markers were successfully identified; however smaller molecular weight markers such as levoglucosan were lost in the sample matrix. Though faster than the extraction approach, this method still requires manual operation and expensive bench top instrumentation. Field-based mass spectrometers, such as the Aerodyne aerosol mass spectrometer, have been used to monitor particulate matter; however they also use a shotgun approach and are limited in terms of organic marker identification due to harsh ionization techniques and a large sample matrix.[22] In cases where the molecules may be intact, the sample matrix is often too large to clearly identify semi-volatile organic compounds (SVOCs).

The major drawback of current techniques is that they do not offer continuous time-resolved information concerning organic markers, or are limited in terms of organic marker identification. Therefore, diurnal patterns are not captured and secondary chemistry (i.e. the

reaction of primary pollutants following emission) is not apparent. For this reason the gas chromatography-mass spectrometry Organic Aerosol Monitor (GC-MS OAM) has been developed to autonomously monitor organic aerosol in the field on an hour averaged basis. The GC-MS OAM is described in Chapter 4, and additional details concerning the GC portion of the GC-MS OAM are discussed in Chapter 5.

1.3 Air Pollution Source Apportionment

One of the purposes of developing the GC-MS OAM is to obtain hourly averaged concentrations of organic markers in order to improve air pollution source apportionment models. Source apportionment studies enable the reduction of air pollution (e.g., $PM_{2.5}$) by relating its composition to specific sources. Source apportionment is performed by using a broad range of instrumentation to obtain time-resolved concentrations of pollutants (gas and particle phase), and then analyzing the data using statistical analysis tools. For example Lee et al. obtained local and regional source profiles of $PM_{2.5}$ by analyzing the inorganic composition data of $PM_{2.5}$ 24-h samples with both positive matrix factorization (PMF) and chemical mass balance (CMB).[23] They found that both analysis tools identified major sources, though the agreement of results varied based on the site. They noted that the lack of sufficient source "markers" was a likely cause of discrepancies between the results.

The enhancement of source apportionment statistical analysis by including organic markers has been previously demonstrated.[24-26] Chow et al. estimated source profiles in Fresno, CA, using the Chemical Mass Balance receptor model.[17] By including organic markers they improved the distinction between gasoline and diesel emissions (using PAHs), and could more accurately estimate cooking source contributions. They also determined the contribution to PM

due to wood burning emissions using markers such as levoglucosan. A limitation of these and other studies is often due to the extended collection time of the samples (4-24 hours). Hence, the time resolution of data collection is limited and important diurnal patterns are not captured. This highlights the need for an automated process of measuring organic markers on a shorter (e.g. hourly) basis.

The importance of hourly measurements to understand secondary chemistry has been demonstrated by Grover et al. They used hourly-averaged $PM_{2.5}$ composition data coupled with gas phase species to identify gasoline and diesel emissions and to better identify secondary fine particulate matter formation.[27] Such studies will be greatly enhanced by the inclusion of hourly averaged organic marker data. Chapter 6 describes a source apportionment study performed in Long Beach, CA. Preliminary testing of the GC-MS OAM was performed as a part of this study.

1.4 Chapter References

1. Heagle, A. S.; Body, D. E.; Neely, G. E., Injury and Yield Responses of Soybean to Chronic Doses of Ozone and Sulfur-Dioxide in Field. *Phytopathology* **1974,** *64* (1), 132-136.
2. Fuhrer, J.; Skarby, L.; Ashmore, M. R., Critical levels for ozone effects on vegetation in Europe. *Environmental Pollution* **1997,** *97* (1-2), 91-106.
3. Kampa, M.; Castanas, E., Human health effects of air pollution. *Environmental Pollution* **2008,** *151* (2), 362-367.
4. Comes, F. J., Recycling in the Earths Atmosphere - the Oh Radical - Its Importance for the Chemistry of the Atmosphere and the Determination of Its Concentration. *Angewandte Chemie-International Edition in English* **1994,** *33* (18), 1816-1826.
5. Sharma, M.; Kishore, S.; Tripathi, S. N.; Behera, S. N., Role of atmospheric ammonia in the formation of inorganic secondary particulate matter: A study at Kanpur, India. *Journal of Atmospheric Chemistry* **2007,** *58* (1), 1-17.
6. Hao, L. Q.; Wang, Z. Y.; Huang, M. Q.; Fang, L.; Zhang, W. J., Effects of seed aerosols on the growth of secondary organic aerosols from the photooxidation of toluene. *Journal of Environmental Sciences-China* **2007,** *19* (6), 704-708.
7. Pandis, S. N.; Harley, R. A.; Cass, G. R.; Seinfeld, J. H., Secondary Organic Aerosol Formation and Transport. *Atmospheric Environment Part a-General Topics* **1992,** *26* (13), 2269-2282.

8. Kroll, J. H.; Seinfeld, J. H., Chemistry of secondary organic aerosol: Formation and evolution of low-volatility organics in the atmosphere. *Atmospheric Environment* **2008,** *42* (16), 3593-3624.
9. Volkamer, R.; Jimenez, J. L.; San Martini, F.; Dzepina, K.; Zhang, Q.; Salcedo, D.; Molina, L. T.; Worsnop, D. R.; Molina, M. J., Secondary organic aerosol formation from anthropogenic air pollution: Rapid and higher than expected. *Geophysical Research Letters* **2006,** *33* (17).
10. Dockery, D. W.; Pope, C. A., Acute Respiratory Effects of Particulate Air-Pollution. *Annual Review of Public Health* **1994,** *15*, 107-132.
11. Smith, R. L.; Davis, J. M.; Sacks, J.; Speckman, P.; Styer, P., Regression models for air pollution and daily mortality: analysis of data from Birmingham, Alabama. *Environmetrics* **2000,** *11* (6), 719-743.
12. EPA National Ambient Air Quality Standards (NAAQS). http://www.epa.gov/air/criteria.html (accessed 08 February, 2013).
13. Elias, V. O.; Simoneit, B. R. T.; Cordeiro, R. C.; Turcq, B., Evaluating levoglucosan as an indicator of biomass burning in Carajas, Amazonia: A comparison to the charcoal record. *Geochimica et Cosmochimica Acta* **2001,** *65* (2), 267-272.
14. Simoneit, B. R. T.; Schauer, J. J.; Nolte, C. G.; Oros, D. R.; Elias, V. O.; Fraser, M. P.; Rogge, W. F.; Cass, G. R., Levoglucosan, a tracer for cellulose in biomass burning and atmospheric particles. *Atmospheric Environment* **1999,** *33* (2), 173-182.
15. Lin, L.; Lee, M. L.; Eatough, D. J., Gas chromatographic analysis of organic marker compounds in fine particulate matter using solid-phase microextraction. *Journal of the Air & Waste Management Association* **2007,** *57* (1), 53-58.
16. Schauer, J. J.; Kleeman, M. J.; Cass, G. R.; Simoneit, B. R. T., Measurement of emissions from air pollution sources. 2. C-1 through C-30 organic compounds from medium duty diesel trucks. *Environmental Science & Technology* **1999,** *33* (10), 1578-1587.
17. Chow, J. C.; Watson, J. G.; Lowenthal, D. H.; Chen, L. W. A.; Zielinska, B.; Mazzoleni, L. R.; Magliano, K. L., Evaluation of organic markers for chemical mass balance source apportionment at the Fresno Supersite. *Atmospheric Chemistry and Physics* **2007,** *7* (7), 1741-1754.
18. Elsasser, M.; Crippa, M.; Orasche, J.; DeCarlo, P. F.; Oster, M.; Pitz, M.; Cyrys, J.; Gustafson, T. L.; Pettersson, J. B. C.; Schnelle-Kreis, J.; Prevot, A. S. H.; Zimmermann, R., Organic molecular markers and signature from wood combustion particles in winter ambient aerosols: aerosol mass spectrometer (AMS) and high time-resolved GC-MS measurements in Augsburg, Germany. *Atmospheric Chemistry and Physics* **2012,** *12* (14), 6113-6128.
19. Schauer, J. J.; Rogge, W. F.; Hildemann, L. M.; Mazurek, M. A.; Cass, G. R.; Simoneit, B. R. T., Source apportionment of airborne particulate matter using organic compounds as tracers. *Atmospheric Environment* **1996,** *30* (22), 3837-3855.
20. Zheng, M.; Ke, L.; Edgerton, E. S.; Schauer, J. J.; Dong, M. Y.; Russell, A. G., Spatial distribution of carbonaceous aerosol in the southeastern United States using molecular markers and carbon isotope data. *Journal of Geophysical Research-Atmospheres* **2006,** *111* (D10).
21. Bruns, E. A.; Perraud, V.; Greaves, J.; Finlayson-Pitts, B. J., Atmospheric Solids Analysis Probe Mass Spectrometry: A New Approach for Airborne Particle Analysis. *Analytical Chemistry* **2010,** *82* (14), 5922-5927.

22. Jayne, J. T.; Leard, D. C.; Zhang, X. F.; Davidovits, P.; Smith, K. A.; Kolb, C. E.; Worsnop, D. R., Development of an aerosol mass spectrometer for size and composition analysis of submicron particles. *Aerosol Science and Technology* **2000,** *33* (1-2), 49-70.
23. Lee, S.; Liu, W.; Wang, Y. H.; Russell, A. G.; Edgerton, E. S., Source apportionment of PM2.5: Comparing PMF and CMB results for four ambient monitoriniz sites in the southeastern United States. *Atmospheric Environment* **2008,** *42* (18), 4126-4137.
24. Docherty, K. S.; Stone, E. A.; Ulbrich, I. M.; DeCarlo, P. F.; Snyder, D. C.; Schauer, J. J.; Peltier, R. E.; Weber, R. J.; Murphy, S. M.; Seinfeld, J. H.; Grover, B. D.; Eatough, D. J.; Jimenez, J. L., Apportionment of Primary and Secondary Organic Aerosols in Southern California during the 2005 Study of Organic Aerosols in Riverside (SOAR-1). *Environmental Science & Technology* **2008,** *42* (20), 7655-7662.
25. Martello, D. V.; Pekney, N. J.; Anderson, R. R.; Davidson, C. I.; Hopke, P. K.; Kim, E.; Christensen, W. F.; Mangelson, N. F.; Eatough, D. J., Apportionment of ambient primary and secondary fine particulate matter at the Pittsburgh National Energy Laboratory particulate matter characterization site using positive matrix factorization and a potential source contributions function analysis. *Journal of the Air & Waste Management Association* **2008,** *58* (3), 357-368.
26. Schauer, J. J.; Cass, G. R., Source apportionment of wintertime gas-phase and particle-phase air pollutants using organic compounds as tracers. *Environmental Science & Technology* **2000,** *34* (9), 1821-1832.
27. Grover, B. D.; Eatough, D. J., Source apportionment of one-hour semi-continuous data using positive matrix factorization with total mass (nonvolatile plus semi-volatile) measured by the R&P FDMS monitor. *Aerosol Science and Technology* **2008,** *42* (1), 28-39.

2 MEASUREMENT OF SCATTERING IN AND URBAN AREA USING A NEPHELOMETER AND $PM_{2.5}$ FDMS TEOM MONITOR: ACCOUNTING FOR THE EFFECTS OF WATER

Chapter 2 of this dissertation was published in the Journal of Air and Waste Management.[28] The contribution of the author was that of data collection for the Lindon study and preparation of the majority of the manuscript.

2.1 Introduction

In June 2012 the US Environmental Protection Agency (EPA) proposed to revise the Particulate Matter National Ambient Air Quality Standard (PM NAAQS).[29] Included in this proposal is a new secondary PM standard, which addresses the effects of visibility on the public. Currently, visibility is regulated in Class I Federal areas such as national parks and wilderness areas by the Regional Haze Program. Under this program, visibility is characterized and monitored using a visibility index, which is calculated in part from $PM_{2.5}$ mass concentrations. Similar to the existing Regional Haze Program, the new secondary PM NAAQS uses speciated $PM_{2.5}$ mass concentrations to calculate a visibility index for urban areas. All concentrations are averaged over 24 hours and combined to calculate a light extinction coefficient using the IMPROVE algorithm. The five $PM_{2.5}$ species which are used in the algorithm are: sulfate, nitrate, organic carbonaceous mass, elemental carbon, and fine soil/crustal, along with relative humidity. Sulfate, nitrate and relative humidity are combined in the moist light extinction efficiency (MLEE) term which accounts for the changes in light extinction at high relative

humidity due to an increase in water bound to particles. The dry light extinction efficiency (DLEE) term accounts for light extinction at low relative humidity. The basic format of the algorithm used in the new standard is represented by the following:[30-31]

$$PM_{2.5} \text{ light extinction} \approx PM_{2.5} \text{ X (DLEE + MLEE)} \quad (2\text{-}1)$$

The speciated data for sulfate and nitrate are often 24-hour samples, while continuous data is used when it is available, and RH levels are recorded hourly. It is important to note, that because 24 hour averaged concentrations are utilized, diurnal cycles are not properly accounted for.

In preparation for this new standard, the EPA referred to many studies on human perception of visibility.[30] These studies verify that we perceive visibility on a short time scale as reported in Class I areas.[30, 32] Therefore our visibility perception is better represented by hourly averaged data than the current 24-h standard. The EPA noted that hourly averaged measurements would better represent human perception as a light extinction indicator; however, short-term variability of current instruments showed that 1-h averaged data can have data quality issues that can be minimized by averaging over 4-24 h.[30] Since current instruments that measure $PM_{2.5}$ mass may introduce larger uncertainty, a 24-h averaging time was chosen. These limitations prevent the new standard from reflecting current understanding of human visibility perception.

The EPA also considered using directly measured $PM_{2.5}$ light extinction as a visibility indicator, as opposed to the proposed calculated mass-based indicator. The EPA discussed numerous advantages of directly measuring light extinction, including the fact that it more directly relates to human perception of visibility. However, the EPA concluded that the

development of a federal reference method (FRM) for direct light extinction measurements would take several years, and it has not yet begun development of such a method. Therefore, the EPA has decided to rely upon the existing network of instrumentation for mass-based concentrations to calculate $PM_{2.5}$ visibility index values.[29-30]

Before the next review of this standard, it is necessary to conduct more scientific studies in urban areas to evaluate the adequacy of the proposed secondary PM NAAQS and the proposed FRM. Included is the need to evaluate a standard based upon hourly averaged concentrations and to further evaluate the instrumentation used. This study is a beginning towards this objective.

2.2 Experimental

The results of two different field studies are used in this paper.

2.2.1 Lindon Utah 2012 Field Study

A field study was conducted in Lindon, Utah, at a Brigham Young University (BYU) air sampling site, which is located adjacent to the State of Utah PM monitoring site. It was conducted from February to March, 2012. Hourly measurements of $PM_{2.5}$ mass were made with an FDMS TEOM and a conventional TEOM heated to 30ºC. PM_{10} mass was also measured with a conventional TEOM at 30ºC. Coarse particulate mass was estimated as the difference between the two conventional TEOM measurements. $PM_{2.5}$ carbonaceous material was measured with a dual oven (DO) semi-continuous OC-EC Field Analyzer[33] from Sunset Laboratory, giving non-volatile carbonaceous material (CM), semi-volatile CM and black carbon.[34] Black carbon and UV absorbing carbon were measured with a McGee Scientific Aethalometer, model AE-22.

Light scattering was measured with a Radiance Research Integrating Nephelometer, model M903. Concentrations of fine particulate sulfate and nitrate were estimated based on the FDMS TEOM, dual oven, and aethalometer data.[34] Hourly averaged data were obtained continuously with some gaps/exceptions as indicated in Figure 2.1.

2.2.2 Roubidoux California 2003 Field Study

A study was conducted during July 2003 at the SCAQMD sampling site in Rubidoux, CA, as has been previously reported.[35] Instruments were compared for semi-continuous measurement of fine particulate mass, including the semi-volatile fraction.[7] Both FDMS and differential TEOM monitors were used and results were compared with the following: 1-h RAMS[35] measurements; 1-h averaged R&P particulate nitrate measurements; 1-h averaged nonvolatile and semi-volatile CM measurements using a DO OC-EC Analyzer; and 3-h integrated PC-BOSS[36] sampler results. During this study, fine particulate mass, including water content,[37] was measured using a GRIMM model 1100 monitor; however, the GRIMM results were not included in the previous publication. The interpretation of these results is included in this manuscript.

2.3 Results and discussion

2.3.1 Lindon Study: Correlation of FDMS and Nephelometer Measurements and the Effect of Relative Humidity

In this study, correlations between the FDMS TEOM and the nephelometer measurements indicate that the FDMS TEOM $PM_{2.5}$ measurements will not adequately characterize light scattering at higher relative humidity when water is absorbed by the aerosol.

This conclusion is reached using the hourly averaged data obtained for $PM_{2.5}$ mass and total light scattering using an FDMS TEOM and nephelometer (corrected for coarse particle scattering). These data, along with relative humidity, are shown in Figure 2.1. Time periods with very high $B_{p,scat}$ values due to the presence of fog are marked with hashed lines.

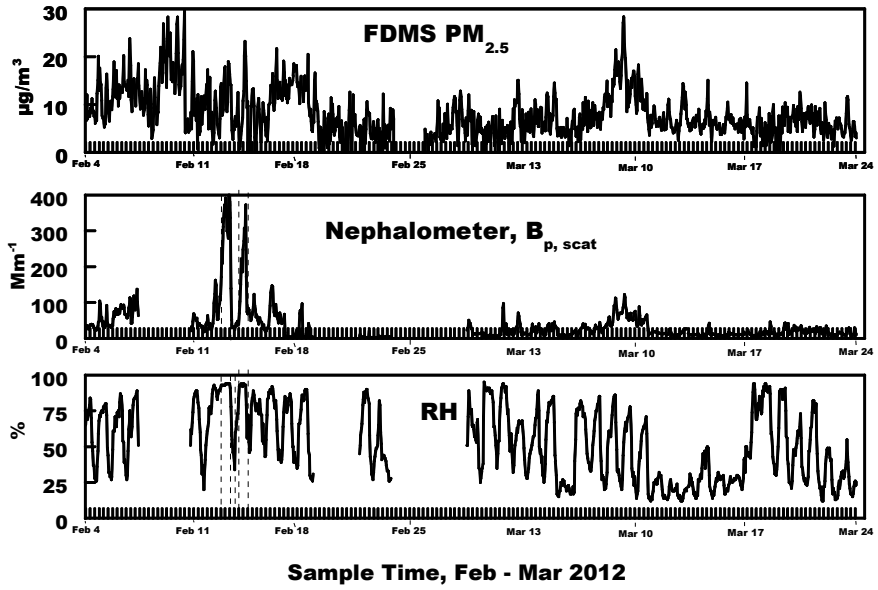

Figure 2.1 Data from the Lindon 2012 Study, including hourly averaged values of FDMS measured PM2.5, nephelometer measured Bp, scat and RH.

The correlation between $PM_{2.5}$ and corrected coarse particle scattering $B_{p,scat}$ (assuming a mass scattering coefficient of 0.5 m^2/g for coarse particles) is shown in Figure 2.2. This is limited to the time periods of Feb 4-7, Feb 10-11, Feb 15-16 and Mar 7-11, when nephelometer data were available and $PM_{2.5}$ concentrations exceeded 15 $\mu g/m^3$. Time periods in which RH exceeded 80% are indicated by solid data points (excluding time periods with fog present). The deviation from linearity of the solid data points is due to the effect of particle associated water, which is not measured by the FDMS TEOM. This can best be understood by considering that the FDMS TEOM first uses a cyclone cut-off, and then passes the sample through a nafion dryer to remove the water, both gas phase and particle bound. Particle-bound water significantly

increases above 80% humidity since this is the deliquescence point of $(NH_4)_2SO_4$ and above the deliquescence point of NH_4NO_3(62%).[38] Thus the particles sharply increase in mass around 80% RH, and cause more light scattering, which is not indicated by the mass measurement since this water is not measured by the FDMS TEOM. This introduces a negative bias to the DLEE, and inclusion of these mass measurements (RH>80%) would underestimate the light extinction coefficient. An appropriate IMPROVE algorithm could account for this, and the EPA has encouraged efforts to better calculate light extinction using the instruments currently deployed in the field (such as the FDMS TEOM).[30] However, in order to reliably calculate hourly averaged extinction, hourly concentrations of NH_4NO_3 and $(NH_4)_2SO_4$ are necessary, which concentrations are often not available.

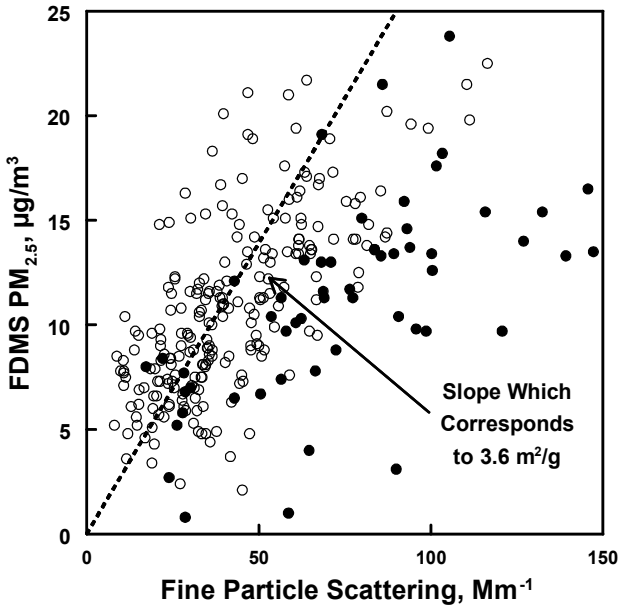

Figure 2.2 Variation of nephelometer response (corrected for coarse particle scattering) with FDMS PM2.5 from the Lindon 2012 study. The open data points are consistent with a mass scattering coefficient of about 3.6 m^2/g. The closed data points are associated with ambient RH > 80%. The increased scattering associated with these data can be attributed to particle bound water which is not measured by the FDMS TEOM.

During the time periods of low humidity when aerosol water content should be small or negligible (open data points in Figure 2.2) the linear relationship between measured $PM_{2.5}$ mass

and light scattering should give the mass scattering coefficient for the dry fine aerosol. Linear regression analysis of the open data points in Figure 2.2 gives a predicted average fine particulate mass scattering coefficient of 3.6 ± 0.5 m^2/g (N = 223, r^2=0.52) with an intercept of 6 ± 15 Mm^{-1}. This value compares favorably to the average dry mass scattering coefficient obtained in a wintertime study in the Salt Lake Valley of 3.0 m^2g and a value of 3.6 m^2/g from the IMPROVE protocols.[39] The IMPROVE protocol value is calculated using the data in Figure 2.4, which is the estimated average composition of fine particulate aerosols during Feb 3-10. This composition is similar to the composition seen in previous studies.[40]

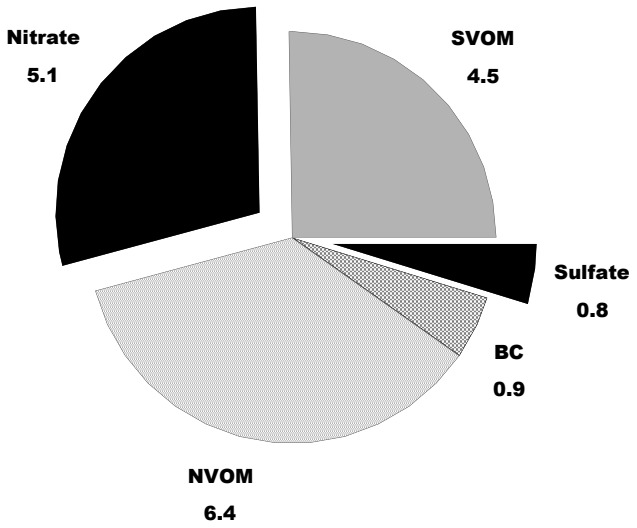

Figure 2.3 Average composition of FDMS measured $PM_{2.5}$ during Feb 9-10 in the Lindon study. Indicated species are NVOM (nonvolatile organic material), SVOM (Semi-volatile organic material), Sulfate and Nitrate (present as the ammonium salts) and BC (black carbon). Concentrations are $\mu g/m^3$.

Further comparison of light scattering with other data obtained in Lindon reveals events in which correlation between primary emissions, formation of secondary aerosol and light scattering can be examined. These relationships are best seen during the episode of high $PM_{2.5}$ concentrations, between March 8 to 12, as shown in Figures 2.1 and 2.4. Figure 2.1 indicates a weak inversion giving rise to increased pollution. Since night time RH did not exceed 80%, the

impact of water uptake by the aerosol is negligible. A 2007 winter study in Lindon included a source apportion analysis[40] which indicated that elevated day-time BC concentrations were associated with emission from mobile sources, and high BC concentrations in the late evening were due to emission from the home combustion of wood. Both day-time and night-time formation of nitrate and organic secondary particulate material were also important. The diurnal trend in BC, RH, $PM_{2.5}$, and $B_{p,\,scat}$ (corrected for coarse particle scattering) are shown in Figure 2.4. The BC and scattering patterns in Figure 2.4 were also mirrored by CO concentrations taken 4 miles away from the Lindon sampling site (not shown here). The evening peaks between about 7 p.m. and 11 p.m. can be attributed to home combustion of wood.[40] While these BC peaks are also associated with increases in scattering, both the scattering and fine particulate mass continue to increase during the period after the end of the BC peak. The apportionment results from the 2007 study[40] indicate that the increasing fine particle concentrations are associated with both organic and nitrate secondary material formed after the wood smoke emission have been released.[40] Fine particle light scattering follows this same trend, Figure 2.4, indicating that secondary aerosol is an important, if not dominant contributor to light scattering at the Lindon sampling site.

2.3.2 Rubidoux Study: Measurement of Fine Particulate Mass Including the Water Content

One weakness of the mass-scattering correlation revealed from the Lindon 2012 data is the lack of measurement of particle associated water using the FDMS TEOM. Such correlations could be improved and the prediction of human perception of visibility better estimated using PM measured mass which did include the particulate water in the measurement. Likewise, using a conventional TEOM will not measure this particle bound water. In addition, because the

sample collection filter is heated, the TEOM will not measure particulate semi-volatile species such as ammonium nitrate or semi-volatile organic material.

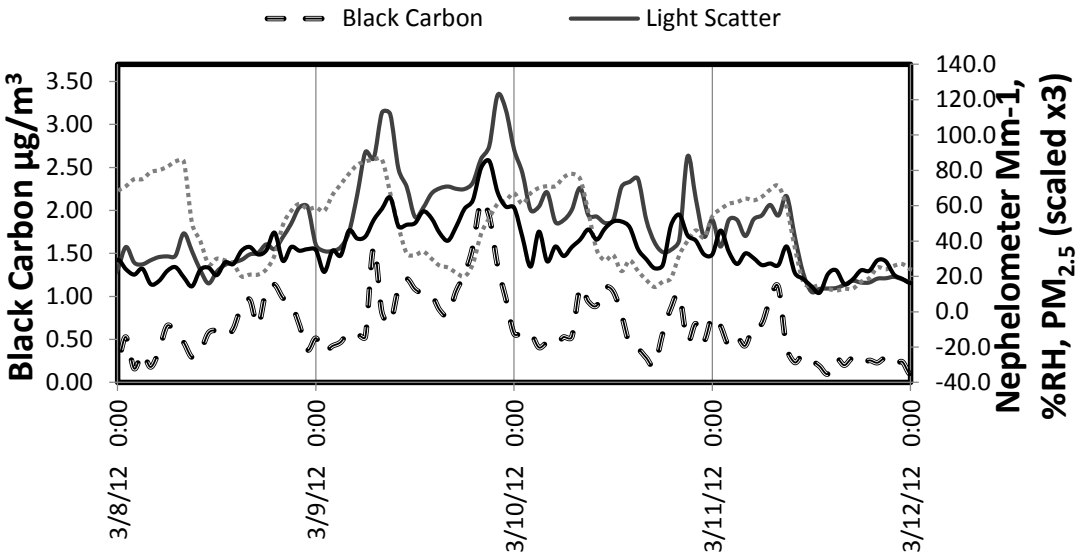

Figure 2.4 A comparison between light scattering, % RH, $PM_{2.5}$ and black carbon from 3/8- 3/11. The trends shown here indicate that secondary aerosol formation is likely the dominant contributor to light scattering since scattering continues to increase after the end of the black carbon peaks.

During the 2003 study at Rubidoux, CA,[41] $PM_{2.5}$ mass was measured with both an FDMS TOEM and the RAMS,[35] two instruments expected to measure total fine particulate mass except for the particle associated water. In addition, $PM_{2.5}$ and $PM_{10\text{-}2.5}$ mass was measured with the GRIMM model 1100. The results of these measurements are shown in Figure 2.5. As indicated, the three measurements agree except for the times of high relative humidity when the GRIMM gave higher results than the other two measurements.

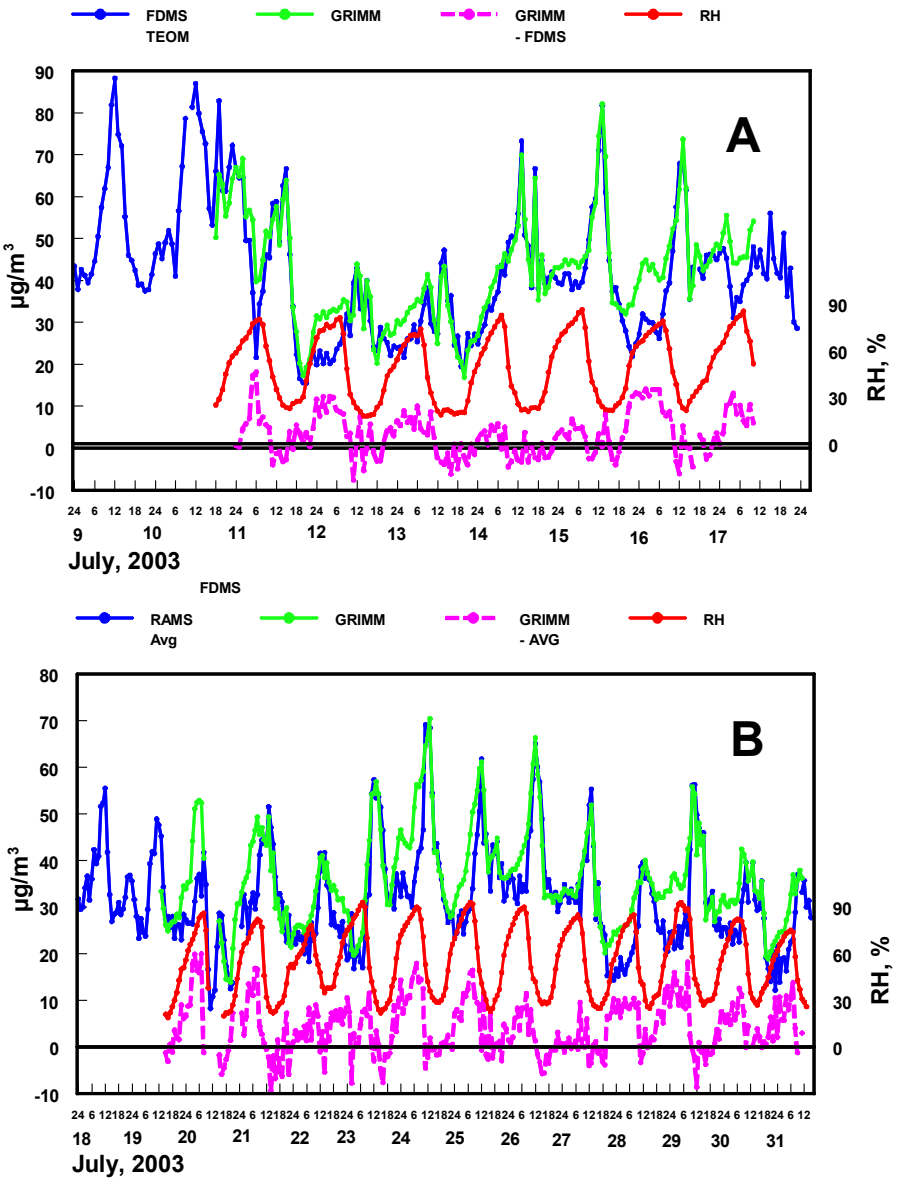

Figure 2.5 Comparisons of $PM_{2.5}$ data obtained using the GRIMM model 1100 with (A) FDMS TEOM $PM_{2.5}$ mass and (B) the average of FDMS TEOM and RAMS measured $PM_{2.5}$ mass. The difference between the GRIMM and other mass measurements is shown, in addition to relative humidity. All results are hourly averaged measurements.

Peaks in the $PM_{2.5}$ concentrations generally occurred during the mid-day period for each sampling day. This was a time of significant secondary ammonium nitrate and semi-volatile organic material formation.[41] Relative humidity was generally low during this mid-day time period. The GRIMM and comparison monitor results are in good agreement during these periods

of low relative humidity, indicating that the protocols used to convert the GRIMM monitor volume distribution data to a $PM_{2.5}$ mass concentration are robust. In contrast, during the overnight periods of high relative humidity, the results obtained with the GRIMM monitor are consistently higher than the results obtained with the comparison monitors. As described above, the comparison monitors do not measure fine particulate water content. It is probable that the higher concentrations measured during the high relative humidity time periods with the GRIMM monitor may reflect the increased volume of aerosol associated with fine particulate water.

The uptake of water by the fine aerosol can be estimated during time periods when NH_4SO_4 and NH_4NO_3 chemical composition data were available (as shown in Figure 2.6). The particle uptake of water with increasing humidity increases significantly due to these two particle-bound species.[42] The effect of relative humidity on water content was estimated from the data of Tang et al. using a previously described protocol to average the hysteresis effects on the data for pure ammonium sulfate.[43-44] The effect of particle-bound ammonium nitrate is slightly less pronounced; however, we have used the same relative humidity curve to approximate the effect of both NH_4SO_4 and NH_4NO_3.[42] Both sulfate and nitrate are expected to exist as NH_4SO_4 and NH_4NO_3 due to the high amount of gas phase NH_3 in the Rubidoux area.

As seen in Figure 2.6, sulfate concentrations did not vary significantly as a function of time of day or relative humidity. However, significant diurnal patterns in ammonium nitrate were seen, with the highest concentrations being present at mid-day. This was also a time of lower relative humidity. The diurnal pattern of the ammonium nitrate indicates the need for a shorter averaging time period than daily averages.

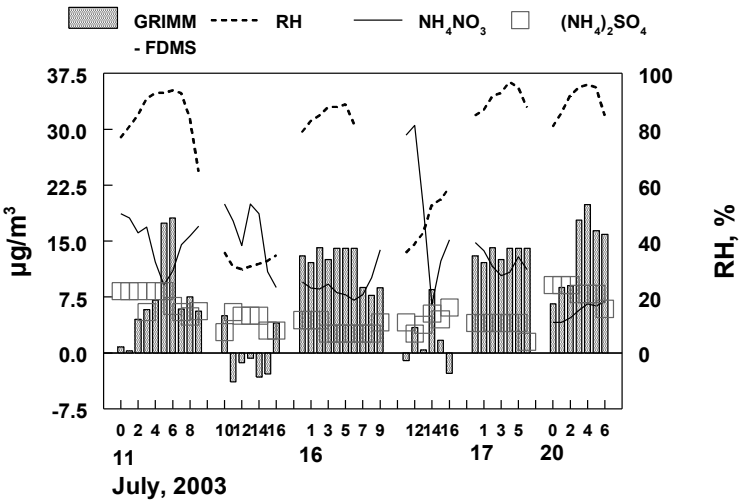

Figure 2.6 Relative humidity, NH_4NO_3 and $(NH_4)_2SO_4$ data used to estimate the uptake of water by the fine aerosol being sampled. The hypothesis was that the positive differences between the GRIMM monitor and comparison samplers were due to aerosol water.

Since the highest concentrations of ammonium nitrate do not occur during periods of highest relative humidity, the calculation of water content using the data in Figure 2.5, provides a stringent test of the origin of the difference between the GRIMM monitor and comparison sampler results. In Figure 2.7, the $PM_{2.5}$ mass difference between the GRIMM monitor and the comparison sampler is compared to the calculated mass of water in the aerosol due to ammonium nitrate, ammonium sulfate and relative humidity changes. Deviations from the slope of 1 are not any larger than the uncertainties in the assumptions used in the calculations, and the data points do scatter uniformly around this line. The assumption that the higher mass measurements seen by the GRIMM 1100 monitor are due to water uptake is reasonable. In should be noted that the GRIMM model 180 monitor with a Nafion dryer system does not measure particle associated water.[45]

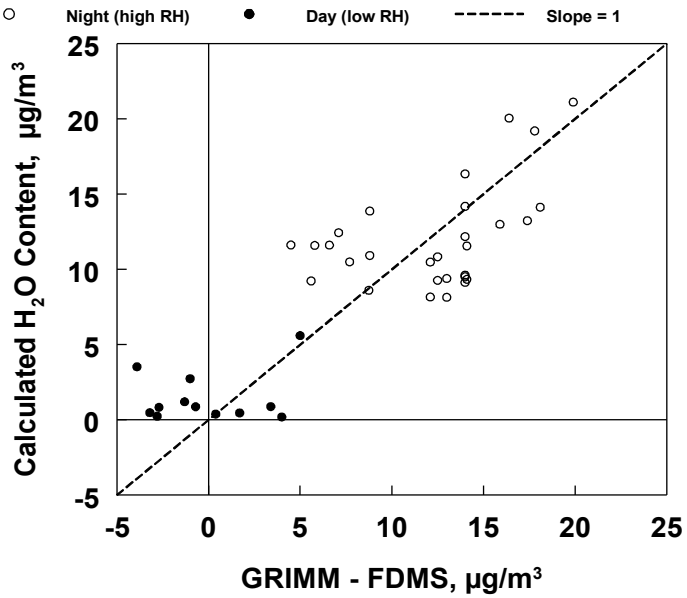

Figure 2.7 Comparison of the GRIMM minus average comparison sampler results and calculated aerosol water content.The line has a slope of one.

2.4 Conclusions

The collection of hourly averaged data in the studies herein signifies the need for alternative instrumentation and the need for shorter averaging times if measured urban visibility is to be related to human perception. In areas where an FDMS TEOM is used to measure $PM_{2.5}$, high humidity causes an underestimation of light extinction due to PM bound water. This occurs because the particle-bound water has a sharp increase once the deliquescence point of NH_4NO_3 and $(NH_4)_2SO_4$ is reached. In areas where hourly speciation data are not available, the calculation of light scattering will be skewed, especially if a 24-h averaged value of NH_4NO_3 is used to calculate the MLEE, thus creating a bias for overestimating light scattering during times when RH is high and NH_4NO_3 levels are actually low. This is especially the case at nighttime. More significantly, the EPA proposed standard will not account for diurnal variation of visibility degradation and, therefore, it will poorly relate to human visibility assessment. The correlations between particle mass and scattering reported here would be improved by the use of instruments

akin to the GRIMM model 1100 monitor, which measures particle associated water. Furthermore, obtaining data using a nephelometer and a GRIMM model 1100 monitor together, would show the accuracy of scattering measurements based on reliable mass measurement systems (such as the GRIMM). Such measurements are recommended.

2.5 Acknowledgments

This research was supported by Southern California Edison. Appreciation is expressed to CIRA, Fort Collins, CO, for the use of their nephelometer

2.6 Chapter References

28. Cropper, P. M.; Hansen, J. C.; Eatough, D. J., Measurement of light scattering in an urban area with a nephelometer and PM2.5 FDMS TEOM monitor: Accounting for the effect of water. *Journal of the Air & Waste Management Association* **2013,** *63* (9), 1004-1011.
29. EPA, U. S. E. P. A. *National Ambient Air Quality Standards for Particulate Matter; Proposed Rule*; FRL-9682-9

EPA-HQ-OAR-2007-0492; Federal Register/ Vo. 77, No. 126, 2012; pp 38889-39055.
30. EPA, U. S. E. P. A., Policy Assessment for the Review of the Particulate Matter National Ambient Air Quality Standards. Agency, U. S. E. P., Ed. Federal Register: 2011; Vol. 77, pp 38889-39055.
31. DeBell, L. J.; Gebhart, K. A.; Hand, J.; Malm, W. C.; Pitchford, M.; Schichtel, B.; White, W. H. Interagency Monitoring of Protected Visual Environments (IMPROVE): Spatial and Seasonal Patterns and Temporal Variability of Haze and its Constituents in the United States: Report IV 2006. (accessed November 2006).
32. Hyslop, N. P., Impaired visibility: the air pollution people see. *Atmospheric Environment* **2009,** *43* (1).
33. Grover, B. D.; Eatough, N. L.; Woolwine, W. R.; Eatough, D. J.; Cary, R. A., Modifications to the Sunset Laboratory Carbon Aerosol Monitor for the Simultaneous Measurement of PM2.5 Nonvolatile and Semi-Volatile Carbonaceous Material. *Journal of the Air & Waste Management Association* **2009,** *59* (8).
34. Grover, B. D.; Eatough, N. L.; Woolwine, W. R.; Cannon, J. P.; Eatough, D. J.; Long, R. W., Semi-continuous mass closure of the major components of fine particulate matter in Riverside, CA. *Atmospheric Environment* **2008,** *42* (2).
35. Obeidi, F.; Eatough, N. L.; Eatough, D. J., Use of the RAMS to measure semivolatile fine particulate matter at Riverside and Bakersfield, California. *Aerosol Science and Technology* **2002,** *36* (2).

36. Ding, Y. M.; Pang, Y. B.; Eatough, D. J., High-volume diffusion denuder sampler for the routine monitoring of fine particulate matter: I. Design and optimization of the PC-BOSS. *Aerosol Science and Technology* **2002,** *36* (4).
37. Grimm, H.; Eatough, D. J., Aerosol Measurement: The Use of Optical Light Scattering for the Determination of Particulate Size Distribution, and Particulate Mass, Including the Semi-Volatile Fraction. *Journal of the Air & Waste Management Association* **2009,** *59* (1).
38. Finlayson-Pitts, B. J.; Pitts, J. N. J., *Chemistry of the upper and lower atmosphere : theory, experiments, and applications.* Academic Press: San Diego, 2000.
39. Pitchford, M.; Malm, W.; Schichtel, B.; Kumar, N.; Lowenthal, D.; Hand, J., Revised algorithm for estimating light extinction from IMPROVE particle speciation data. *Journal of the Air & Waste Management Association* **2007,** *57* (11).
40. Hansen, J. C.; Woolwine, W. R., III; Bates, B. L.; Clark, J. M.; Kuprov, R. Y.; Mukherjee, P.; Murray, J. A.; Simmons, M. A.; Waite, M. F.; Eatough, N. L.; Eatough, D. J.; Long, R.; Grover, B. D., Semicontinuous PM2.5 and PM10 Mass and Composition Measurements in Lindon, Utah, during Winter 2007. *Journal of the Air & Waste Management Association* **2010,** *60* (3).
41. Grover, B. D.; Kleinman, M.; Eatough, N. L.; Eatough, D. J.; Hopke, P. K.; Long, R. W.; Wilson, W. E.; Meyer, M. B.; Ambs, J. L., Measurement of total PM(2.)5 mass (nonvolatile plus semivolatile) with the Filter Dynamic Measurement System tapered element oscillating microbalance monitor. *Journal of Geophysical Research-Atmospheres* **2005,** *110* (D7).
42. Tang, I. N.; Wong, W. T.; Munkelwitz, H. R., The relative importance of atmospheric sulfates and nitrate in visibility reduction. *Atmospheric Environment* **1981,** *15* (12).
43. Malm, W. C.; Gebhart, K. A.; Molenar, J.; Cahill, T.; Eldred, R.; Huffman, D., Examining the relationship between atmospheric aerosol and light extinction at Mount-Rainier-National-Park and North-Cascades-National-Park. *Atmospheric Environment* **1994,** *28* (2).
44. Sisler, J. F.; Malm, W. C.; Gebhart, K. A.; Molenar, J.; Cahill, T. In *The effect of relative humidity on visibility - Continental distributions*, Annual AWMA Meeting, Air and Waste Management Association, Pittsburgh, Pittsburgh, 1992.
45. Long, R. W.; Modey, W. K.; Smith, P. S.; Smith, R.; Merrill, C.; Pratt, J.; Stubbs, A.; Eatough, N. L.; Eatough, D. J.; Malm, W. C.; Wilson, W. E., One- and three-hour PM2.5 characterization, speciation, and source apportionment using continuous and integrated samplers. *Aerosol Science and Technology* **2005,** *39* (3), 238-248.

3 COMPOSITION AND SECONDARY FORMATION OF FINE PARTICULATE MATTER IN THE SALT LAKE VALLEY: WINTER 2009

Chapter 3 of this dissertation was published in the Journal of Air and Waste Management.[46] The author's contribution was that of addressing the reviewers concerns, clarifying and rewriting many sections of the manuscript, and preparing it for final publication. For a complete list of contributing authors see the associated reference.

3.1 Introduction

Under the National Ambient Air Quality Standards put in place as a result of the Clean Air Amendments of 1990, three regions in the State of Utah, Salt Lake County, Ogden City and Utah County, are in violation of the 24-h National Ambient Air Quality Standard (NAAQS) for PM_{10} and $PM_{2.5}$. The valleys in which these counties are located are susceptible to strong winter inversions that can persist for days to weeks. The strong inversions coupled with the metropolitan nature of this region (Salt Lake Valley population of 1.2 million) contribute to its violation of the NAAQS for PM during the winter. These meteorological conditions and the metropolitan nature of these regions have existed for decades. However, the maximum concentrations seen during inversions has decreased in response to air pollution control measures of the past, but the improvements have not been sufficient to put these regions into attainment. High concentrations of fine particulate matter are generally associated with inversions. In general fine particulate matter and anthropogenic pollutant gases are dominated by local emissions and not by transport from other regions. High concentrations of coarse particulate

matter are sometimes observed due to transport of crustal material associated with high winds; however, these conditions were not important during the current study.

The Hawthorne Elementary School sampling site (AQS Station Code 490353006) located in Salt Lake City, Utah has been designated as one of 55 urban, long-term, nationwide multi-pollutant NCore sites.[47] The NCore network is designed to enhance existing monitoring capabilities in an effort to produce an integrated multi-pollutant approach to air quality monitoring. In addition to collecting information on criteria pollutants, NO_X, O_3, CO and PM, emphasis has been placed on measuring non-criteria pollutants, specifically NH_3 and HNO_3 because of their importance in secondary PM formation. These species are measured in an effort to improve emission control strategies as well as to obtain more complete information for scientific, public health and ecosystem assessments.

Characterization of the $PM_{2.5}$ mass on a semi-continuous basis and the 3-h average determination of $PM_{2.5}$ mass and components have been previously studied at the Hawthorne site. [45, 48] These studies were directed towards the understanding of fine particulate health effects and source characterization.[45, 49] These previous air sampling campaigns have shown that a major component of PM in the Salt Lake Valley during the winter is ammonium nitrate (NH_4NO_3). Ammonium nitrate is primarily formed from gas phase ammonia and nitric acid via reaction:

$$NH_{3(g)} + HNO_{3(g)} \rightarrow NH_4NO_{3(s,aq)} \qquad (3\text{-}1)$$

Ammonium nitrate forms particles of the appropriate size to scatter visible light which reduces visibility. It is also expected to be a major contributor to $PM_{2.5}$ in the Salt Lake Valley and thus contribute to both NAAQS violations and exacerbation of human cardiopulmonary

health problems by increasing fine particulate matter.[49] One of the goals of this study is to identify the limiting reagent in the formation of $PM_{2.5}$ ammonium nitrate in the Salt Lake Valley.

3.2 Materials and methods

Samples were collected at the Hawthorne Elementary School air quality monitoring site from January 3 through February 25, 2009. One-hour averaged concentrations of $PM_{10-2.5}$, $PM_{2.5}$, NO_x (NO and NO_2), O_3, CO, and NH_3 were measured. Particulate phase nitrate, nitrite and sulfate, and gas phase HONO, HNO_3 and SO_2 were also measured on a one-hour average basis. Speciation data was collected for $PM_{2.5}$, as it is the focus of this paper. $PM_{10-2.5}$ is given for completeness; however, no speciation data is available on the coarse particle fraction.

One-hour averaged $PM_{10-2.5}$ and $PM_{2.5}$ masses were measured using a Thermo Environmental model 1405DF Tapered Element Oscillating Microbalance (TEOM) with a Filter Dynamics Measurement System (FDMS). The sampler used firmware version 1.22. The 1405DF sampler incorporates a virtual impactor to separate the sampled air into two fractions, $PM_{2.5}$ and $PM_{10-2.5}$. Manual methods collected daily samples for PM_{10} and $PM_{2.5}$ using Thermo Environmental model 2025 samplers. Particulate samples were collected every third day for the National Speciation Trends Network using MetOne SASS and URG 3000N samplers. An intensive sampling program was initiated during inversions to collect samples for speciation every other day.

A URG-9000C Ambient Ion Monitor (AIM) provided 1-h averaged measurements of particulate nitrate, nitrite and sulfate in $PM_{2.5}$, and of gas phase HONO, HNO_3 and SO_2; this model does not measure cations. We have previously demonstrated the equivalence of hourly ion chromatography data with appropriate integrated data using valid diffusion denuder

techniques.[50] The instrument draws in air at a rate of 3 L/min through a $PM_{2.5}$ sharp-cut cyclone filter. The air is passed through a liquid diffusion denuder where gases are removed by reaction with a dilute aqueous solution of H_2O_2 (0.3% in water). The oxidant solution in the denuder is used to convert SO_2 to sulfate. Particles are subsequently collected. The air stream after the denuder enters an aerosol super-saturation chamber. Both the gas phase and particle phase are collected for one hour and then analyzed with ion chromatography (Dionex ICS-1000). An inertial particle separator collects and dissolves these particles in deionized water and injects them into the ion chromatograph for analysis. The lower limit of detection for both particle and gas phase ions is species dependent and approximately 0.05 $\mu g/m^3$. The AIM instrument was calibrated according to the user manual instructions every two weeks with a seven anion standard purchased from Dionex (P/N 56933). The denuder membrane was changed every four weeks.

To avoid sampling artifacts as well as weather interferences, sampling with the AIM was done through a manifold. The manifold was constructed from a 2.44 meter long PVC pipe with 15.2 cm diameter. A high volume air blower was connected to the air pipe and was set so that the air velocity inside the pipe was no more than 5 mph (8 km/h). A weather cap was attached to the top of the manifold to avoid collection of precipitation and large objects. The sampling manifold was raised about 2 m over the roof of the sampling trailer and at least 0.5 m above the closest sampling intake of other instruments. The sampling line from the manifold to the AIM inlet was a 75-cm long, Teflon-coated, 2.5-cm O.D. aluminum diameter pipe. This set-up is to minimize nitric acid loss in the inlet.

Hourly averaged NO_X (NO and NO_2), CO, NH_3, and O_3 concentrations were monitored using EPA reference designated method analyzers. NO_X (NO and NO_2) was monitored using a Thermo Environmental model 42C analyzer operated on 0 to 1 ppm range for NO and NO_X and

0 to 0.5 ppm range for NO_2. This instrument measured NO_X and NO and calculates NO_2 as the difference. CO was monitored using a Thermo Environmental model 48C operated on 0 to 50 ppm range. NH_3 was monitored using a Thermo Environmental model 17C operated on 0 to 100 ppb range. O_3 was monitored using a Teledyne API model 400E operated on 0 to 500 ppb range. All instruments were operated following the EPA Quality Assurance Handbook for Air Pollution Measurement Systems [51].

3.3 Meteorology

The Salt Lake Valley sits in the heart of the Intermountain Region and is bordered on the east and west by high mountain ranges (rising to 1,850 m above the valley floor) and to the north by the Great Salt Lake. During winter, and under stable high pressure systems, long nights and occasional snow cover trap cold air at the surface and produce stable valley temperature inversions. Several times each winter, strong ridges of high pressure are situated over Northern Utah producing clear skies, light winds, and weak mixing. Over time, the diurnal valley heat deficit increases and a cold pool forms within the confines of the valley.[52] In these cases, the atmosphere is stable through at least 700 mbar, but the core of the cold pool, where most pollutants are trapped, ranges from 200 m to 600 m above the valley floor. Cold pools can persist for 1 to 3 weeks and require a strong synoptic scale weather event to fully disperse pollutants from the valley floor.

Weather during the January and February 2009 sampling period was typical of most winters in the Salt Lake Valley. Occasional storm systems from the southwest and northwest brought heavy mountain snow and moderate amounts of snow to the valley floor. Two

significant cold pools formed during the sampling period on January 14-24, 2009 and on January 29 to February 6, 2009, resulting in stable inversions and clear skies on these days.

3.3.1 January 14-24 Cold Pool

A deep trough over the central United States allowed a strong ridge of high pressure to build west over the intermountain region. Between January 16 and 23 the ridge was centered over Utah and produced light winds and cloudless skies. During this time, daily high temperatures on the valley floor (1288 m) at the Salt Lake City International Airport (KSLC) ranged from 2 to 6 °C. Daily low temperatures ranged from -4 to -7 °C. Wind speeds in the cold pool were light and averaged between 3 and 6 km/h. The last significant snowfall on the valley floor occurred on January 8, but the snow cover melted completely by January 12 and no additional snow fell during the cold pool event. The Salt Lake Valley has significant gradients of elevation and precipitation, so on the eastern bench areas, snow cover likely persisted throughout the cold pool event. The stability of the cold pool was significant. Using the morning and afternoon radiosonde data from KSLC, vertical lapse rates of -12 to -23 °C per 1000 m were measured. The vertical lapse rate gradient of a fully mixed, dry, stable atmosphere is 10 °C per 1000 m. The negative lapse rate is indicative of a strong inversion.

3.3.2 January 29 - February 6 Cold Pool

On January 26 a cold front moved through Northern Utah dropping 8 cm of snow at KSLC. Following the cold front, a ridge of high pressure moved from the west and was centered over Utah on January 30. Temperatures during this cold pool were warmer and ranged from 3 to 12 °C. At KSLC, snow cover melted on February 1, but likely persisted in Eastern Salt Lake

Valley. Wind speeds during the core of the cold pool averaged 8 km/h. Stability, as assessed from KSLC vertical temperature gradients, was weaker than during the first cold pool, but a negative lapse rate of -17 °C per 1000 m was recorded during the morning of February 5.

3.4 Results & Discussion

Figure 3.1 shows the hourly averaged concentrations of $PM_{2.5}$, $PM_{10-2.5}$ and measured fine particulate anions. The data set for the PM and gas measurements have four gaps in the URG particle composition data (a total of 10 % of the data is missing) because of instrument malfunction. For PM composition analysis, assumptions were made that (1) nitrite was present as the sodium salt, (2) ammonium nitrite was volatile enough that it would not exist in PM, and (3) the remainder of the anions were present as the ammonium salts. The mass not accounted for by the measured anions is presented as "Missing $PM_{2.5}$ Mass" in Figure 3.1, and consisted mostly of fine particulate carbonaceous material including elemental carbon (EC) and organic material (OM). EC and OM were measured by the Improve method on 24-h averaged filters. Measured OC was converted to OM using a factor of 1.6. The hourly averaged concentrations of the criteria gas phase pollutants CO, NO_x (NO and NO_2), O_3 and SO_2 are shown in Figure 3.2. The hourly averaged concentrations of gas and fine particulate nitrite, nitrate and gas phase ammonia are shown in Figure 3.3.

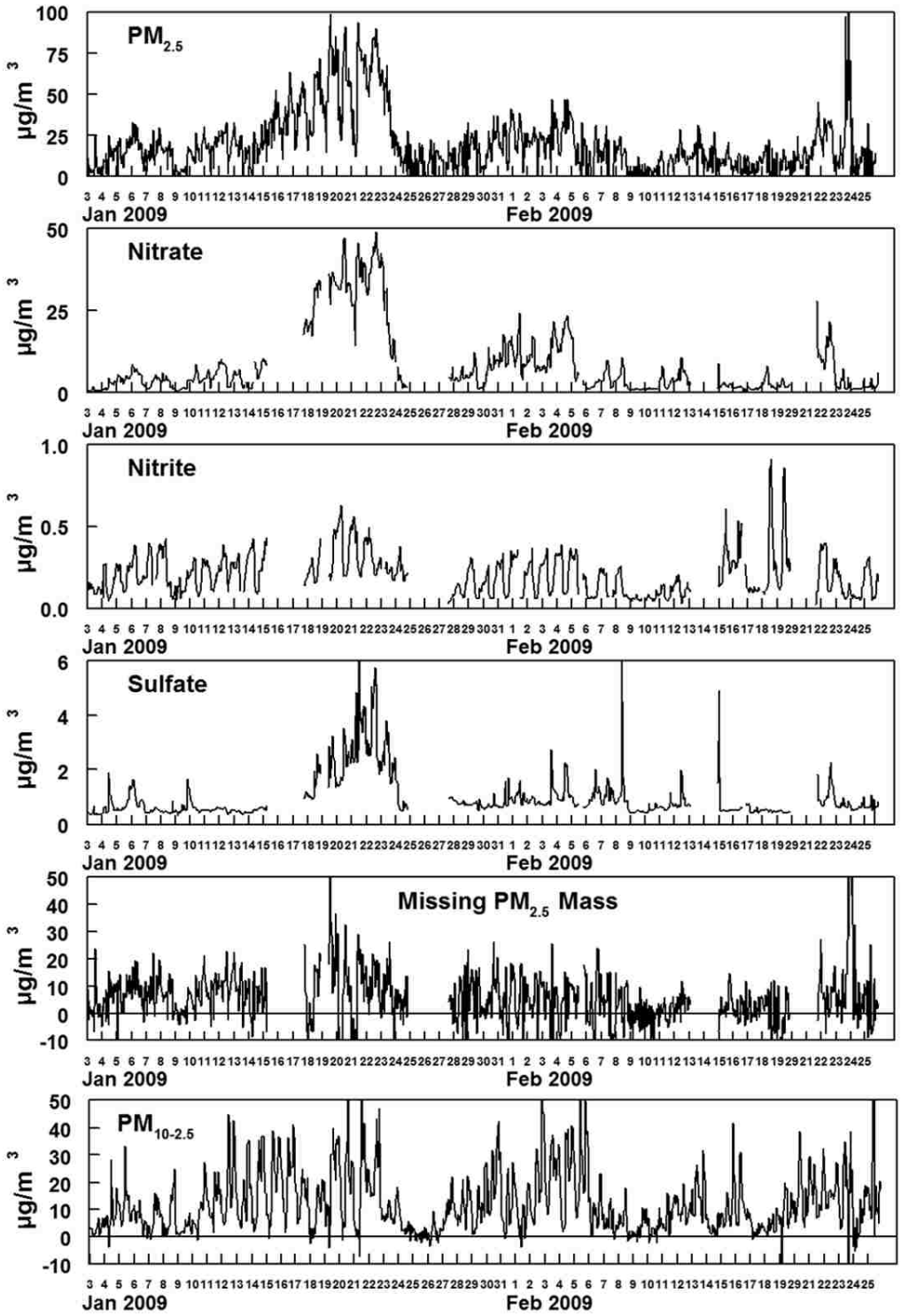

Figure 3.1 Hourly averaged concentrations of $PM_{2.5}$, $PM_{10-2.5}$, and fine particulate species at Hawthorne during the study. Missing $PM_{2.5}$ is calculated as the difference between measured fine particulate mass and the other measured species assuming sulfate and nitrate are present as ammonium compounds and nitrite is present as the sodium salt. Missing mass is dominantly carbonaceous material.

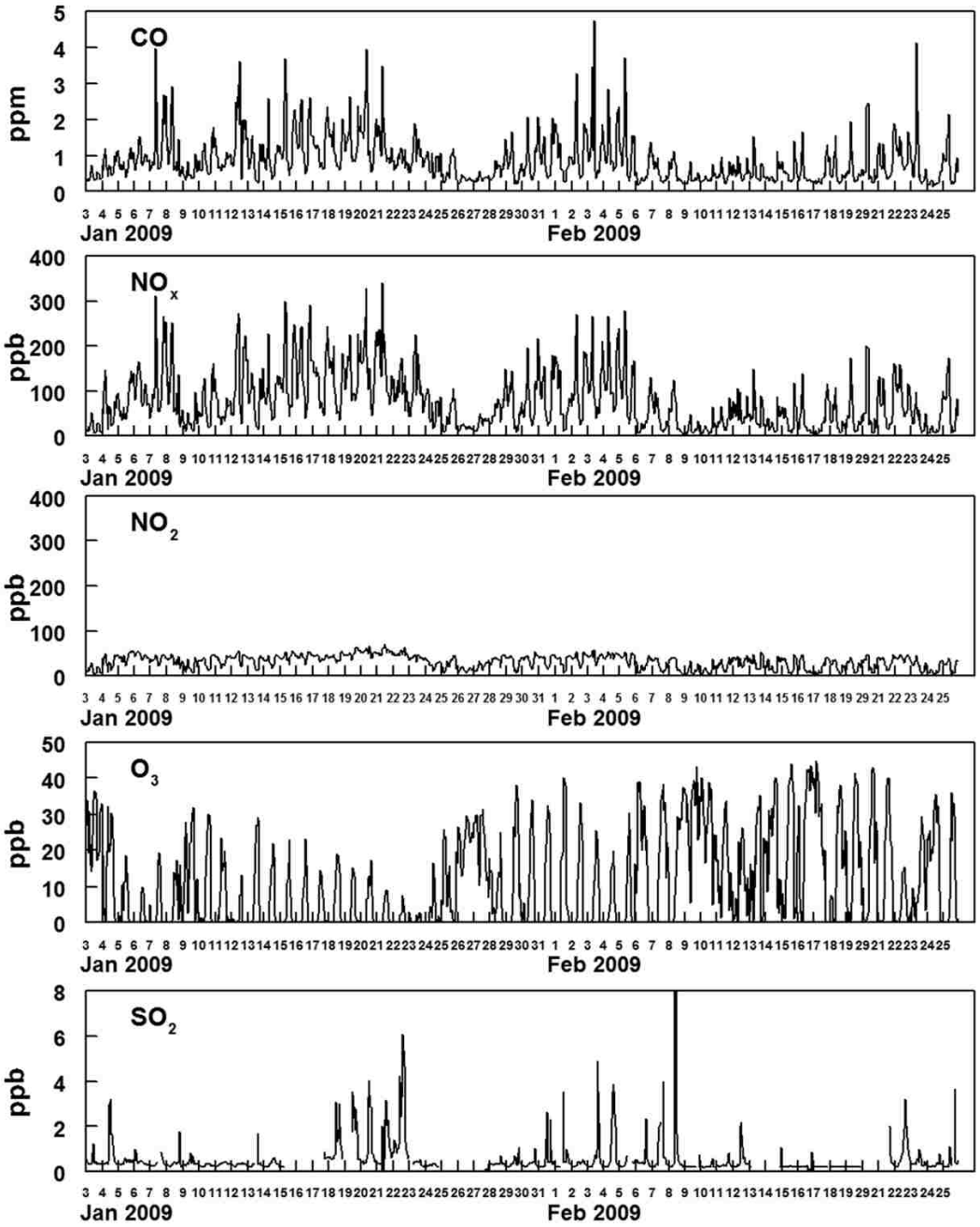

Figure 3.2 Hourly averaged concentrations of criteria pollutant gas phase species measured at Hawthorne during the study.

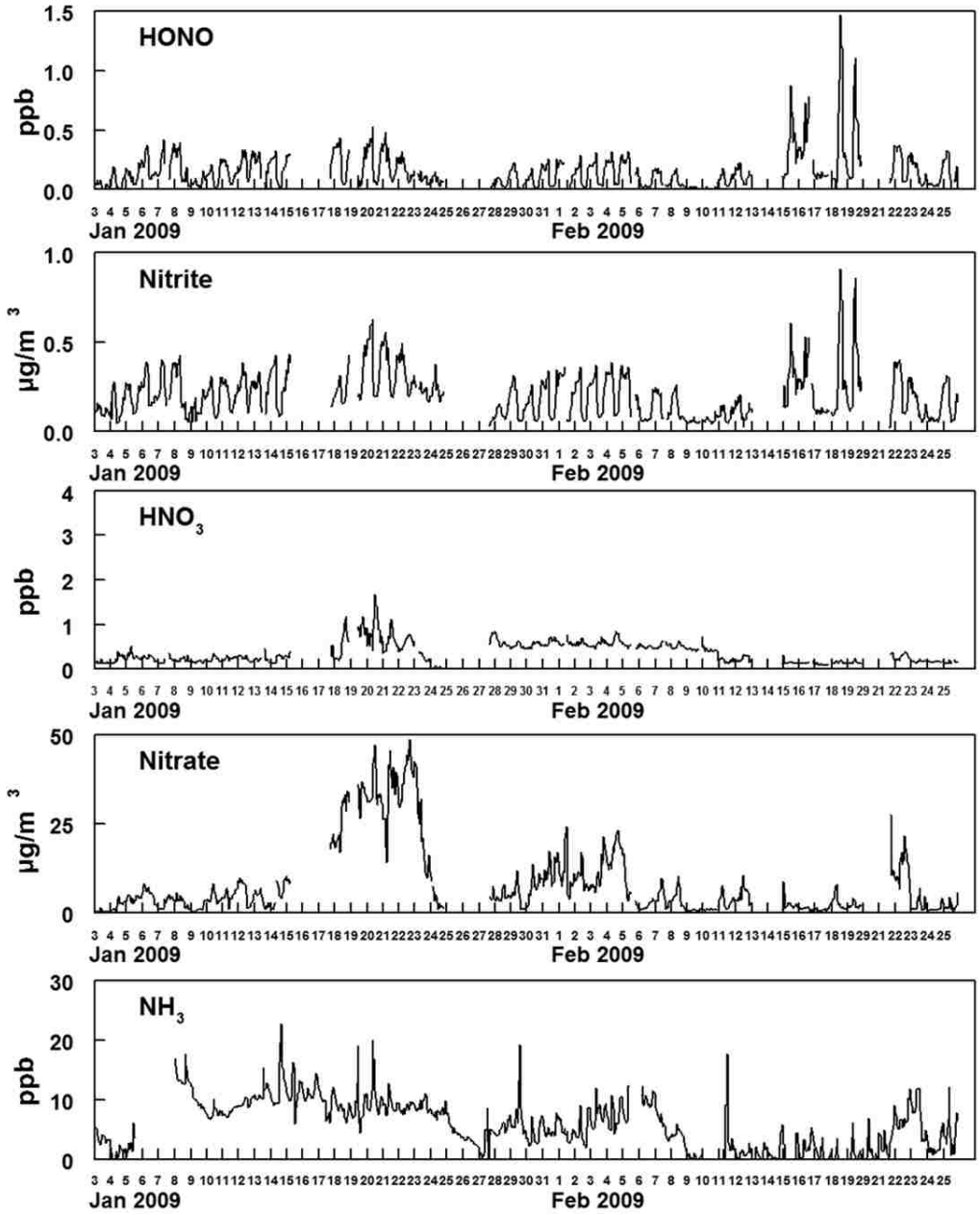

Figure 3.3 Hourly averaged concentrations of gas and particulate phase nitrite and nitrate species and gas phase ammonia at Hawthorne. The particulate phase species given in Figure 3.1 are repeated here to allow comparison with the gas phase species.

3.4.1 Comparisons of Gas Phase Species and Particulate Phase Mass and Components

Two distinct, persistent inversions occurred during the study. The first inversion began on January 14th and continued through January 24th. The second inversion period occurred from January 29th to February 6th (indicated in Figures 3.1-3.3). Both inversions were

broken by a low-pressure air mass followed by snowfall. On January 24th, the frontal passage brought 7 cm of snow along with approximately 0.5 cm of water. A sharp temperature increase (~4 °C) was observed on February 6th. Both episodes were broken by an increase in wind speed (from ~5 to above 11 km/h) and change of wind direction from north during the inversion to south at the end. Several other inversions lasting between 2 and 3 days were observed during the study, but none were as intense and persistent as the two mentioned above. Elevated concentrations of $PM_{2.5}$, nitrate, sulfate (see Figure 3.1), CO, NO_x and SO_2 (see Figure 3.2) were observed during the two major inversion events relative to non-inversion periods. The concentrations of other species were less effected during the inversion (see Figures 3.1-3.3).

The composition of $PM_{2.5}$ for (a) the major inversion periods and (b) the remainder of the study are shown in Figure 3.4. A high concentration of NH_3 prevailed during the sampling campaign (Figure 3.3) and therefore it was assumed that nitrate and sulfate were predominately in the form of their ammonium salts. Other inorganic species (e.g. chloride, fluoride, phosphate, etc.) were measured by IC, but these concentrations were usually below the detection limits and none of these species contributed significantly to the fine particulate mass. Figure 3.4 illustrates that the dominant fine particulate component was ammonium nitrate, averaging 69% of the fine particulate mass during the inversion periods and 40% during the remainder of the study. The next largest contributor to fine particulate matter was the missing mass, averaging 21% during the inversion periods and 39% for the remainder of the study. All fine particulate components have been accounted for (ammonium ion is inferred) except crustal and carbonaceous material. Water is excluded by the FDMS TEOM, which specifically excludes particle bound water from the measurement.[37, 40-41] The fraction of crustal material in fine particulate matter during the study was small, from 0.1 to 0.5 $\mu g/m^3$. This was based on 24-h average measurements of Al

and Si in fine particles from the NCore program. Therefore the missing mass is predominately EC and OM. Furthermore, the calculated missing mass is consistent with the average of 22% EC and OM obtained from four 24-h quartz filter NCore samples. Since the ratio of EC and OM in the carbonaceous material is unknown, no discussion is included on the diurnal variation in these species.

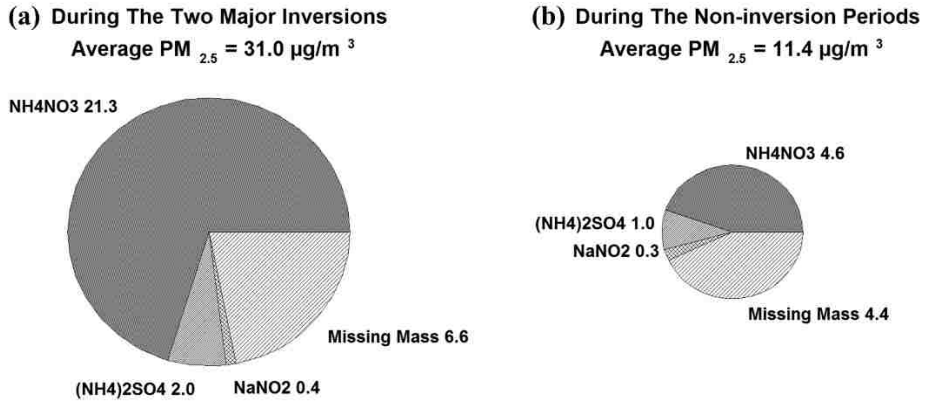

Figure 3.4 Average concentrations,g/m^3, of fine particulate species at Hawthorne (a) during the two major inversions and (b) during the remainder of the 2009 winter study.

Figure 3.5 shows total $PM_{2.5}$ (non-volatile plus semi-volatile mass) plotted against particulate nitrate and sulfate (both expressed as their ammonium salts) and CO (as a measure of primary emissions). Linear regression analyses for the data shown in Figure 3.5 are presented in Table 3.1. This analysis indicates that both ammonium nitrate and, to a lesser degree, ammonium sulfate account for much of the increase in fine particulate matter during the inversions. This is further supported by the lack of association between increasing concentrations of CO and fine particulate mass (see Figure 3.5). While CO, a primary pollutant, is higher during the inversion (see Figure 3.2), increases in CO are not correlated with increases in secondary pollutants.

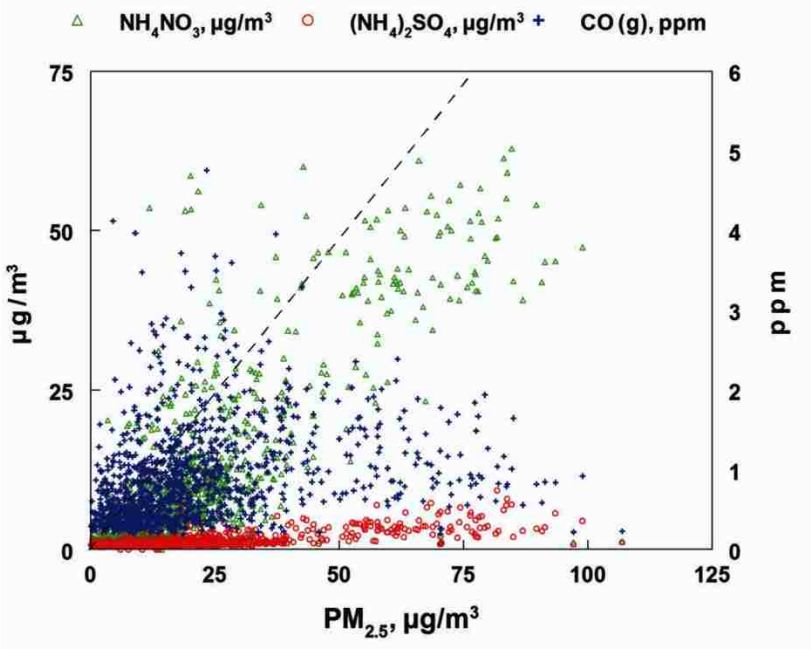

Figure 3.5 Comparison of $PM_{2.5}$ vs fine particulate ammonium nitrate, ammonium sulfate, and gas phase CO during the Hawthorne 2009 winter study. The dashed line is the 1:1 line for $PM_{2.5}$ mass. Linear regression results for the data are given in Table 1. The fine particulate species are correlated with $PM_{2.5}$ mass, but CO is not.

Table 3.1. Conventional Linear Regression Analysis Comparison of $PM_{2.5}$ Mass (g/m^3), or NO_x (ppb), and Other Measured Species.

	N	R^2	Slope	Intercept
x = $PM_{2.5}$ ($\mu g/m^3$)				
NH_4NO_3 ($\mu g/m^3$)	1035	0.777	0.627 ± 0.010	-1.0 ± 6.3
$(NH_4)_2SO_4$ ($\mu g/m^3$)	1035	0.495	0.043 ± 0.001	0.5 ± 0.8
$CO_{(g)}$ (ppm)	1273	0.131	0.011 ± 0.001	0.6 ± 0.5
x = NO_X (ppb)				
$CO_{(g)}$ (ppm)	1286	0.933	0.00902 ± 0.00007	0.16 ± 0.15
x = NO_2 (ppb)				
NH_4NO_3 + HNO_3 (ppb)	114	0.685	0.33 ± 0.02	-4.1 ± 3.5

The mass fraction of ammonium nitrate in $PM_{2.5}$ differed between the inversion periods and the less polluted days (Figure 3.4). PM during the major inversions averaged 66% ammonium nitrate whereas on days outside the major inversion periods, ammonium nitrate averaged 40% of the $PM_{2.5}$ mass. Interestingly, the mass fraction of ammonium sulfate slightly decreased during the two major inversion periods when compared to the non-inversion days. The average mass percent ammonium sulfate of total $PM_{2.5}$, 6.5%, was only one tenth the mass

percent of ammonium nitrate. Even though most of the sulfur oxides were in the particulate phase, the primary source appears not to be associated with a major PM source. Total sulfur oxides (ammonium sulfate plus SO_2 on a mole basis) were also not correlated with CO, a marker for primary emission sources (predominantly mobile sources). Factors which may contribute to the formation of nitrate and sulfate are discussed later.

Figure 3.6 shows the diurnal variations for many of the measured species for January 7 through 23 (a period preceding and during the first major inversion). First, $PM_{2.5}$ mass had a strong diurnal pattern during the January 14 - 24 inversion period, with daily maxima occurring in the noon to late evening time periods [Figure 3.6(a)]. In contrast, the primary emission species CO and NO_x have a different pattern [Figure 3.6(b)]. A strong linear relationship between these two species is illustrated in Figure 3.7A and Table 3.1. Furthermore, Figure 3.6 illustrates that CO and NO_x both peak in daily concentrations during morning commute hours and evening hours when home combustion of wood smoke is significant for this study area.[53] Morning NO_x and CO peaks decreased during weekends and holidays (e.g., January 19, Martin Luther King Day) and evening peaks showed slight decreases during weekends [Figure 3.6(b)]. CO and NO_X are frequently present in highest concentrations when $PM_{2.5}$ is at a minimum (Figure 3.6). These diurnal trends suggest that $PM_{2.5}$ is strongly influenced by secondary fine particle formation. This conclusion is also consistent with the data shown in Figures 3.4 and 3.5.

Figure 3.6 shows that particulate nitrite had a very strong diurnal variation with highest concentrations during the night and lower concentrations during the day [Figure 3.6(a)]. This pattern can be attributed to the nighttime formation of nitrite from primary NO_X emissions and absence of solar radiation initiated oxidative chemistry.[54] Finally, ozone also showed a marked diurnal pattern with mid-day maxima, and was highly correlated with solar radiation [Figure

3.6(c)]. However, another gas which is primarily secondary, NO_2, was not correlated with solar radiation. This chemistry is further explored in the next section.

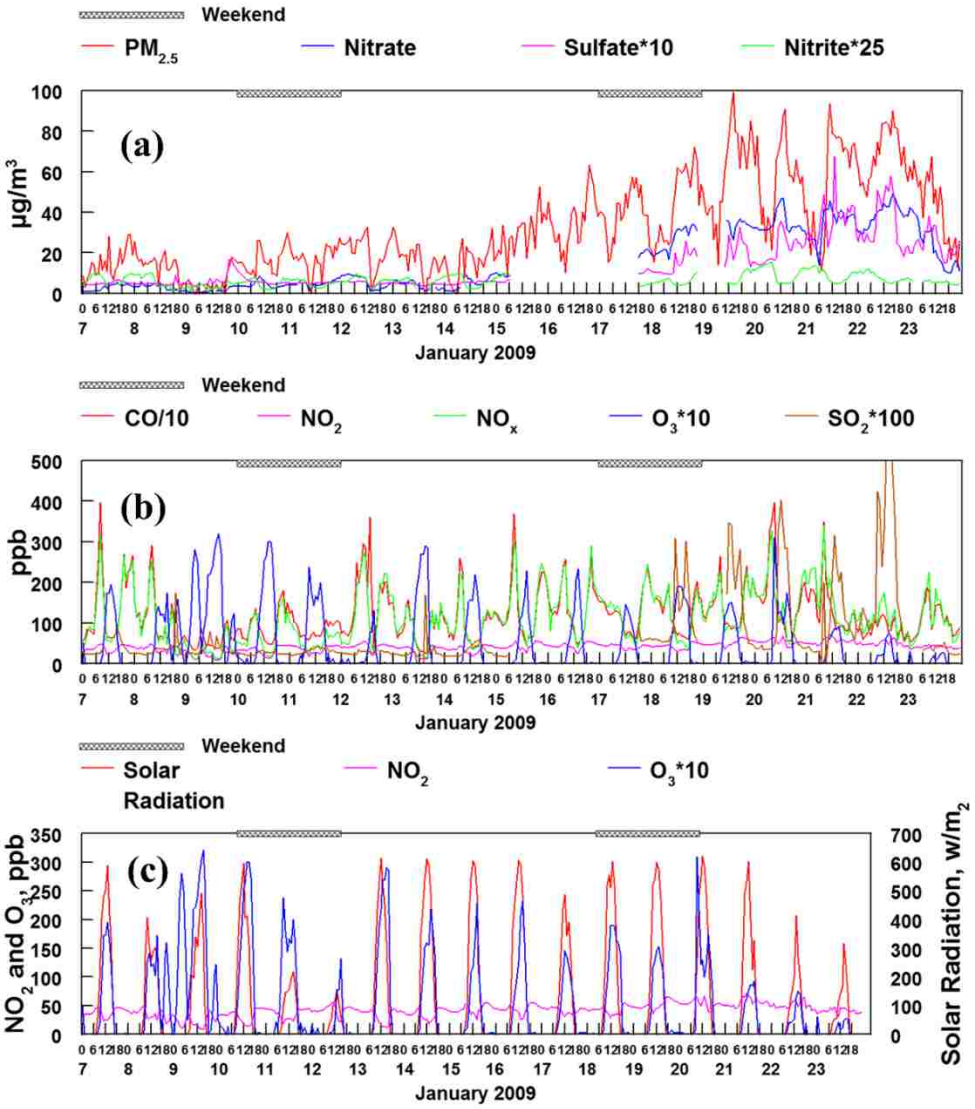

Figure 3.6 Hourly averaged time sequence of measured species just before and during the January 16-23 inversion. (a) Fine particulate mass and measured components. (b) Measured gas phase species. (c) Comparison of the secondary species NO_2 and O_3 with solar radiation. O_3 formation is correlated with solar radiation, but NO_2 formation is not.

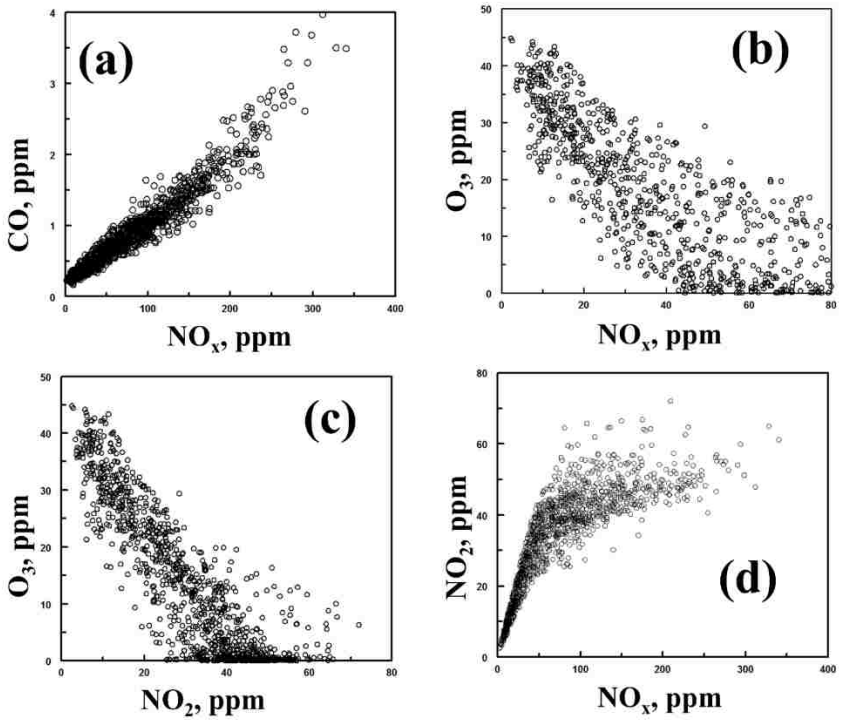

Figure 3.7 Comparison of several pollution species. (a) Hourly averaged concentrations of NO_x and CO during the Hawthorne study (see Table 3.1 for linear regression comparison of this data). (b) Hourly averaged concentrations of NO_x and O_3 during the Hawthorne study (the negative correlation between these two species suggests the formation of ozone is limited by the concentrations of VOCs during the study). (c) Hourly averaged concentrations of NO_2 and O_3 during the Hawthorne study (the negative correlation between these two species suggests the formation of ozone is limited by the concentrations of VOCs during the study). (d) Hourly averaged concentrations of NO_x and NO_2 during the Hawthorne study (the tailing off of NO_2 concentrations at high NO_x concentrations suggests the atmosphere is oxidant limited during the study).

3.4.2 Nitrogen Oxide Chemistry

The majority of primary nitrogen oxides are emitted from combustion sources in the form of NO(g).[54] In the presence of ozone, $HO_2\cdot$ or $RO_2\cdot$, NO is oxidized to NO_2 via the following:

$$NO(g) + O_3(g) \rightarrow NO_2(g) + O_2(g) \quad (3\text{-}2)$$

$$NO(g) + HO_2\cdot(g) \rightarrow NO_2(g) + OH\cdot(g) \quad (3\text{-}3)$$

$$NO(g) + RO_2\cdot(g) \rightarrow NO_2(g) + RO\cdot(g) \quad (3\text{-}4)$$

Ozone is formed by the photolysis of NO_2; $OH\cdot$ is formed by the photolysis of O_3 followed by the reaction of O^1D with H_2O; and $HO_2\cdot$ and $RO_2\cdot$ are formed from the reaction(s) of $OH\cdot$ (and at night $NO_3\cdot$) radical(s) with gas phase volatile organic compounds (VOCs). Thus,

the relative concentrations of NO_X and VOCs control the concentration of ozone in a complex manner described by an ozone isopleth. [54] In general, at low NO_X concentrations the concentrations of ozone is not significantly influenced by the concentration of VOCs and the system is NO_X limited. However, at low VOC concentrations, O_3 concentrations can decrease with increasing NO_X, as NO reacts with O_3, and NO_2 competes with VOC for the OH· radical by the irreversible formation of nitric acid:

$$NO_{2(g)} + OH\cdot_{(g)} \rightarrow HNO_{3(g)} \qquad (3\text{-}5)$$

Nitric acid may also be formed at night through the NO_3· radical. However, since O_3 and NO_2 do not co-exist at night [Figure 3.6(c)], this pathway will not be important. An analysis of the NO_x and O_3 data was carried out using the method described by Clapp and Jenkin [55] Figure 8 shows the oxidant concentration, $[NO_2] + [O_3]$ (defined at OX), plotted against the NO_x mixing ratio ($NO_x = NO + NO_2$) for daylight hours.

The intercept of the best fit line through the data represents the regional contribution to the oxidant concentration. The difference between the intercept and the measured OX concentration represents the local contribution to the oxidant concentration. The regional contribution to the oxidant concentration is calculated to be 43 ppb. Comparison of the best fit line through the data to the analysis of Clapp and Jenkin [55] of airmass in the UK show a large amount of scatter in this data. The relatively large amount of scatter in Figure 3.8 may be due to scavenging of NO_2 by OH radical to produce HNO_3 instead of O_3. As shown in Figures 3.1 and 3.5, production of ammonium nitrate was particularly significant during inversions.

It is worthwhile to note the assumption that all nitrogen oxides are of local origin and that ozone production above the background is due to local chemistry and not advection of either

nitrogen oxides or ozone from transported sources. This is true due to the stable nature of the inversions studied that result in little ventilation between layers.

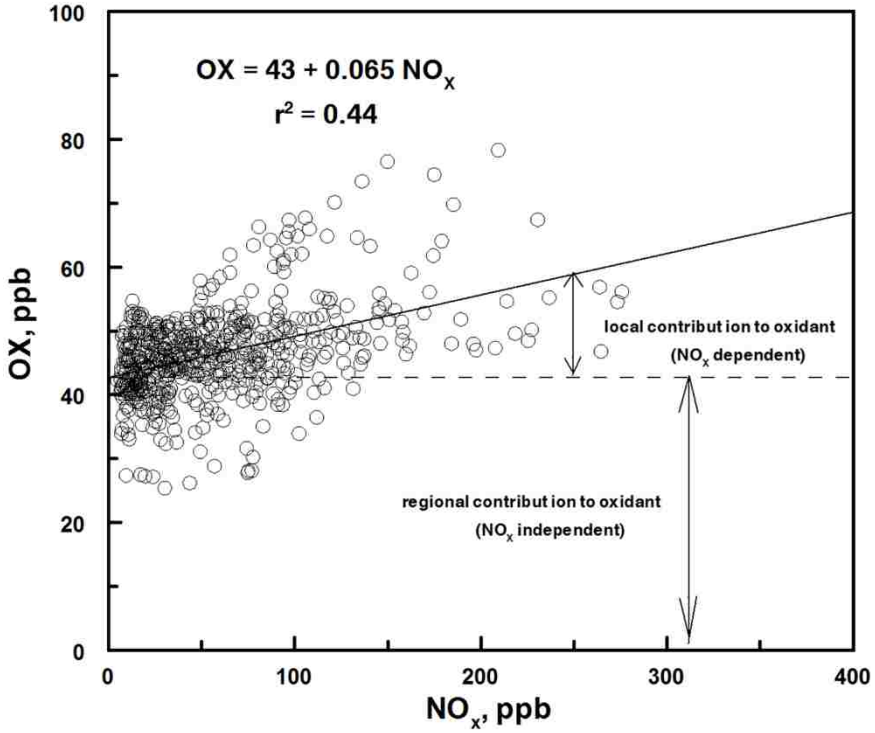

Figure 3.8 Variation of O_x mixing ratios ($O_x = NO_2 + O_3$) as a function of NO_x ($NOx = NO + NO_2$) during daylight hours.

During the study, hourly ozone concentrations peaked at 45 ppb (well within EPA regulations, as expected for a winter study). The highest ozone concentrations did not occur during the two major inversions, but peaked between inversions. The diurnal variation of ozone was generally characterized by a sharp increase in ozone concentration beginning at 7:00 a.m., peaking at 2:00 p.m., followed by a sharp decline below the limit of detection of the instrument in the next four to five hours, with a very strong correlation, as expected, between O_3 and solar radiation [Figure 3.6(c)]. The relationships of NO_X to O_3 and NO_2 to O_3 are shown in Figures 3.7(b) and 3.7(c), respectively. The inverse relationships shown in Figure 3.7(b & c) suggests ozone scavenging by NO and competition of the NO_2 molecule for the OH radical, thus limiting

the formation of ozone. The sharp downward trend in the O_3/NO_X and O_3/NO_2 relationships indicates an oxidant limited air mass with VOC concentrations low, relative to NO_x.[54] This conclusion is further strengthened by Figure 3.7(d), showing NO_2 plotted against NO_x. Upwards of 90% of NO_x is NO_2 at concentrations below 40 ppb. The linearity of the data deteriorates at concentrations of NO_x above 40 ppb. At 100 ppb of NO_X and higher, the relative NO_2 concentrations seldom exceeded 40-60 ppb, indicative of the lack of oxidant species necessary to convert NO to NO_2. This deficiency can also be explained by low VOC concentrations. Although VOC's were not measured directly, it can be assumed that they were relatively low due to the decrease of the ozone concentration with the increase of NO_X, signifying the lack of $RO_2\cdot$ radicals and the use of ozone to convert NO to NO_2. Obtaining VOC data to supplement the data given here would be valuable.

Another contributing factor to low ozone concentrations with higher NO_X and NO_2 concentrations is the reaction of NO_2 with $OH\cdot$ to produce nitric acid, which can then be converted to particulate nitrate and reduce the effectiveness of the peroxy radicals in the formation of ozone. The coexistence of nitrate formation and reduced ozone formation with high solar radiation is seen during the January 16-23 cold pool, as shown in Figure 3.9. The peak concentrations of ozone during the inversion occurred when nitrate concentrations were lower than 30 $\mu g/m^3$. When nitrate concentrations ranged from 20 to 50 $\mu g/m^3$, and when solar radiation peaked at greater than 400 W/m^2, ozone averaged only 50% of the ozone concentrations seen before and after the cold pool. The effect of nitrate formation on the reduction in ozone formation is apparent. A relationship can also be seen between the concentrations of $NO_{2(g)}$ and total nitrate as shown in Figure 3.10. Concentrations of the two species are correlated, particularly for the 9:00 a.m. to 5:00 p.m. time periods (noted as midday

data points in Figure 3.9) during inversions when the formation of the OH· radical occurs. The linear regression results for the concentration of NO_2 and total nitrate (HNO_3 and PM ammonium nitrate) during inversions for the 9:00 a.m. to 5:00 p.m. time periods are given in Table 3.1. During these time periods, total nitrate is equal to about 1/3 the NO_2.

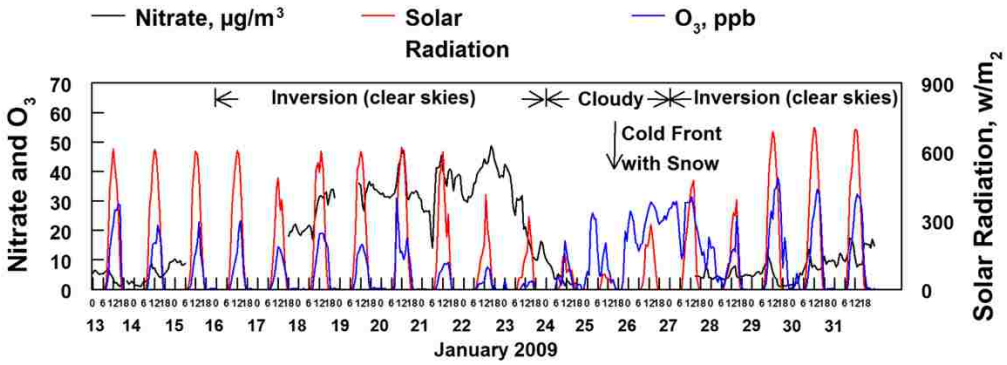

Figure 3.9 Correlation of the hourly averaged concentrations of nitrate and O_3 with solar radiation during the two major inversion time periods. Ozone concentrations are closely linked to solar radiation during the inversions but nitrate concentrations are not.

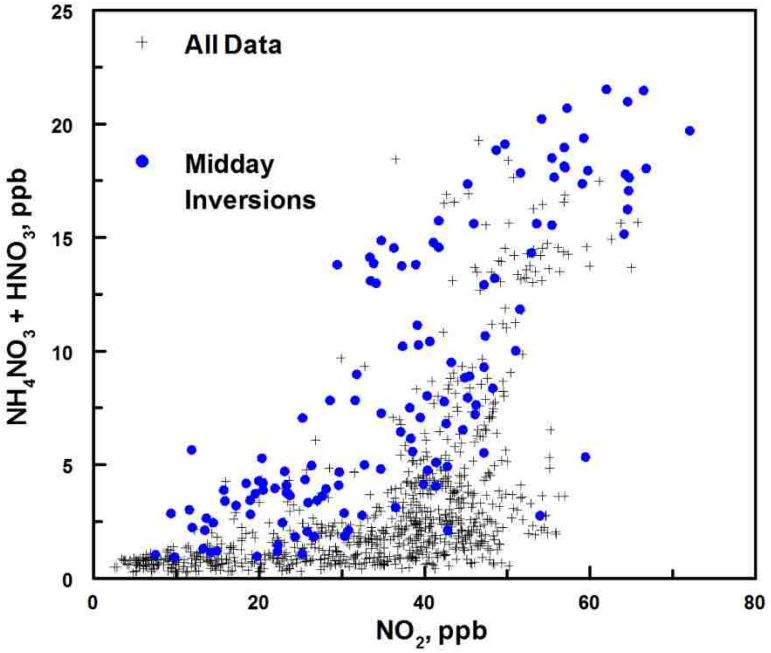

Figure 3.10 Correlation of hourly averaged concentrations of NO_2 and the sum of NH_4NO_3 plus HNO_3. The time periods of maximum solar radiation (high OH· radical formation) from 9:00 a.m. to 5:00 p.m. during the two inversion episodes are indicated as filled (blue) circles. Linear regression analysis for the circle data points is given in Table 3.1.

Figure 3.11 shows the fractions of total nitrogen oxides, NO_Y, present as either $HNO_3(g)$ or fine particulate nitrate and as either $HONO_{(g)}$ or fine particulate nitrite. The highest fractions of NO_Y present as a nitrate species are found during the two strongest inversion periods when the concentrations of fine particulate nitrate are also highest. During the inversion periods, as much as 25% of the NO_Y can be present as $HNO_{3(g)}$ or fine particulate nitrate (see Figures 3.11 and 3.12). During both of the inversion periods (and usually outside these inversion periods) there is a dominant diurnal pattern in the fraction of NO_Y present as a nitrate species, with a midday maximum (see Figure 3.12). There is also a strong temporal relationship between the maxima in the $nitrate_{(Total)}/NO_Y$ and solar radiation values (see Figure 3.12), although the maximum value in these two quantities is not strongly related. This reflects the dominant role of the OH· radical on nitric acid formation (see Equation 4), and the expected complex relationships among NO_2, VOC, RH, solar radiation and other factors and the formation of OH·. In contrast, the diurnal pattern in the fraction of NO_Y present as a nitrite species shows little variation over the study, with a nighttime maximum generally less than 5% of the total NO_Y. The nighttime maximum reflects the decay of $HONO_{(g)}$ during the day due to solar radiation. Nitrite is observed to peak during daytime hours, between February 15 to 20. This is inconsistent with the observed diurnal pattern for nitrite and the photochemically labile nature of HONO. The meteorology over this timeframe was not unusual and, consequently, cannot explain this unusual data pattern. The origin of this unique pattern is unknown.

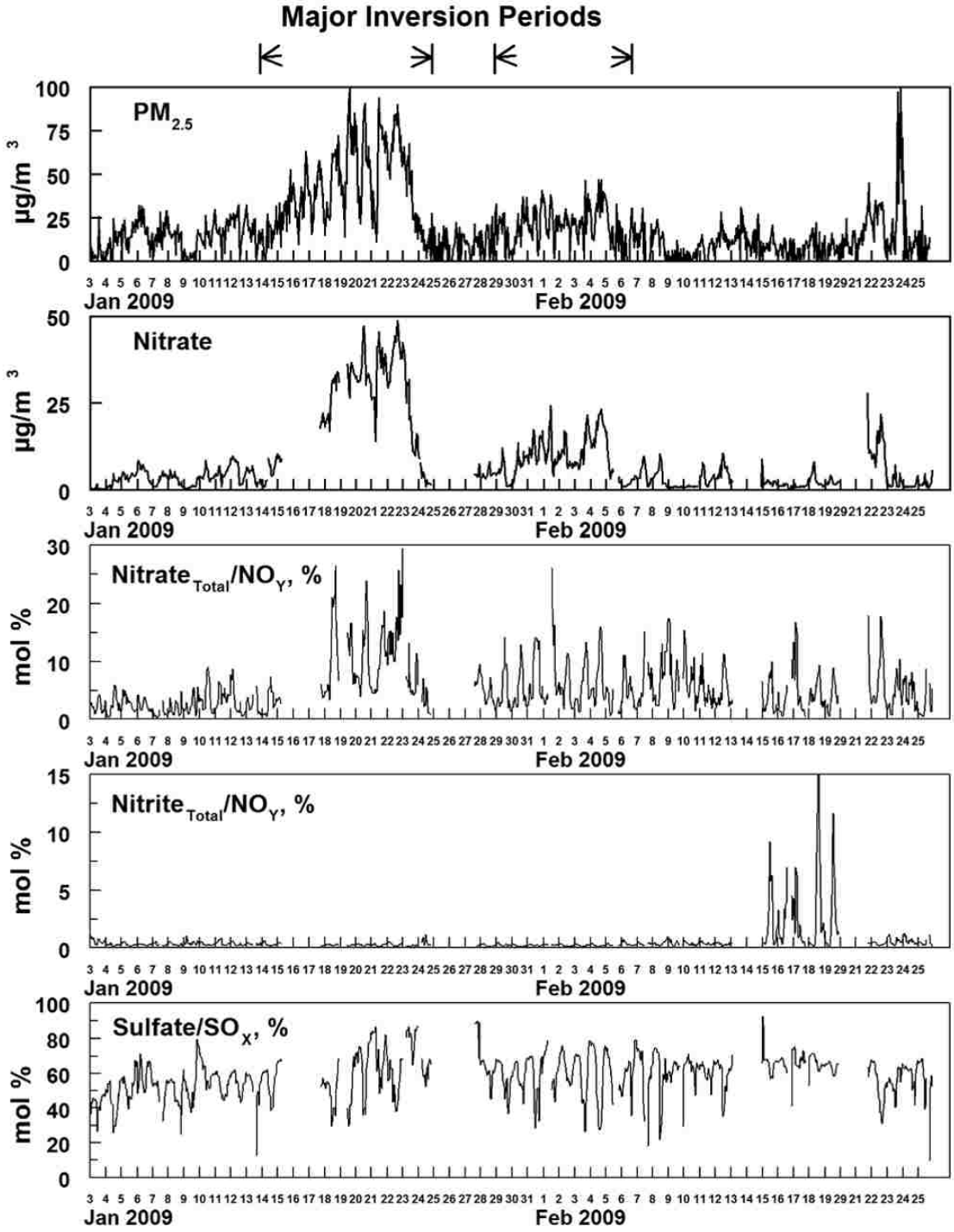

Figure 3.11 Time sequence of hourly averaged $PM_{2.5}$, fine particulate nitrate and the ratio of total nitrate and nitrite to NO_Y and sulfate to SO_X. The time period of the two major inversions during the study is indicated. Nitrate formation is enhanced during the inversions but the formation of nitrite and sulfate is not.

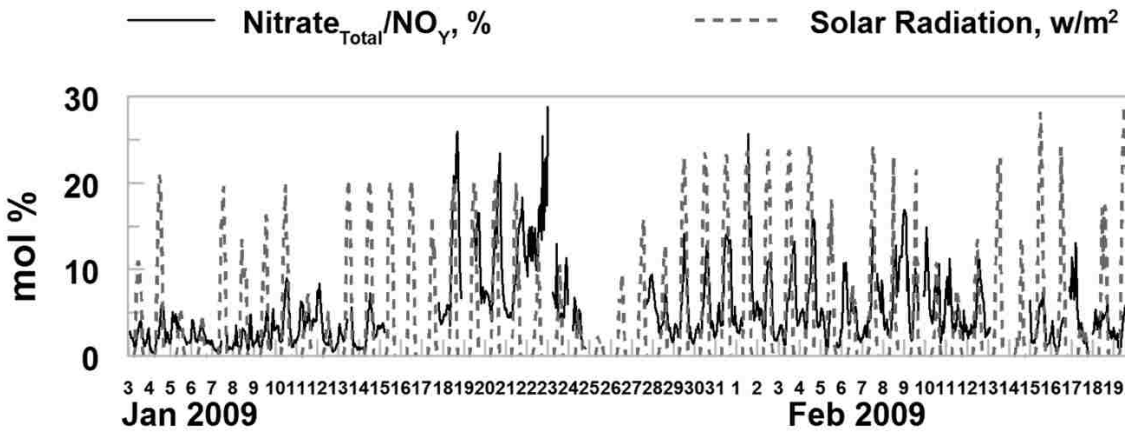

Figure 3.12 Correlation of NO_Y. While the formation of fine particulate ammonium nitrate is enhanced during high solar radiation, the fraction of NOY present as nitrate is not correlated with solar radiation across the study.

The data also provide insight concerning equilibrium between ammonium nitrate and gas phase nitric acid and ammonia:

$$NH_4NO_{3(s,aq)} = HNO_{3(g)} + NH_{3(g)} \quad (3\text{-}6)$$

The equilibrium constant, K_S, for Equation 6 [56] and the effect of temperature and relative humidity on the equilibrium for ammonium nitrate have been described previously [28, 38]. At 0 °C (the average temperature during the study) and below the deliquescence point of pure NH_4NO_3 (62% RH), K_S is 13.1 ppb.[48] The actual equilibrium described by Equation 6 for fine particulate matter deviates from the predicted equilibrium for pure NH_4NO_3 because of the influence of water and the complex mixture of PM.[57] The most significant effect is usually the effect of RH. Above the deliquescence point of ammonium nitrate, the equilibrium is shifted towards the condensed phase. The dissociation constant then decreases with increasing RH, up to about an order of magnitude lower as 100% RH is approached.[54]

The theoretical K_S values are compared to calculated K_S values in Figure 3.13. Theoretical values were calculated by assuming pure ammonium nitrate has no effect due to the presence of water in the aerosol. The calculated K_{exp} value is based on the measured

concentrations of HNO_3(g) and NH_3(g) for the time period from January 10 through February 7.[57] This time is chosen because it includes the two major inversion events when the concentrations of particulate nitrate were high (Figure 3.1) and the gas phase species were also elevated (Figure 3.3). As expected, the ratio of K_{exp}/K_S was very dependent on the relative humidity. The ratio approached or equaled unity only when the RH was below the ammonium nitrate deliquescence point of 62%. As the RH increased, the ratio decreased and approached 0.1 when the RH was above 75%. These results are consistent with the expectations described above. More detailed analysis of this gas/particle partitioning would be possible if PM ammonium and PM water data were available.

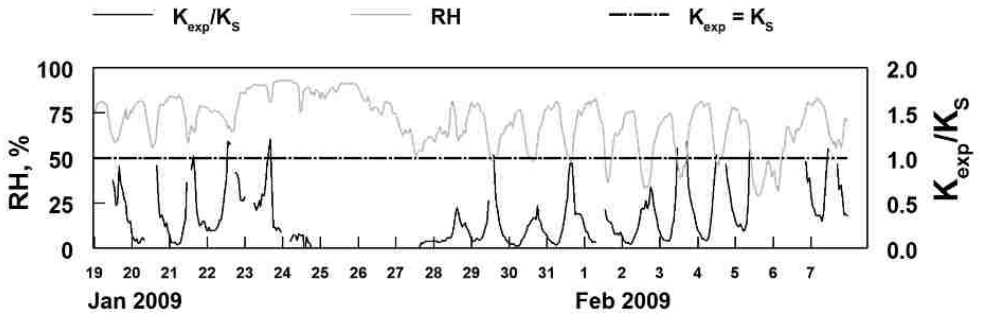

Figure 3.13 Comparison of hourly averaged RH and the ratio of the experimental product of $HNO_{3(g)}$ and $NH_{3(g)}$ (K_{exp}) and the equilibrium constant for the dissociation of pure ammonium nitrate at low humidity (KS).

3.4.3 Sulfur Oxide Chemistry

The chemistry involving sulfur oxides is not as complex as the nitrogen oxide chemistry. The sources are also expected to be simpler. Nitrogen oxides are emitted from mobile sources, home fuel burning, and major industrial sources. Industrial sources are the most significant emitters of sulfur dioxide, though small amounts of sulfur oxides are emitted from mobile sources. Industrial sources in the Salt Lake Valley include a copper smelter to the west and several small oil refineries to the north-northeast of the sampling site. The impact of the smelter

is likely low because sulfur dioxide is emitted from a 366 m stack, usually above inversion heights. Figure 3.14 suggests that the refineries may be important contributors to sulfur dioxide at the Hawthorne site, where it is shown that the highest concentrations of sulfur dioxide are associated with winds at the Hawthorne site from the north-northwest, and to a lesser extent from the west.

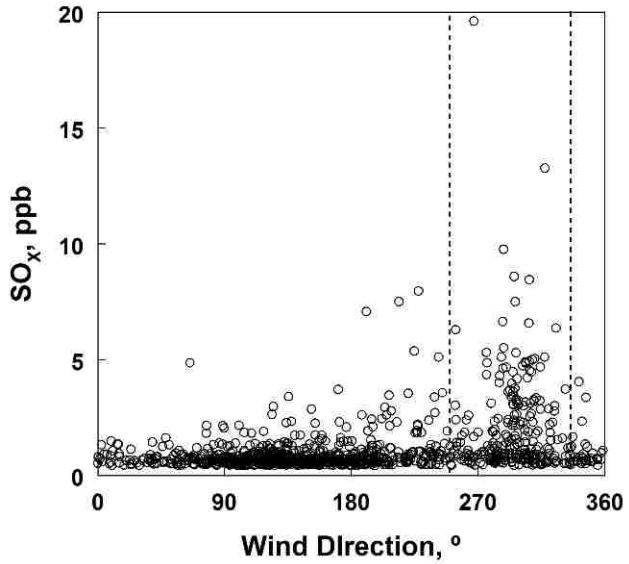

Figure 3.14 Relationship between wind direction and hourly averaged concentration of SO_x. The complex of oil refineries in the Salk Lake Valley are located about 20 km north-northwest of the site. The expected ranges of directions for direct flow from the refineries are included in the dashed lines given in the figure.

Conversion of SO_2 to sulfate can occur due to the OH· radical homogeneous oxidation, or via aqueous phase chemistry.[58] The current data give little information on which may be the dominant mechanism during this study. The ratio of sulfate to total sulfur oxides (sulfate plus SO_2) during the study is given in Figure 3.11. Typically, sulfate accounts for about 50 to 60 mol% of the total sulfur oxides with no clear effects due to time-of-day or presence of an inversion. While the fraction of total sulfur oxides present as particulate ammonium sulfate is high, the concentrations relative to total $PM_{2.5}$ mass are low, averaging only 7% of the $PM_{2.5}$ mass (Figures 3.1 and 3.4).

3.5 Conclusions

Ammonium nitrate averaged 40% of the total $PM_{2.5}$ in the absence of inversions and 69% during strong inversions in this Salt Lake Valley 2009 study. Ammonium nitrate formation was nitric acid limited, with a large excess of ammonia present. Sulfates and nitrites together constitute 7% during inversion and 11% outside of inversion periods of the total $PM_{2.5}$ and are not as significant as ammonium nitrate. Ozone levels throughout the study remained well below EPA limits. Overall, the lower boundary layer in the Salt Lake Valley was found to be oxidant and VOC deficient with respect to ozone formation. Because ozone levels during the study remained well within EPA standards, the most effective way of reducing contributions of ammonium nitrate to secondary particle formation during the inversion periods is to decrease NO_x emissions. However, a decrease in NO_x will increase ozone concentrations. A complete ozone isopleth would further inform this decision.

3.6 Chapter References

28. Cropper, P. M.; Hansen, J. C.; Eatough, D. J., Measurement of light scattering in an urban area with a nephelometer and PM2.5 FDMS TEOM monitor: Accounting for the effect of water. *Journal of the Air & Waste Management Association* **2013,** *63* (9), 1004-1011.
37. Grimm, H.; Eatough, D. J., Aerosol Measurement: The Use of Optical Light Scattering for the Determination of Particulate Size Distribution, and Particulate Mass, Including the Semi-Volatile Fraction. *Journal of the Air & Waste Management Association* **2009,** *59* (1).
38. Finlayson-Pitts, B. J.; Pitts, J. N. J., *Chemistry of the upper and lower atmosphere : theory, experiments, and applications.* Academic Press: San Diego, 2000.
40. Hansen, J. C.; Woolwine, W. R., III; Bates, B. L.; Clark, J. M.; Kuprov, R. Y.; Mukherjee, P.; Murray, J. A.; Simmons, M. A.; Waite, M. F.; Eatough, N. L.; Eatough, D. J.; Long, R.; Grover, B. D., Semicontinuous PM2.5 and PM10 Mass and Composition Measurements in Lindon, Utah, during Winter 2007. *Journal of the Air & Waste Management Association* **2010,** *60* (3).
41. Grover, B. D.; Kleinman, M.; Eatough, N. L.; Eatough, D. J.; Hopke, P. K.; Long, R. W.; Wilson, W. E.; Meyer, M. B.; Ambs, J. L., Measurement of total PM(2.)5 mass (nonvolatile plus semivolatile) with the Filter Dynamic Measurement System tapered element oscillating microbalance monitor. *Journal of Geophysical Research-Atmospheres* **2005,** *110* (D7).
45. Long, R. W.; Modey, W. K.; Smith, P. S.; Smith, R.; Merrill, C.; Pratt, J.; Stubbs, A.; Eatough, N. L.; Eatough, D. J.; Malm, W. C.; Wilson, W. E., One- and three-hour PM2.5

characterization, speciation, and source apportionment using continuous and integrated samplers. *Aerosol Science and Technology* **2005,** *39* (3), 238-248.
46. Kuprov, R. Y.; Eatough, D. A.; Cruickshank, T.; Olson, N.; Cropper, P. M.; Hansen, J. C., Composition and Secondary Formation of Fine Particulare Matter in the Salt Lake Vally: Winter 2009. *Journal of the Air & Waste Management Association* **2014,** *64* (8), 957-969.
47. EPA NCore. http://www.epa.gov/ttnamti1/ncore/ (accessed August 18).
48. Long, R. W.; Eatough, N. L.; Mangelson, N. F.; Thompson, W.; Fiet, K.; Smith, S.; Smith, R.; Eatough, D. J.; Pope, C. A.; Wilson, W. E., The measurement of PM2.5, including semi-volatile components, in the EMPACT program: results from the Salt Lake City Study. *Atmospheric Environment* **2003,** *37* (31), 4407-4417.
49. Pope, C. A.; Hansen, M. L.; Long, R. W.; Nielsen, K. R.; Eatough, N. L.; Wilson, W. E.; Eatough, D. J., Ambient particulate air pollution, heart rate variability, and blood markers of inflammation in a panel of elderly subjects. *Environmental Health Perspectives* **2004,** *112* (3), 339-345.
50. Grover, B. D.; Eatough, N. L.; Woolwine, W. R.; Cannon, J. P.; Eatough, D. J.; Long, R. W., Semi-continuous mass closure of the major components of fine particulate matter in Riverside, CA. *Atmospheric Environment* **2008,** *42* (2), 250-260.
51. EPA, Quality Assurance Handbook for Air Pollution Measurement Systems Volume II. 2008. http://www.epa.gov/ttnamti1/files/ambient/pm25/qa/QA-Handbook-Vol-II.pdf.
52. Whiteman, C. D.; Bian, X. D.; Zhong, S. Y., Wintertime evolution of the temperature inversion in the Colorado Plateau basin. *Journal of Applied Meteorology* **1999,** *38* (8), 1103-1117.
53. Long, R. W.; Eatough, N. L.; Eatough, D. J.; Meyer, M. B.; Wilson, W. E., Continuous determination of fine particulate matter mass in the Salt Lake City Environmental Monitoring Project: A comparison of real-time and conventional TEOM monitor results. *Journal of the Air & Waste Management Association* **2005,** *55* (12), 1839-1846.
54. Finlayson-Pitts, B. J., *Chemistry of the upper and lower atmosphere : theory, experiments, and applications.* Academic Press: San Diego, 2000; p 969.
55. Clapp, L. J.; Jenkin, M. E., Analysis of the relationship between ambient levels Of O-3, NO2 and NO as a function of NO chi in the UK. *Atmospheric Environment* **2001,** *35* (36), 6391-6405.
56. Pio, C. A.; Harrison, R. M., The Equilibrium of Ammonium-Chloride Aerosol with Gaseous Hydrochloric-Acid and Ammonia under Tropospheric Conditions. *Atmospheric Environment* **1987,** *21* (5), 1243-1246.
57. Mozurkewich, M., The Dissociation-Constant of Ammonium-Nitrate and Its Dependence on Temperature, Relative-Humidity and Particle-Size. *Atmospheric Environment Part a-General Topics* **1993,** *27* (2), 261-270.
58. Eatough, D. J.; Caka, F. M.; Farber, R. J., The Conversion of So2 to Sulfate in the Atmosphere. *Israel Journal of Chemistry* **1994,** *34* (3-4), 301-314.

4 DEVELOPMENT OF THE GC-MS ORGANIC AEROSOL MONITOR (GC-MS OAM) FOR IN-FIELD DETECTION OF PARTICULATE ORGANIC COMPOUNDS

Chapter 4 of this dissertation has been submitted for publication to the Journal of Aerosol Science and Technology. The contribution of the author was the development and testing of the GC-MS OAM, and preparation of the manuscript.

4.1 Introduction

Tropospheric fine particulate matter (PM) poses serious health risks and has a significant impact on global climate change.[11, 59-60] The organic fraction of PM (i.e., organic aerosol) ranges from 10-90% of the PM total mass.[61-63] Monitoring the organic aerosol composition is a significant challenge due to the hundreds of compounds present, and their broad range of chemical properties. Routinely monitoring these organic compounds provides invaluable information to better characterize pollution sources, and further understanding of secondary organic aerosol formation.[64] However, routine measurement of particle phase organics is difficult.

Traditionally, filter collection and impaction techniques have been used for identification and quantification of organic aerosol species. These methods usually involve liquid extraction followed by GC-MS analysis. Using these methods, hundreds of important organic compounds have been identified and have been used as organic markers to link pollution to specific emission sources. However, analysis of samples collected by filtration or impaction require laboratory analysis and bench top equipment; therefore, the cost is high and time resolution can be poor.

Rapid methods to analyze samples collected by filtration or impaction without liquid extraction have been developed.[21, 65] However, these methods do not capture important diurnal variations in ambient organic compound (OC) concentrations, and time-relevant correlations between OCs and other pollutants cannot be made. Therefore, a need exists to develop in-field techniques to continuously monitor individual PM OC species.

Field monitoring of ambient particles has been significantly enhanced with the development and commercialization of particle beam mass spectrometry methods such as the Aerodyne aerosol mass spectrometer (AMS) and the TSI aerosol time-of-flight mass spectrometer. Instruments such as these provide important time-resolved, and size-resolved chemical composition data including total carbon and inorganic species. However, these instruments are not designed to identify or quantify organic compounds due to the harsh ionization techniques used and large sample matrix effects. These instruments are also limited in use because of their size and limited portability.

An instrument capable of continuously monitoring particulate phase OC has been reported by Williams et al.[66] This instrument uses inertial impact of particles for collection, followed by thermal desorption into a GC-MS system for separation and detection. The instrument was deployed in the field during two month-long periods, where multiple species of primary and secondary organic aerosols were identified.[67] Results from Williams et al. further illustrate the importance of information that can be obtained by continuously monitoring organic marker compounds, and the overarching need to further develop in-field techniques for monitoring these compounds.

Lin et al. described a similar instrument for semi-continuous determination of organic marker compounds.[68] While the instrument previously described was related in concept to the

instrument described herein, the application for collection and analysis of particles was not published.

This paper demonstrates the use of a new automated in-field detection system for measurement of organic compounds in $PM_{2.5}$ using filtration, followed by thermal desorption into a compact GC-MS system. Automated sampling and the use of a compact GC-MS system make it possible to easily deploy the instrument in the field for long-term monitoring.

4.2 Experimental

4.2.1 Instrument Description

An overall schematic of the OAM is shown in Figure 4.1. Details of each component are included below.

Sample Collection. A sample is collected by drawing air with a flow of 4-8 L/min through a $PM_{2.5}$ sharp cutoff cyclone inlet (Sunset Laboratory). A 0.375 in. (o.d.) 6 ft long stainless steel tube connects the cyclone inlet (located outside) to the instrument (located indoors). $PM_{2.5}$ samples are collected on a 0.385 in. diameter chemically deactivated quartz filter, which is housed in the collection/thermal desorption chamber shown in Figures 1 and 2. The flow across the filter is obtained using a Gast DOA-P707-AA vacuum pump. In order to prevent surface catalyzed pyrolysis, the quartz filter is deactivated using a solution of 10% hexamethyl disilazane in toluene.[69] This filter is submersed in the silazane solution for 30 min, and then rinsed with toluene and dried at room temperature.

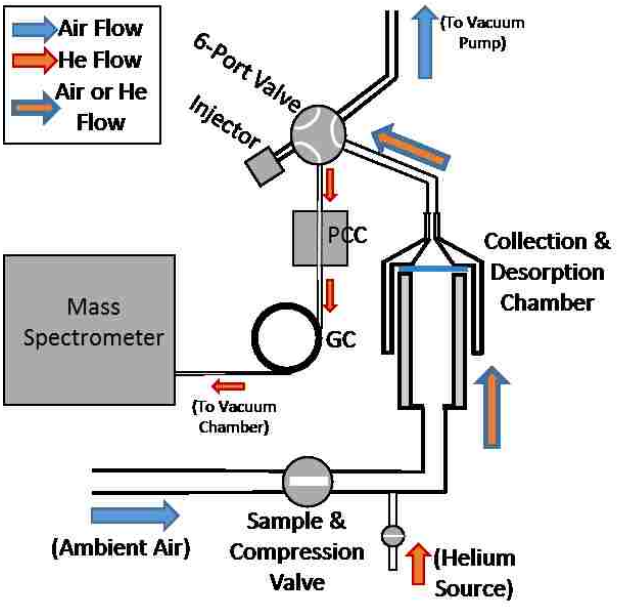

Figure 4.1 Schematic of the GC-MS Organic Aerosol Monitor

Thermal Desorption Chamber. The thermal desorption chamber is made of stainless steel, and has a compression seal inside the chamber to seal the quartz filter. Air flows through the filter and chamber followed by a 6-port valve shown in Figure 4.1. After a sample is collected the entire collection chamber is purged with helium at a flow of 100 mL/min for 3 minutes. After purging, the 6-port valve rotates and opens the desorption chamber to the GC column. The chamber is pressurized to 20 psi to achieve a flow of approximately 10 mL/min through the chamber and GC column. The chamber is heated at a rate of ~150 °C/min and the temperature is held at 150-300 °C (depending on the compounds of interest) for 10 minutes using PID (proportional-integral-derivative) controlled resistive heating. The chamber is heated using a 22 gauge nichrome heating coil that is wrapped around the outside of the chamber. The analyte is transferred through both the valve and stainless steel transfer lines into a cooled pre-column concentrating (PCC) region of the transfer line. The chamber and all transfer lines were deactivated to reduce degradation using Inertium (AMCX). The 6-port valve was deactivated with Sulfinert (Restek).

After the sample is transferred, the filter and desorption chamber undergo a cleaning cycle. The aim of the cleaning cycle is to drive off refractory organic material left on the filter. The chamber and filter are heated to 300 °C for 5 min, with helium flowing at 60 mL/min through the side arm. Even after the cleaning cycle, some residual species are present, such as non-volatile organic carbon, black carbon and other inorganic species. These species build up on the filter over time, necessitating changing of the filter due to reactions between refractory material remaining on the filter after the cleaning cycle and target compounds. The frequency of a filter change is dictated by the air sample collected; but for air masses representative of urban areas is usually required every 7-14 days. The current method assumes that volatile organics pass through the filter and are not adsorbed, and that the organics collected are in the particle phase.

Pre-Concentrator and Gas Chromatograph. As thermal desorption of the sample takes place, organic compounds are concentrated onto a pre-column concentrator (PCC). Analysis occurs when the PCC is flash heated and the sample is transferred into the GC column. The PCC is made by inserting a 35 mm length of the column capillary into a nickel tube (0.02 inch i.d.). The nickel tube is tightly wrapped with heating wire (32 gauge Constantan wire, insulated with a double glass layer), and the entire assembly is placed on a thermoelectric cooling device (Hi-Z, model HZ-2). During desorption of the sample from the collection filter, the PCC is kept at 10 ºC. The chamber is swept at 10 mL/min for 12 minutes during desorption. Increased desorption time resulted in no significant increase in MS signal. The chamber has a volume of 10 mL, resulting in complete flushing of the volume 12 times during the desorption period. The PCC is then flash heated, reaching 250 °C within 2 s.

The compact gas chromatograph is composed of a 5 m long Rxi-5Sil fused silica column, with an inner diameter of 0.25 mm, and a film thickness 0.25 μm. The column is wrapped inside an aluminum tube with a diameter of 43 mm and a wall thickness of 1 mm. The outside of the aluminum is wrapped with resistive heating wire. The GC column is temperature programed to start at 35 °C and ramp at 2 °C/s up to 300 °C and hold at 300 °C for one min. From the time that the GC program begins, the PCC delays heating for a set amount of time (delay time), and is then flash heated. A delay time of 100 s was used for this study, which correlates to the time at which the column temperature is 195 °C. Total GC-MS analysis occurs in less than 5 min, and total analysis, including desorption, occurs in 20 min. Further details concerning the PCC and compact GC performance are described elsewhere.[70]

Toroidal Ion Trap Mass Spectrometer. The mass spectrometer is a modified Guardian 7, manufactured by Torion Technologies. This portable-miniaturized system uses a toriodal ion trap.[71-72] Modifications to the Guardian 7 include a larger turbo pump (Pfeiffer TMH 1601 P) to accommodate the helium flow during thermal desorption, and a larger column inner diameter. Other modifications include the GC described previously, and software changes performed by Torion Technologies to allow autonomous sampling.

4.2.2 Chemicals and System Testing

Standards used to test system performance included levoglucosan, dehydroabietic acid, stearic acid, and a standard mixture of polycyclic aromatic hydrocarbons (EPA 525 PAH mix-B in acetone), each purchased from Sigma-Aldrich and used without further purification. Levoglucosan, dehydroabietic acid, and stearic acid standards were prepared in acetone with 150 and 30 ppm of each compound.

All standard mixtures were loaded directly onto the collection filter using 0.1-5.0 μL injections, followed by helium purge, thermal desorption and GC-MS analysis as described above. In this way, standard mixtures were used to calibrate the instrument for organic compounds of interest. Desorption temperature was optimized for the chemicals used in this study by varying the temperature from 180 °C to 250 °C while keeping the amount of standard constant between runs. The optimal temperature for compounds such as levoglucosan and DHA was close to 180 °C. However 230 °C was used in this study in order to extend the range of compounds desorbed from the filter, while minimizing thermal degradation. This was consistent with previous work done by Lin et al.[15] The desorption time was optimized by varying the time between 5-17 min while holding the temperature constant at 230 °C. A desorption time of 12 min was used for this study as no increase in signal was apparent after this time.

An atmospheric chamber was used in this study to provide repeatable wood smoke pollution samples for system testing. The chamber is a 45 m^3 Teflon bag. The bag is constructed with Teflon film that is heat sealed with a Vertrod sealing blade iron, and adhesive polysilicone tape is used on the seams for added mechanical support. The bag is elliptical in shape and collapsible for air removal. The chamber is equipped with UV lamps and sampling ports to sample air directly from the bag. A fan is placed in the bag to gently stir the contents. For more information about the atmospheric chamber and the pollution source, refer to Kuprov et al.[73] Particles from the combustion of aged pine wood were blown into the bag from a wood burning stove. Smoke samples were collected at 5.0 L/min for approximately 2 min, with a total particulate concentration of about 100 $\mu g/m^3$ in the atmospheric chamber. As particles in the bag were lost by deposition to the walls and the concentration decreased, the collection time was adjusted so that the same mass was collected on the filter each time. In the case where standard

addition was performed, the sample was collected followed by directly loading the standard on the filter for standard addition. No cyclone cut-off was used in conjunction with the atmospheric chamber.

4.2.3 In-Field Testing

The instrument was field tested on the campus of Brigham Young University (Provo, UT) during January-March 2015. It was housed in a trailer, which was positioned on a ridge where no tall buildings or trees were near enough to cause irregular air mixing. Several additional instruments were run simultaneously including the following: FDMS TEOM (R&P model 8500); Aethelometer (Magee Scientific); Ambient Ion Monitor (URG, model 9000D); gas monitors including NO_x, and O_3 (Teledyne, models 200E and 300E); Optical Particle Sizer (TSI, model 3330); OC-EC Analyzer (Sunset Laboratory Inc.); and an integrating nephelometer (NGN-2, Optec).

During this study, the filter was changed every 7-14 days. The need to change the filter was tested at least once a week by loading the filter with standards while it was deployed in the field, and testing for degradation loss. When degradation of the loaded standard was apparent by a >50% decrease in signal, the filter was replaced.

4.3 Results and Discussion

4.3.1 Laboratory Performance

The primary objective of this project was to develop an instrument that can autonomously monitor airborne particulate organic compounds on an hourly basis. Thermal desorption is a viable option for autonomously transferring analyte into a detector; however, the filter must be

inert towards organic compounds. Quartz fiber and stainless steel frits were tested for inertness inside the collection and desorption chamber made of quartz, gold coated aluminum, and Inertium coated stainless steel. Inertium coated stainless steel provided the most inactive surface for the collection and desorption chamber. Quartz fiber filters coated with hexamethyldisilazane provided the most inert filter surface while allowing for thermal cycling, and surface catalyzed degradation was dramatically reduced. Figure 4.2 illustrates the results of desorbing several atmospherically relevant organic compounds from a chemically deactivated quartz filter into the GC-MS.[68] Compounds 2, 3 and 4 are isomers of levoglucosan, products of the combustion of cellulose and often used as markers for wood smoke emissions. The eight compound is stearic acid, which is a marker for cooking. The ninth peak includes dehydroabietic acid (DHA), a component of wood resin and is also a marker for wood smoke. The remaining compounds are polycyclic aromatic hydrocarbons (PAHs). The two acids and levoglucosan isomers were particularly selected because they are historically difficult to analyze.[66, 74] Also, these compounds readily react with most surfaces at high temperatures; therefore, their use as standards serves to characterize the quality of deactivation of the sampling environment.

Without deactivation of the quartz fiber filter, almost complete degradation of thes acids and levoglucosan isomers occurs due to the reactive surface of the quartz. Figure 4.2 shows some degradation, with peaks indicative of stearic acid degradation appearing at 1.95 min (see peak set 6). Other compounds, such as PAHs appear to desorb from the filter without pyrolysis regardless of the quartz surface being deactivated. It is also important to note that the three isomers of levoglucosan were successfully separated without derivatization. This is due to the use of the PCC as described by Cropper et al.; however, this is the first demonstration of the separation of these isomers without derivatization using this method.[70]

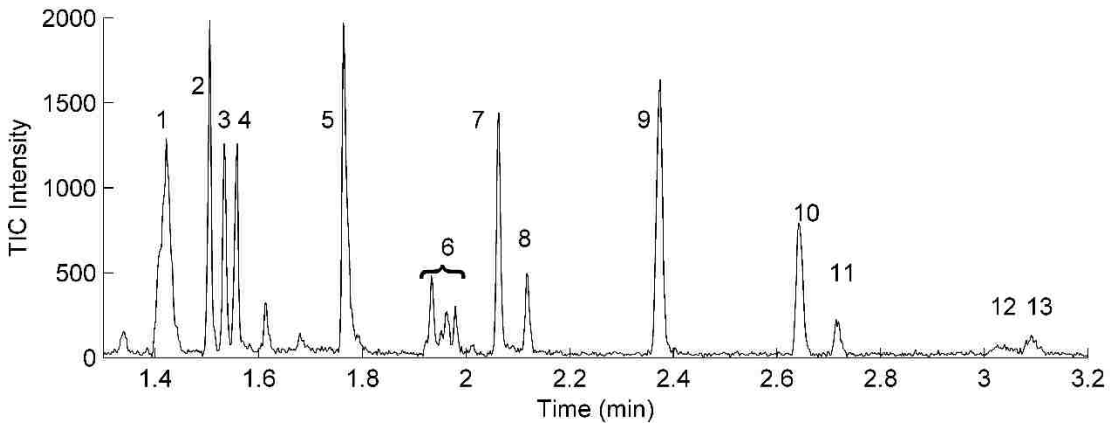

Figure 4.2 Total ion chromatogram (TIC) of several organic markers desorbed off a deactivated quartz filter. The compounds are (1) fluorene, (2) galactosan, (3) manosan, (4) levoglucosan, (5) anthracene and phenanthrene, (6) degradation products attributed to steric acid, (7) pyrene, (8) stearic acid, and (9) dehydroabietic acid, chrysene and benzo(a)anthracene, (10) benzo(b)fluoranthene and benzo(k)fluoranthene, (11) benzo(a)pyrene, (12) indeno(1,2,3-cd)pyrene and dibenzo(a,h)anthracene, (13) benzo(ghi)perylene. An amount of 2.5 ng of each PAH (compounds 1,5,7,9,10,11,12,13) was loaded on the filter, and 60 ng of each of the remaining species, 2,3,4,8, and 9(dehydroabietic acid fraction).

The limits of detection (LOD), limits of quantitation (LOQ) and linear ranges for a variety of compounds are listed in Table 4.1. LOD is reported as three times the standard deviation in the baseline with no sample. LOQ is reported as 10 times the standard deviation in the baseline. The reconstructed ion chromatogram (RIC) for the ion with the highest intensity (base peak) was chosen to determine the detection limit using peak height. Isomers that co-elute are listed together.

Calibration curves for levoglucosan are shown in Figures 4.3 and 4.4. Calibration curves were generated using the reconstructed ion chromatrogram (RIC) of the ion with the greatest intensity. Levoglucosan amounts were calculated using m/z 60. The response curve is fit to a polynomial, and becomes linear at concentrations above 60 ng (see Figure 4.3). Figure 4.4 shows that though the lower concentrations are not linear, they are reproducible and, thus, are quantitative. Figure 4.5 shows the calibration curve for pyrene (m/*z* 202), and the response is linear from 1 to 12 ng. The non-linearity of levoglucosan may be due to a combination of the

nonlinear response of the ion trap at lower concentrations for levoglucosan, loss of levoglucosan while purging with helium, or active sites on the filter leading to thermal degradation, since levoglucosan is more reactive than pyrene.

Table 4.1 Limits of Detection for Several Compounds Commonly Found in Organic Aersol.

	m/z	LOD (ng)[1]	LOQ (ng)	Linear Range (ng)
Anthracene\Phenanthrene	178	0.08	0.12	0.2-16
Benzo(ghi)perylene	276	2.5	7.5	2.5-50
Benzo[a]anthracene\ Chrysene	228	0.2	0.64	0.2-15
Benzo[a]pyrene	252	0.3	1.1	0.5-16
Benzo[b]fluoranthene/ Benzo[k]fluoranthene	252	0.3	0.96	0.5-15
Dehydroabietic acid	240	1.3	4.6	10-150
Dibenzo(a,h)anthracene/ Indeno(1,2,3-cd)pyrene	276	2.5	7.5	2.5-50
Fluorene	166	0.02	0.079	0.2-15
Galactosan	60	3.1	10.3	60-450
Levoglucosan	60	3.1	10.3	60-450
Mannosan	60	3.1	10.3	60-450
Pyrene	202	0.06	0.2	0.5-15
Stearic Acid	130	3	10	10-80

[1] *LOD and LOQ were calculated using 3 and 10 times (respectively) the standard deviation in the baseline of the reconstructed ion chromatogram.*

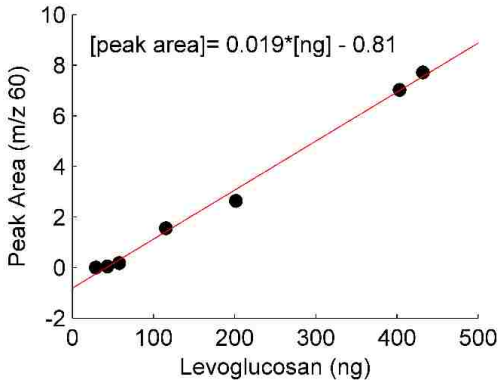

Figure 4.3 Calibration curve for levoglucosan illustrating linear range. The red line is the best linear fit. The equation displayed represents the best linear fit, where y is the peak area and x is the amount of levoglucosan in ng.

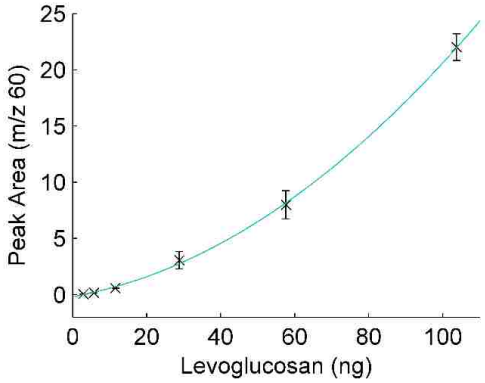

*Figure 4.4 Calibration curve for levoglucosan illustrating the lower detection limits. The blue line is the quadratic fit to the data (y = 0.0020*x2 + 0.033*x – 0.00039 where y is the peak area and x is ng of levoglucosan). Error bars represent +/- one standard deviation of 3 trials at each amount. For these runs, the detector voltage was set to -1850 V, and the filament current was set to 0.65 Amp.*

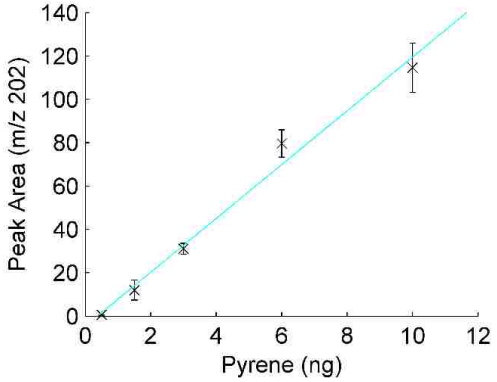

*Figure 4.5 Calibration curve for pyrene. The blue line is the linear fit to the data (y = 12*x - 4.6, where y is the peak area and x is ng of pyrene). Error bars represent +/- one standard deviation of 3 trials at each amount. For these runs, the detector voltage was set to -1850 V, and the filament current was set to 0.65 Amp.*

In order to test how well the combination of the thermal desorption, GC and MS systems overcome matrix effects in a real sample, particulate matter was created by burning wood (pine) in a wood burning stove and pulling a fraction of the smoke into an atmospheric chamber. In order to test for chemical change in the sample, consecutive samples were taken and the signal from several species were compared to each other. To compensate for the slow loss of particles on the walls of the atmospheric chamber, the collection time was adjusted so that approximately the same mass of sample was collected on the filter. Particle mass concentration in the bag was measured using a DataRam4 (Thermo Scientific). Table 4.2 shows the deviation of the signal for various species in the sample. The standard deviation of the peak heights was approximately 10% of the average signal for each of the peaks described. Therefore, it was assumed that the chemical composition remained constant for consecutive samples.

Table 4.2 Chemical Change of 7 Consecutive Smoke Samples.

Species[1]	Retention Time	Mean Peak Height	% RSD
Levoglucosan (m/z 60)	1.92	360	10
Compound 1 (m/z 205)	2.41	2494	13
Compound 2 (m/z 205)	2.36	2310	11
Compound 3 (m/z 155)	1.86	1205	6
Compound 4 (m/z 155)	3.09	623	11

[1]*Identities of compounds 1-4 are unknown*

Standard addition of DHA was performed on a smoke sample in order to compare the response curves between standard addition with a large sample matrix and calibration with standards. Figure 4.6 shows the total-ion-chromatogram of one of these smoke samples (no standard is added to this sample). Figure 4.7 shows the response curves for both a calibration and a standard addition experiment using the smoke sample contained in the pollution chamber.

The slopes of the calibration and standard addition response curves (Figure 4.7) can be considered the same at a 95% confidence level. The amount of DHA collected on the filter was 113 ng, according to the calibration curve. The similarity in the slopes shows that for the sample studied here, the sample matrix does not significantly alter the response of the GC-MS OAM to DHA.

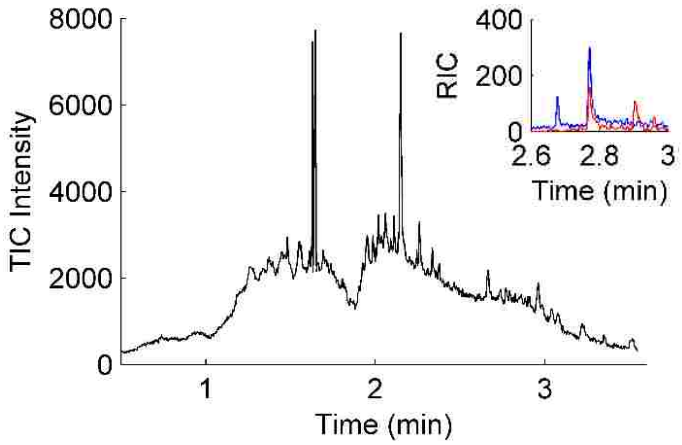

Figure 4.6 Total-ion-chromatogram (TIC) for a wood smoke sample collected from an atmospheric chamber. The inset plot shows the reconstructed ion chromatogram (RIC) for ions m/z 239 (blue) and 285 (red), two significant fragments of DHA. Identification of DHA at 2.79 min is confirmed by these fragments and the retention time.

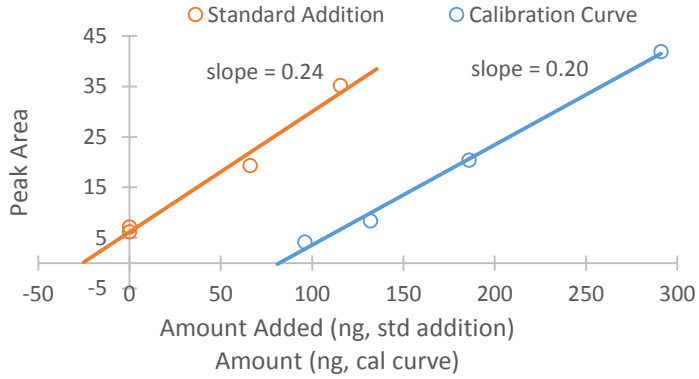

Figure 4.7 Calibration curve and standard addition of dehydroabietic acid (DHA) for 4 consecutive wood smoke samples. The detector voltage was set to -1900 V, and the filament current was set to 0.70 Amp. The total mass collected on the filter for each sample in the standard addition curve was 1.1 µg. Applying the calibration curve to the smoke sample predicts that 113 ng DHA was present on the filter, corresponding to a total concentration of 11µg/m^3 in the pollution chamber.

As seen in Figure 4.7, the calibration response curve does not pass through the origin over the range of concentrations measured. Therefore, the method of standard addition cannot be applied to determine the amount of DHA in the smoke sample using the x-intercept as is usually done. However comparison of the slopes of the two curves over the linear range (80-300 ng) indicates that the instrument successfully overcomes matrix effects for the sample studied herein.

Similar results were obtained for levoglucosan (Figure 4.8), where the slopes for the standard addition and calibration curves were 0.047 ng^{-1} and 0.052 ng^{-1}, respectively. These two slopes can be considered the same at the 85% confidence level.

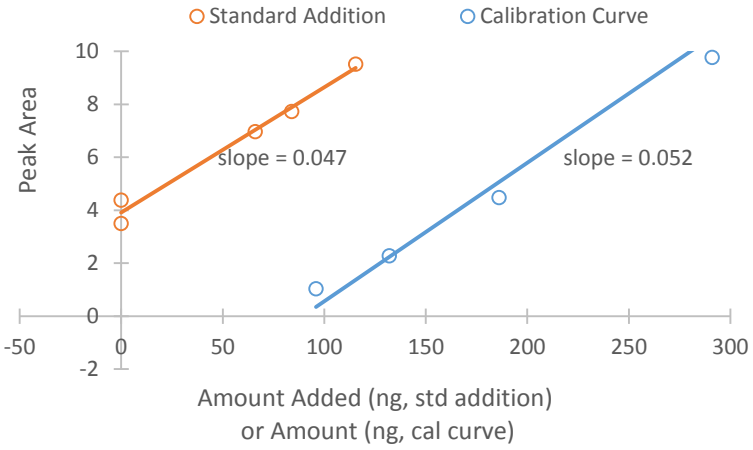

Figure 4.8 Calibration curve and standard addition of levoglucosan. PM was sampled from the atmospheric chamber and analyzed as described in Figure 6. According to the calibration curve 156 ng levoglucosan was present on the filter, which corresponds to a total concentration of 14 +/- 2 µg/m^3 in the pollution chamber.

4.3.2 In-field performance

The GC-MS OAM was tested between January-March, 2015, in Provo UT on Brigham Young University campus. It was housed in an air sampling trailer on campus in an area impacted by anthropogenic emissions from the Utah Valley region. The total ion chromatogram of a single hour-long sample is shown in Figure 4.9. The peaks of several species that were detected are shown. These were identified using their retention times and m/z ratios listed in

Table 4.1. Figure 4.10 shows a 2-day series of chromatograms collected every 90 min that show evidence for levoglucosan. Levoglucosan is identified by the major mass-to-charge peak of m/*z* 60, and the retention time of 1.6 min. The identification of levoglucosan using the complete mass spectrum is also possible, but is not shown here for simplicity.

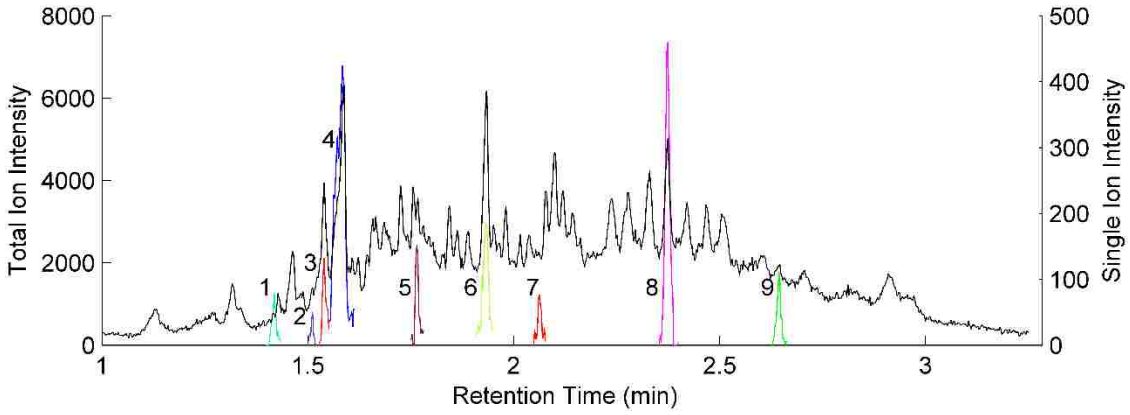

Figure 4.9 Total-ion-chromatogram (black trace) of a single air pollution sample collected on Jan 11, 2016 between 00:00-1:00 a.m. The colored peaks are various compounds identified in the sample: (1) fluorine, (2) galactosan, (3) mannosan, (4) levoglucosan, (5) phenanthrene, (6) stearic acid, (7) pyrene, (8) dehydroabietic acid, (9) benzo(b&k)fluoranthene. Compounds were identified by m/z spectra and retention times.

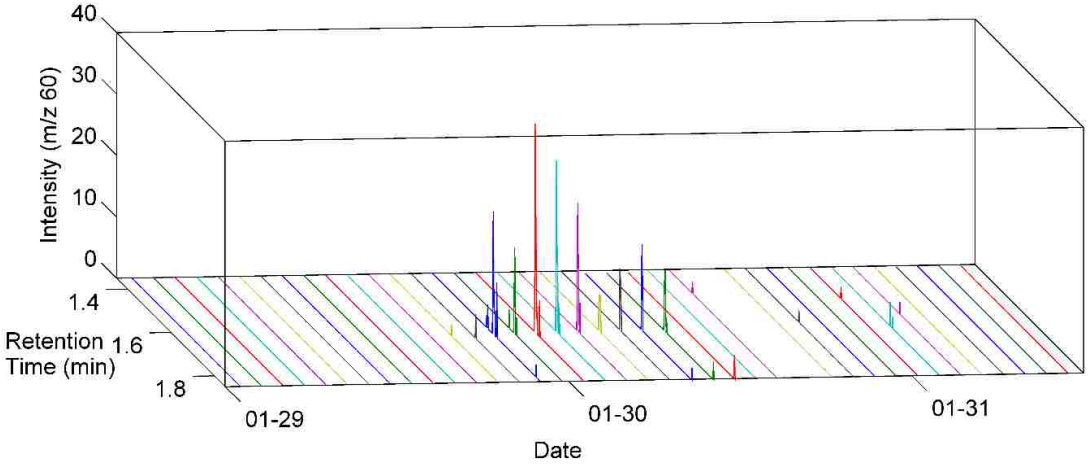

Figure 4.10 Hourly reconstructed ion chromatograms for m/z 60, corresponding to levoglucosan, with a retention time of 1.62 minutes. These samples were collected from Jan 29, 2015 to Jan 31, 2015.

Results from deploying the GC-MS OAM in the field for 14 consecutive days are shown in Figure 4.11. The diurnal variation in pyrene, levoglucosan, and the unknown compound with

m/*z* 203 is shown. Each of these species has a unique diurnal patterns. On the morning of Feb 5, 2015, pyrene and levoglucosan peaks coincide, levoglucosan being indicative of wood smoke. At other times, such as Jan 30, 2015, pyrene appears without levoglucosan, indicative of a difference source of pyrene such as gasoline or diesel combustion. Figure 4.12 shows concentrations of elemental carbon, NO_x and levoglucosan during this 14 day period. Evening elevated levels of elemental carbon and levoglucosan occur simultaneously (See evening peaks on 1-27, 1-30, 2-1, 2-2, 2-6, and 2-9). Evening peaks of elemental (black) carbon and total $PM_{2.5}$ in Utah Valley, UT, have long been attributed to wood smoke,[40, 45] but this was confirmed chemically for the first time by directly monitoring levoglucosan.

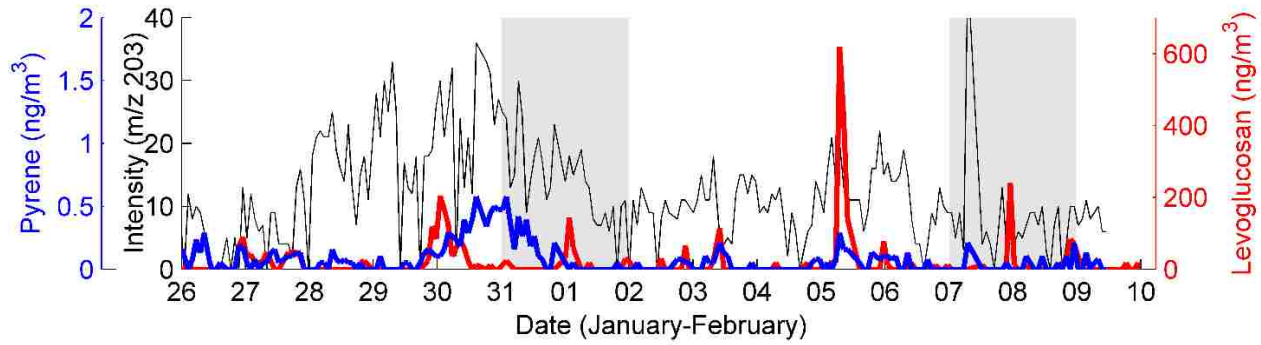

Figure 4.11 Variations in pyrene, levoglucosan, and m/z 203 from Jan 26, 2015 to Feb 10, 2015. . Shaded times indicate weekends.

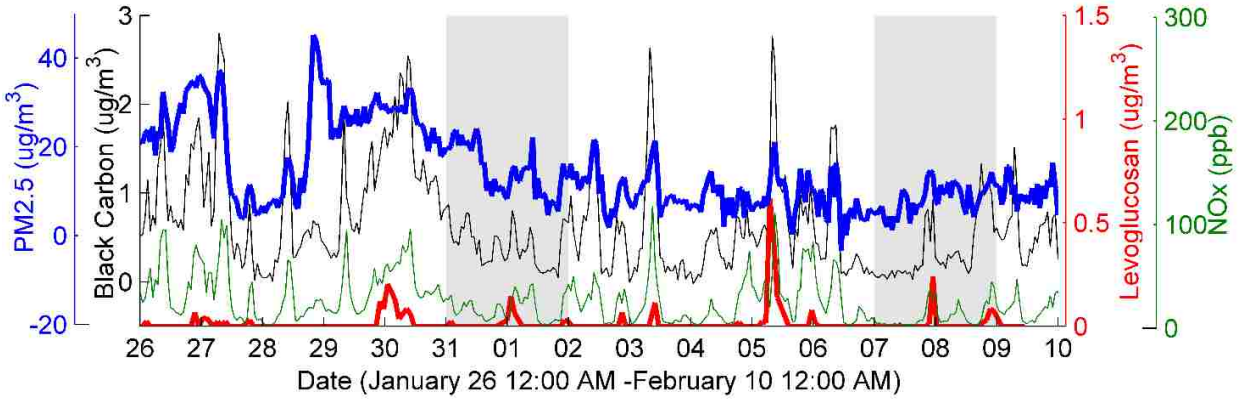

Figure 4.12 Plot of PM2.5 mass (blue), elemental (black) carbon (black), levoglucosan (red), and NOx (green) from Jan 26, 2015 to Feb 10, 2015. Shaded areas indicate weekends.

The simultaneous evening peaks in Figure 4.12 for levoglucosan and black carbon on Jan 30 and Feb 5 and 8 can be used to estimate the ratio of levoglucosan in wood smoke. The assumption is made that these peaks can be attributed to wood smoke. Previous source apportionment results in Utah Valley have indicated that wood smoke is 10% black carbon. This is consistent with peaks on Jan 30 and Feb 8, however the percentage is higher on Feb 5 (29%).[18] The composition of wood smoke during the current study was estimated using levoglucosan and $PM_{2.5}$ data. The ambient concentration was 0.028 ± 0.006 g levoglucosan/g wood smoke. This is comparable to compositions previously reported (0.036, Bari et al., 2009)[75] and is further indication of the validity of the data reported in Figures 4.11 and 4.12

A problem inherent to filter collection methods is the loss of volatile components from the sample. While the instrument has the advantage of virtually no loss of the sample post collection, because the sample is immediately analyzed, it is still subject to evaporative loss during collection. Eatough et al. has reported that 10-50% of a sample can be lost due to loss of volatile species.[76]

An important issue in field GC-MS methods is how instrument performance is related to relative humidity. Water can be detrimental to GC column performance. Field results using the GC-MS OAM show no apparent effect of relative humidly or decrease of column performance due to water. The authors suspect this is due to purging the sample with helium, when the large majority of the water in the sample is vented. Should water present a problem, inclusion of a Nafion drier is possible. Furthermore, as the current method assumes volatile gas phase organics pass through the filter and are not adsorbed, the inclusion of a carbon impregnated denuder may further ensure the sample is composed of particle phase species.

4.4 Conclusions

The GC-MS Organic Aerosol Monitor provides invaluable information concerning air pollution and its sources by obtaining speciated data for individual organic compounds with time resolution of 1 h. Laboratory results indicate that the OAM performs well at overcoming matrix effects for the samples collected in this study. Field results show that daily peaks in levoglucosan and elemental carbon are highly correlated and confirm the presence of evening wood smoke for the region studied herein. By running autonomously in the field, the OAM has the capability to monitor organic aerosol in depth and further characterize air pollution and its sources.

4.5 Chapter References

11. Smith, R. L.; Davis, J. M.; Sacks, J.; Speckman, P.; Styer, P., Regression models for air pollution and daily mortality: analysis of data from Birmingham, Alabama. *Environmetrics* **2000,** *11* (6), 719-743.

15. Lin, L.; Lee, M. L.; Eatough, D. J., Gas chromatographic analysis of organic marker compounds in fine particulate matter using solid-phase microextraction. *Journal of the Air & Waste Management Association* **2007,** *57* (1), 53-58.

21. Bruns, E. A.; Perraud, V.; Greaves, J.; Finlayson-Pitts, B. J., Atmospheric Solids Analysis Probe Mass Spectrometry: A New Approach for Airborne Particle Analysis. *Analytical Chemistry* **2010,** *82* (14), 5922-5927.

40. Hansen, J. C.; Woolwine, W. R., III; Bates, B. L.; Clark, J. M.; Kuprov, R. Y.; Mukherjee, P.; Murray, J. A.; Simmons, M. A.; Waite, M. F.; Eatough, N. L.; Eatough, D. J.; Long, R.; Grover, B. D., Semicontinuous PM2.5 and PM10 Mass and Composition Measurements in Lindon, Utah, during Winter 2007. *Journal of the Air & Waste Management Association* **2010,** *60* (3).

45. Long, R. W.; Modey, W. K.; Smith, P. S.; Smith, R.; Merrill, C.; Pratt, J.; Stubbs, A.; Eatough, N. L.; Eatough, D. J.; Malm, W. C.; Wilson, W. E., One- and three-hour PM2.5 characterization, speciation, and source apportionment using continuous and integrated samplers. *Aerosol Science and Technology* **2005,** *39* (3), 238-248.

59. Mannucci, P. M.; Harari, S.; Martinelli, I.; Franchini, M., Effects on health of air pollution: a narrative review. *Internal and Emergency Medicine* **2015,** *10* (6), 657-662.

60. Fiore, A. M.; Naik, V.; Spracklen, D. V.; Steiner, A.; Unger, N.; Prather, M.; Bergmann, D.; Cameron-Smith, P. J.; Cionni, I.; Collins, W. J.; Dalsoren, S.; Eyring, V.; Folberth, G. A.; Ginoux, P.; Horowitz, L. W.; Josse, B.; Lamarque, J. F.; MacKenzie, I. A.; Nagashima, T.; O'Connor, F. M.; Righi, M.; Rumbold, S. T.; Shindell, D. T.; Skeie, R. B.; Sudo, K.; Szopa, S.;

Takemura, T.; Zeng, G., Global air quality and climate. *Chemical Society Reviews* **2012,** *41* (19), 6663-6683.
61. Turpin, B. J.; Saxena, P.; Andrews, E., Measuring and simulating particulate organics in the atmosphere: problems and prospects. *Atmospheric Environment* **2000,** *34* (18), 2983-3013.
62. Lee, S. H.; Allen, H. C., Analytical Measurements of Atmospheric Urban Aerosol. *Analytical Chemistry* **2012,** *84* (3), 1196-1201.
63. Wilson, W. E.; Grover, B. D.; Long, R. W.; Eatough, N. L.; Eatough, D. J., The measurement of fine-particulate semivolatile material in urban aerosols. *Journal of the Air & Waste Management Association* **2006,** *56* (4), 384-397.
64. Williams, B. J.; Goldstein, A. H.; Kreisberg, N. M.; Hering, S. V., In situ measurements of gas/particle-phase transitions for atmospheric semivolatile organic compounds. *Proceedings of the National Academy of Sciences of the United States of America* **2010,** *107* (15), 6676-6681.
65. Falkovich, A. H.; Rudich, Y., Analysis of semivolatile organic compounds in atmospheric aerosols by direct sample introduction thermal desorption GC/MS. *Environmental Science & Technology* **2001,** *35* (11), 2326-2333.
66. Williams, B. J.; Goldstein, A. H.; Kreisberg, N. M.; Hering, S. V., An in-situ instrument for speciated organic composition of atmospheric aerosols: Thermal Desorption Aerosol GC/MS-FID (TAG). *Aerosol Science and Technology* **2006,** *40* (8), 627-638.
67. Williams, B. J.; Goldstein, A. H.; Kreisberg, N. M.; Hering, S. V.; Worsnop, D. R.; Ulbrich, I. M.; Docherty, K. S.; Jimenez, J. L., Major components of atmospheric organic aerosol in southern California as determined by hourly measurements of source marker compounds. *Atmospheric Chemistry and Physics* **2010,** *10* (23), 11577-11603.
68. Lin, L.; Lee, M. L.; Eatough, D. J., Review of Recent Advances in Detection of Organic Markers in Fine Particulate Matter and Their Use for Source Apportionment. *Journal of the Air & Waste Management Association* **2010,** *60* (1), 3-25.
69. Kong, R. C.; Woolley, C. L.; Fields, S. M.; Lee, M. L., Deactivation of Small-Diameter Fused-Silica Capillary Columns for Gas and Supercritical Fluid Chromatography. *Chromatographia* **1984,** *18* (7), 362-366.
70. Cropper, P. M.; Goates, S. R.; Hansen, J. C., A compact gas chromatograph and pre-column concentration system for enhanced in-field separation of levoglucosan and other polar organic compounds. *Journal of Chromatography A* **2015,** *1417*, 73-78.
71. Austin, D. E.; Wang, M.; Tolley, S. E.; Maas, J. D.; Hawkins, A. R.; Rockwood, A. L.; Tolley, H. D.; Lee, E. D.; Lee, M. L., Halo ion trap mass spectrometer. *Analytical Chemistry* **2007,** *79* (7), 2927-2932.
72. Lammert, S. A.; Rockwood, A. A.; Wang, M.; Lee, M. L.; Lee, E. D.; Tolley, S. E.; Oliphant, J. R.; Jones, J. L.; Waite, R. W., Miniature toroidal radio frequency ion trap mass analyzer. *Journal of the American Society for Mass Spectrometry* **2006,** *17* (7), 916-922.
73. Kuprov, R. Y.; Buck, D.; Pope, C. A.; Eatough, D. J.; Hansen, J. C., Design and Characterization of a Two-Stage Human Subject Exposure Chamber. *Journal of the Air & Waste Management Association* **2011,** *61* (8), 864-871.
74. Schkolnik, G.; Rudich, Y., Detection and quantification of levoglucosan in atmospheric aerosols: A review. *Analytical and Bioanalytical Chemistry* **2006,** *385* (1), 26-33.
75. Bari, M. A.; Baumbach, G.; Kuch, B.; Scheffknecht, G., Wood smoke as a source of particle-phase organic compounds in residential areas. *Atmospheric Environment* **2009,** *43* (31), 4722-4732.

76. Eatough, D. J.; Long, R. W.; Modey, W. K.; Eatough, N. L., Semi-volatile secondary organic aerosol in urban atmospheres: meeting a measurement challenge. *Atmospheric Environment* **2003,** *37* (9-10), 1277-1292.

5 COMPACT GAS CHROMATOGRAPH AND PRE-COLUMN CONCENTRATION SYSTEM FOR ENHANCED IN-FIELD SEPARATION OF LEVOGLUCOSAN AND OTHER POLAR ORGANIC COMPOUNDS

Chapter 5 of this dissertation was published in the Journal of Chromatography A.[70] The contribution of the author was the development and testing of the pre-column concentration unit and compact GC, and preparation of the manuscript.

5.1 Introduction

The quantitation of levoglucosan has received much attention because levoglucosan is produced from the combustion of cellulose and is, therefore, a marker for wood smoke in air pollution. The separation and detection of levoglucosan is usually performed by gas chromatography (GC). However, derivatization (typically silylation) is often required to achieve adequate separation, detection and quantification.[74] To readily measure levoglucosan in the field, methods for separation and detection without silylation are required. This study incorporates a compact GC unit and a pre-concentration unit with a mass spectrometer to enhance in-field separation and detection of organic markers commonly used to identify sources of pollution, including levoglucosan. Other organic markers that can be detected include polycyclic aromatic hydrocarbons (markers for gasoline, diesel, or other emissions), organic acids (e.g., dehydroabietic acid, a product of wood burning), and cholesterol (a marker for meat cooking).[26, 77]

Portability of the instrument is made possible in part by compact gas chromatography. Primary considerations in the design of a compact gas chromatograph include reduced overall size, reduced power consumption, and rapid temperature programming. Because compact systems usually heat faster than conventional systems, faster separations can be achieved.[78] There are two major categories of providing heat to gas chromatographic columns: direct heating and indirect heating. Indirect heating can further be divided into contact of the column with the heating/cooling element and air bath designs. In contrast, direct heating involves applying a current to an electrically conductive column material. While many different heating systems exist, only a few are discussed below.

Indirect heating has been accomplished in multiple ways. One of the earliest methods[79] was introduced by PerkinElmer in 1962. Their design was composed of a capillary column embedded into a flat metal disk that was placed on a similarly shaped heating disk. PerkinElmer reported that this model provided extremely accurate temperature control, though a compact design was not necessarily a goal and the thermal mass and power consumption was likely high. A cylindrical fixture was developed by Sides and Cates [80] by wrapping a GC column on the outside of a tubular heat conductor, and applying heat on the inside of the tube. The inside of the tube also incorporated a fan for cooling. Heating rates of up to 210 °C/min were achieved; however, power consumption was not reported. Another method described by Roundehler et al.[81] placed a cylindrically wound column in a small diameter stainless steel sheath, with a small air gap between the sheath and the column; the sheath was used as the heater. They obtained heating rates up to 100 °C/s, but minimizing power was not a goal of this method. Maswadeh et al.[82] also designed a cylindrical metal fixture with deep grooves on both the interior and exterior of the cylinder. They wound multiple layers of capillary into the interior groove,

placed the heater in the exterior groove, and covered both grooves with insulation. They reported good chromatographic performance, and the power consumption was under 20 W for a 1-m column.

In contrast to indirect heating, direct heating of the column typically provides the advantage of lower thermal mass due to the absence of an external fixture; therefore, less power is consumed by the system. These methods can also provide very fast GC separation; many commercially available fast GC systems utilize direct heating. The difficulties with these systems usually arise from electrical shorting of heaters that extend the length of the column. Accurately measuring the temperature of these systems has also been an issue. One commercially available system that appears to have overcome these issues is the Calidus GC (Falcon Analytical), which directly applies current to a steel column to resistively heat the column. Another commercially available system is the Hapsite ER (Inficon), which resistively heats a 15-meter, fused silica capillary. It has an operating temperature range of 45–200 °C and has been used for detection of volatile and semi-volatile organic compounds. However, the disadvantage of this system is that many environmentally relevant compounds, such as levoglucosan and large organic acids, do not elute until temperatures greater than 200 °C are reached.

Another significant contribution to the miniaturization of GC systems is the application of microchip technology.[83] For these systems, lithography is used to print the GC onto a chip.[83] Although such systems offer promise, they currently are subject to a number of serious limitations. The materials used are often not suitable for elevated temperatures (>200 °C). The columns must be short and have a large diameter, which may prevent obtaining the resolution necessary to separate real atmospheric samples.[84-85] Furthermore, the detectors that have been

used with microchip GCs are often tuned for specific compounds and lack sensitivity to compounds of interest in the atmosphere.[84] Finally, the footprint of the microchip-based unit (including electronics and platform) is not much different than other compact systems.

In addition to compacting the column/heater assembly, many systems utilize pre-concentration and injection focusing to concentrate analyte prior to separation. Pre-concentration can be performed either by chemical trapping (e.g., sorbent tubes or coated capillary traps) or by cold trapping.[86-88] Although these approaches extend GC in-field use, pre-concentration has not been applied for enhanced separation of non-volatile polar organic compounds, such as levoglucosan.

An important part of in-field analysis of levoglucosan or any other compound is sample collection, whether the pollutant is in water or air. Collection can take place on a filter, sorbent tube, or solid-phase microextraction device. Williams et al.[66] has described an automated instrument that uses particle impaction for sample collection. Filter collection followed by thermal desorption has also been suggested.[68] These and other collection methods are discussed elsewhere and are not discussed in detail in this paper.

In this paper, we report improvements that allow enhanced detection of polar, nonvolatile species for in-field analysis using a compact GC which utilizes an indirect heating method. Also discussed in this paper is the use of a pre-column concentration device and its application to the analysis of levoglucosan. This is an initial step in developing a system to analyze levoglucosan in the field at environmentally significant levels. The instrument is fast compared to conventional GC and uses minimal power, conducive to field use. Furthermore, construction of the pre-concentrator and column assembly is simple and can be readily adapted to any applicable injection or detection method. It is especially useful for in-field GC analysis.

5.2 Experimental

5.2.1 Pre-Column Concentrator/ Flash Heater

The pre-column concentrator (PCC) operates by cold-trapping the less-volatile components of a sample in a segment of the column capillary and then releasing the trapped band onto the GC by flash heating. For this study less volatile components refers to compounds with a boiling point above about 350 °C. Cold trapping is used in this case, as opposed to an adsorbent trap, because it can be performed directly on the column for increased simplicity. The PCC assembly, shown in Figure 5.1, is relatively simple. The column is threaded through a 35-mm long nickel tubing jacket (0.02 inch i.d.), which is tightly wrapped with heating wire (32 gauge Constantine wire, insulated with a double glass layer). The entire assembly is placed on a thermoelectric cooling device (HZ-2, Hi-Z Technology, San Diego, CA) and compressed onto the device using a clamp for efficient heat transfer. The HZ-2 is placed on an aluminum heat sink that is continuously fan cooled, and the entire assembly is covered with insulation. The HZ-2 is a high temperature thermoelectric module, which can withstand temperatures up to 350 °C. A high temperature heat sink provided by Hi-Z Technology was used in this setup.

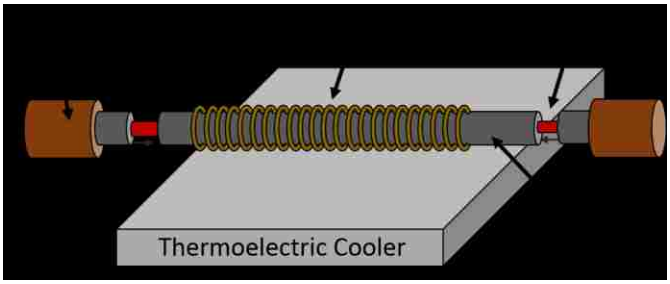

Figure 5.1 Pre-column concentrator (PCC). Sample is trapped in a 35-mm length of column inserted in nickel tubing cooled by a 30×30-mm thermoelectric cooler. Flash heating by a heated wire in contact with the pre-concentrator releases the sample to the column. The junction between the PCC and the transfer line is made up of nickel tubing which extends from the copper tubing/transfer line to the PCC. In this way cold spots are eliminated. For clarity, the assembly is shown with the capillary exposed, but when installed the nickel tubing on each end abuts the tubing of the PCC, as indicated by small arrows.

PCC heating can be programmed with a time delay relative to the beginning of a temperature-programed GC run, which effectively provides an additional degree of separation as the solvent and more volatile compounds travel through the cooled PCC while the analyte band is still trapped. This also decouples the band of analyte from any aspect of manual injection that could broaden the peak, as well as eliminating extra-column broadening from the junction of the injector to the column. Alternatively, the PCC can be held constant at the injection port temperature and, thereby, be used as a heated transfer line to the column heater assembly.

Critical to performance is elimination of cold spots in the transfer lines leading from the injector to the PCC and from the PCC to the column assembly. Heated transfer line segments are depicted in Figure 5.1. Transfer lines were constructed from 1/8-inch (o.d.) copper tubing, through which the capillary column was passed. Nickel tubing was used to thermally bridge the gap between the copper tubing and the PCC. Copper and nickel were used due to their high thermal conductivity to ensure even heating. A thermocouple was mounted on the outside of the copper tubing and heating wire was wrapped around the outside of the copper tubing. In this way, an even temperature was maintained throughout the transfer line due to the high heat conductivity of copper. The transfer line temperature was maintained at 270 °C.

The PCC temperature is measured using a type K thermocouple mounted in direct contact to the outside of the nickel tubing using silica/sodium silicate-based adhesive cement (Sauereisen No. 1 paste, Pittsburgh, PA). Heating is controlled with an Omega 4200 series temperature controller. In the studies reported here, the auto tune function was used to set the variables of the PID (proportional integral derivative) controller, and the time control period was set to 0.8 s. The controller temperature was set to 270 °C. The temperature of the PCC decreased to a

minimum of 3 °C during cooling. When the heater was triggered, the PCC reached 270 °C within 3 s, and maintained a constant temperature with a variation of less than 1 °C.

5.2.2 Column Assembly

The column assembly was designed to overcome common problems with compact GC of uneven heating of the column and limited lifetime of the heater. The design results in substantial improvements in elution band shape and chromatographic efficiency, as described below in characterization of the assembly. As depicted in Figure 5.2, the column assembly is composed of a cylindrical aluminum support with a diameter of 40 mm, height of 12 mm, and thickness of about 1 mm. The GC column is wound on the inside of the aluminum tube. Small lips (1 mm) on the inside of the tube support the column and prevent the capillary from springing out of the tube. A miniature resistance temperature detector (RTD) is used to measure and control the temperature (Omega F2020-100-B, Stamford, CT). The RTD is mounted on the outside of the aluminum support using ceramic cement. Resistive heating wire is evenly wound around the outside of the aluminum support. Thirty-two gauge, double glass insulated, advance alloy wire, 80-cm in length, with a total resistance of 12 Ohms was used to resistively heat the column assembly. The entire assembly is wrapped with silver foil to ensure even heating, and to improve the effectiveness of the heating wire by wicking away the heat on all sides. Finally, the assembly was covered with a layer of polyimide tape.

The high heat conductivity of aluminum gives an even temperature all along the column, and winding the column in a single layer on the inside of the support causes the column to press firmly against the aluminum wall, helping to ensure uniform contact between the capillary and the aluminum. The insulated heating wire is easily wrapped around the outside of the assembly.

Placing the RTD on the aluminum support allows the temperature of the heater to be monitored and controlled at a single point that accurately reflects the rest of the assembly due to the high thermal conductivity of aluminum.

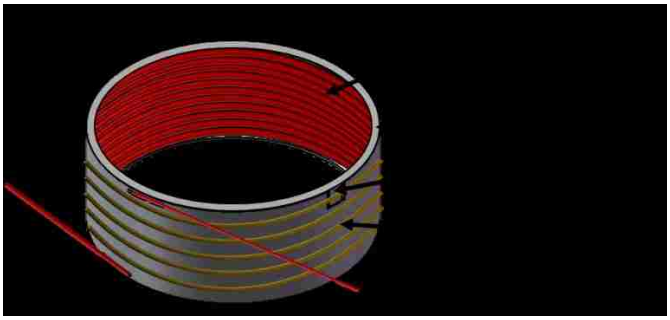

Figure 5.2 Column Assembly. . The column support has a diameter of 40 mm and is 12 mm in height.

All experiments were performed with a 5-m long, 250-µm I.D. fused silica column, with a 0.25 µm thick Rxi-5Sil MS (Restek) stationary phase. This stationary phase is primarily dimethyl polysiloxane, and was chosen because of its stability to thermal cycling up to 350 °C. This stationary phase is also optimized for nonpolar compounds which are often found in ambient air pollution samples such as polycyclic aromatic hydrocarbons (PAHs).

The column assembly and the PCC were easily incorporated into a Guardian-7 portable GC-MS (gas chromatography-mass spectrometer) produced by Torion Technologies,[89] with overall dimensions of 35 x 44 x 18 cm. The Guardian-7 controls column temperature with a pulse-width modulated signal. Detection is accomplished with a toriodal ion trap mass spectrometer. The mass spectrometer was set to scan m/z 38-450, with 14.1 scans/s.

Power consumption by the column assembly for a typical temperature program is less than 15 W. Power and PID control for the column assembly are provided by the Guardian 7, with a peak voltage of 26 V. With this configuration the maximum heating rate is 2.7 °C/s from 25 °C to 200ºC. Due to the loss of heat the maximum heating rate from 200 °C to 250 °C is

1.6 °C/s, and from 250 °C to 300 °C, 1.1 °C/s. These heating rates are constrained by the 26-volt power supply of the Guardian-7; therefore, the maximum heating that the GC assembly can handle is unknown, and the maximum temperature that can be reached is 310 °C. The GC assembly is fan cooled using room air, and cooling of the GC assembly from 220 °C to 30 °C occurs in 100 seconds. Helium is used as the carrier gas for all experiments in this paper, and is supplied by an external cylinder with a flow rate of approximately 1.0 mL/min. In order to maintain the flow the inlet pressure is gradually increased for each run.

5.2.3 Standard Mixtures

Chromatographic performance was tested with three different standard mixtures. EPA 525 PAH Mix-B was obtained from Supelco and diluted in acetone to 5 µg/mL. Levoglucosan, stearic acid, and dehydroabietic acid were purchased from Aldrich, Matheson Coleman & Bell, and Pfaltz & Bauer, respectively, and used without further purification. A mixture of these three compounds was prepared in acetone, with 150 µg/mL each. A mixture of n-alkanes (250 µg/mL for each alkane) was also used to characterize the instrument.

5.3 Results and Discussion

5.3.1 Pre-Column Concentration Unit

The effect of using the PCC at various delay times is shown in Figure 5.3, and levoglucosan peak descriptions are reported in Table 5.1. These results show that using the PCC and delaying the injection of levoglucosan with respect to the start of the temperature-programmed GC run significantly reduces the peak width of levoglucosan without the need for silylation. It is possible that this decrease in peak width acts to improve separation, but

selectivity and resolution of the mass spectrometer is still necessary to resolve levoglucosan from any co-eluting peaks. Included in Table 5.1 is the separation number (SN), which is the number of peaks that can be resolved between two peaks. In this study SN is used as a metric for comparing different delay times. This was calculated from the following equation:

$$SN = (t_{R(x+1)} - t_{R(x)})/(w_{h(x+1)} + w_{h(x)}) - 1 \quad [90] \qquad (5\text{-}1)$$

where t_R is the retention time (corrected using the delay time) and w_h is the full width at half maximum. The subscripts x and x+1 refer to levoglucosan and the subsequent stearic acid peak.

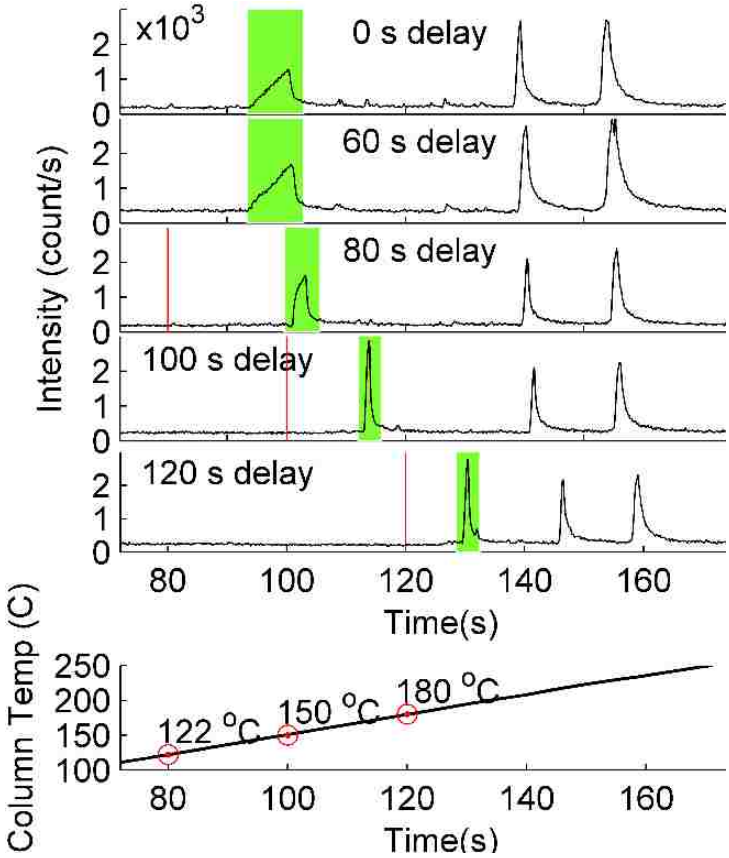

Figure 5.3 Improvement in chromatographic separations of levoglucosan by increasing the time delay for initiating flash-heating in the PCC relative to the start of the temperature-programed GC run. . The levoglucosan peaks are marked with green, and the initiation time of flash heating the PCC is indicated by red lines and corresponding red circles in the bottom temperature plot. The time before 70 seconds has been omitted. In each plot, the second and third peaks are stearic acid and dehydroabietic acid. The improvements in peak shape are shown qualitatively, and peak area differences can be attributed to imprecise split flow injection. For the temperature program, the column was held at 35 °C for 10 s, ramped at 1.5 °C/s to 280 °C, and held there for 60 s.

Table 5.1 Characterization of levoglucosan peaks in Figure 5.3.

Delay Time (s)	FWHM (s)	RT (s)	Separation Number (eq. 1)
0	3.7	103	7.4
60	4.0	103	6.5
80	2.8	103	9.3
100	1.1	113	14.2
120	1.0	130	8.2

Figure 5.3 shows that when levoglucosan is injected onto the column at 35 °C, its peak has considerable fronting despite the use of temperature programming. Fronting and otherwise poor band shape continues until flash heating is delayed longer than 80 s. Fronting is likely due to overloading of the column. As the delay time and corresponding temperature of the GC increases, the sample is retained less on the column and fronting is reduced. Figure 4.3 shows that at an 80-s delay time, the fronting decreases and the peak begins to take a different shape. At 80 s the GC column temperature is 122 °C, which allows levoglucosan to travel through the column faster. (Note that the actual retention time for levoglucosan is relative to the flash-heating event.) After 100 s, the GC temperature has reached 150 °C, and fronting is completely eliminated. With a further increase in delay time from 100 s to 120 s, the FWHM of levoglucosan is slightly reduced from 1.1 s to 1.0 s, but the separation number decreases (see Table 5.1). Consequently, there is no advantage to further increasing the delay time. Furthermore, with a 120 s delay time, the elution time of levoglucosan is 10.5 seconds. This is equal to the hold-up time for the system, thus no retention is taking place. The elution time during the 100 s delay is 13.0 s. Thus, while some separation is still taking place for a 100 s delay time, levoglucosan is not retained using a 120 s delay time.

At high concentrations, the PCC can reach saturation at which point sample is lost into the column. Saturation occurs at approximately 300 ng for levoglucosan, but varies for different compounds with varying chemical properties (such as polarity and vapor pressure). For the compounds in this study, when the PCC is overloaded, 2 peaks for the same compound are observed. If a second peak is not seen, it is assumed that the entire sample is retained in the PCC and is not lost during the delay time.

A calibration curve for levoglucosan with use of the PCC and a 100 s delay time is shown in Figure 5.4. The limit of detection for levoglucosan from this method is 2.2 ng and was approximated from three times the standard deviation in the baseline for m/z 60 (a prominent and unique ion in the levoglucosan mass spectrum). The limit of quantitation is approximately 7 ng (approximated using ten times the standard deviation in the baseline). The baseline window used was 1 min prior to the peak. The concentration of levoglucosan in ambient air pollution can range from 10–8000 ng/m^3; therefore, this method is capable of detecting atmospherically relevant quantities, depending on the collection technique and the amount of air sampled.[15]

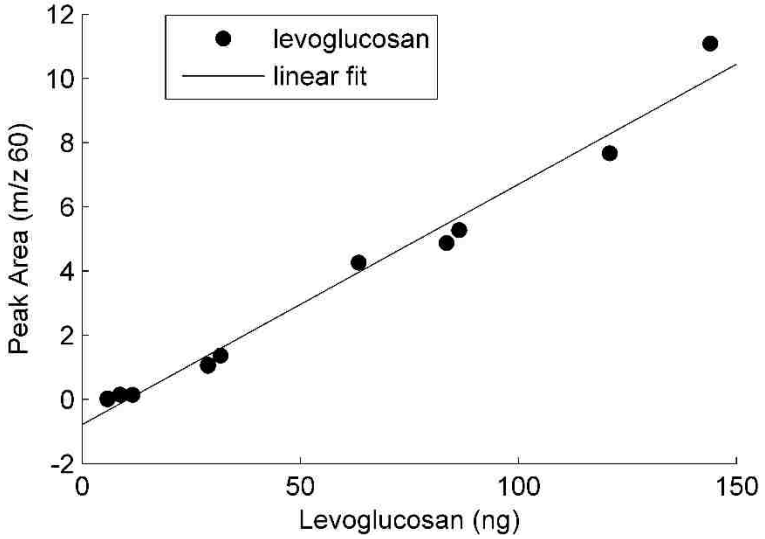

Figure 5.4 Calibration curve for levoglucosan. The equation for the best fit line for the data is Peak Area = 0.075 x [levoglucosan] – 0.78. The standard deviation in the slope (s_m) for this line is 0.003.

To illustrate the usefulness of the instrument, a sample of wood smoke was collected on a quartz fiber filter, followed by thermal desorption off the filter onto the PCC and subsequent separation and analysis. The details concerning sample collection and desorption are described in Chapter 4. Figure 5.5 shows the total ion chromatogram (TIC) for the smoke sample, and the reconstructed-ion-chromatogram (RIC) for m/z 60 and 73 (two significant peaks in the mass spectra for levoglucosan). Levoglucosan is identified from its mass spectrum and retention time (115 s).

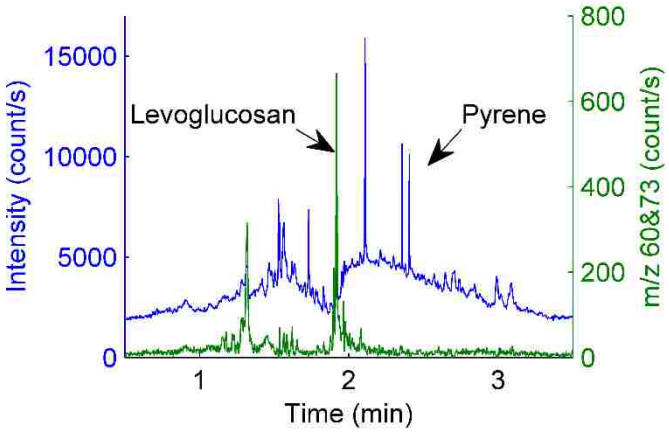

Figure 5.5 A smoke sample analyzed with the PCC and GC system.The top trace in blue is the total-ion-chromatogram, and the bottom trace in green is the reconstructed-ion-chromatogram for m/z 60 and 73, two ion peaks characteristic of levoglucosan. Levoglucosan appeared at 115.2 seconds. Pyrene (retention time, 144 s) and several other PAHs could also be detected in the sample.

5.3.2 Characterization of the Column Assembly

Performance of the column assembly without the use of the PCC was evaluated from separations of a simple hydrocarbon mixture. Figure 5.6 illustrates the quality of temperature control for a temperature programed run with a ramp rate of 1.5 °C/s. Power consumption for a similar temperature program, which is the same as that used for the runs in Figure 5.3, is illustrated in Figure 5.7. The mean power is 14 W, which is at least 70 times less than the average power consumption of a conventional GC oven, making it conducive to field

instrumentation.[91] This power profile illustrates the power usage for a typical temperature program. With the peak voltage of 26 V provided by the Guardian 7, maximum heating rates were 2.7 °C/s from 25 °C to 200 ºC, 1.6 °C/s from 200 °C to 250 °C, and 1.1 °C/s from 250 °C to 300 °C. The maximum heating rate is reduced at higher temperatures due to the loss of heat and the limited power supplied to the unit (a 26-V power supply was used); therefore, the maximum heating rate that the GC assembly can handle is unknown. However, a constant heating rate of 1.5 °C/s was used for this study. A fan in the unit was able to cool the GC assembly from 220 °C to 30 °C in 100 s.

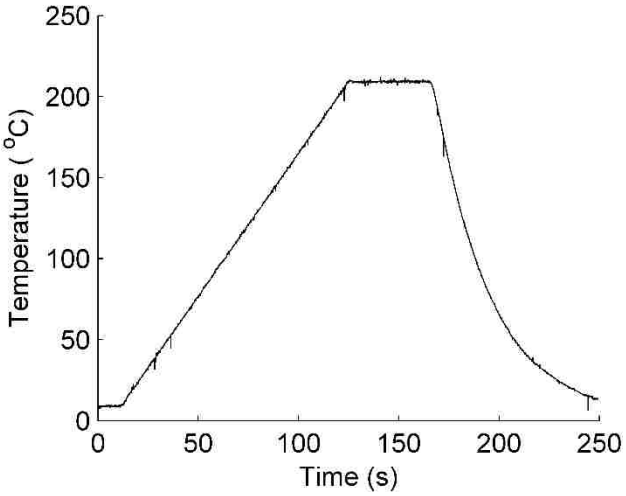

Figure 5.6 Column temperature profile of the compact GC. The column was heated at 1.5 °C/sec to 220 °C. The temperature was held at 220 °C for 60 seconds, and was subsequently fan cooled to 30 °C in 100 s. The above temperatures were recorded at 10 points/s. The average standard deviation in the temperature for 3 runs using the same temperature program is 0.3 °C.

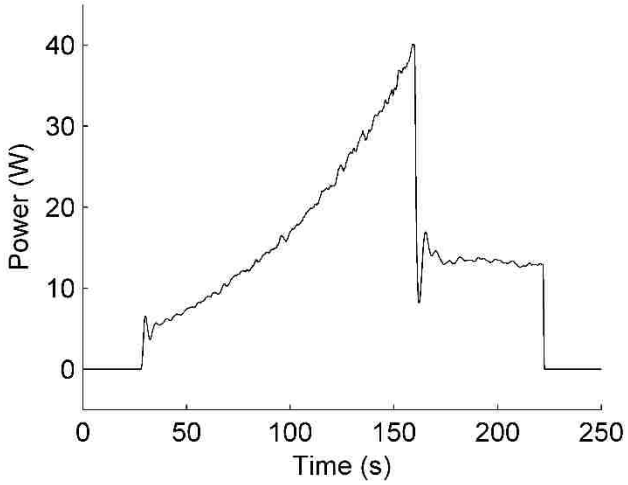

Figure 5.7 Power profile for the temperature program in Figure 5.6. Temperature was held at 35 °C for 10 s, and then ramped at 1.5 °C/s to 280 °C and held there for 60 s. Peak power consumption was 56 W, and the average was 14 W.

The reliability of the resistive heating wire has been an issue in compact systems, and shorts are known to occur that limit the life of the column heater.[92] Our design protects the heating wire; it was cycled over 2000 times with no visible wear on the wire and insulation other than the insulation turning from tan to dark brown.

The reproducibility in retention times for a simple mixture is shown in Table 5.2, and a chromatogram for this mixture is shown in Figure 5.8. The standard deviation of the mean value for each compound is close to 1 s. The reproducibility in retention times is limited by the precision of the software timer of 0.5 s. Combined with the mass spectrometric information for each peak, this variability is acceptable. The reproducibility of isothermal separation is shown in Table 5.3. The column was held at 100 °C for these runs.

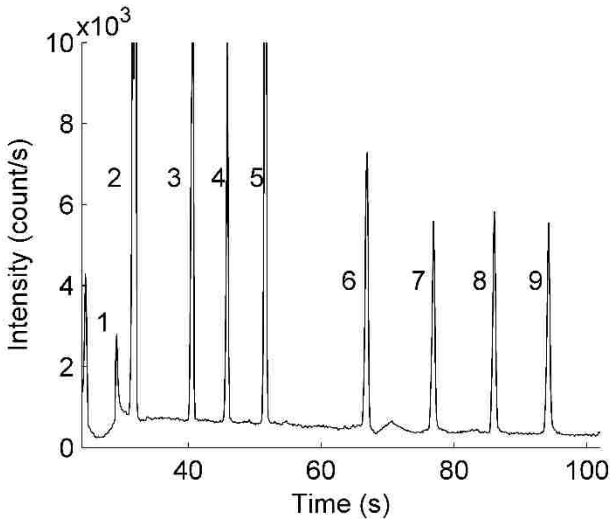

Figure 5.8 Separation of a hydrocarbon mixture. The column temperature began at 35 °C for 10 seconds and was then ramped at a rate of 1.5 °C/s, and the helium flow was kept at 1.0 mL/min. From left to right the compounds are: (1) n-octane, (2) p-xylene, (3) n-propylbenzene, (4) n-decane, (5) n-butylbenzene, (6) n-dodecane, (7) n-tridecane, (8) n-tetradecane, (9) n-pentadecane. Large peaks have been cropped.

Table 5.2 Variation in retention times over the course of a week.

Compound[a]	Retention Time (s)	SD (s)[b]
n-propylbenzene	42	± 1
n-decane	47	± 1
n-butylbenzene	53	± 1
n-dodecane	68	± 1
n-tridecane	77	± 1
n-tetradecane	86	± 0.9
n-pentadecane	94	± 0.9

[a]*About 0.5 µL of the hydrocarbon mixture was injected each time.*

[b]*The standard deviation (SD) of the mean is reported.*

Table 5.3 Isothermal runs for two n-alkanes at 100 °C.

Compound	N Plates	S.D.	Retention Time (s)	S.D. (s)
n-tetradecane	1300	± 200	106	7
n-pentadecane	3000	± 400	210	20

The separation of polycyclic aromatic hydrocarbons (PAHs) is illustrated in Figure 5.9. PAHs are useful for in-field measurements because of their environmental importance.[93] They can be found in drinking water and organic aerosols and are considered priority pollutants by the EPA. The compact GC was able to separate the isomers phenanthrene and anthracene. Larger isomers in the standard were not resolved due to the relatively short 5-m column.

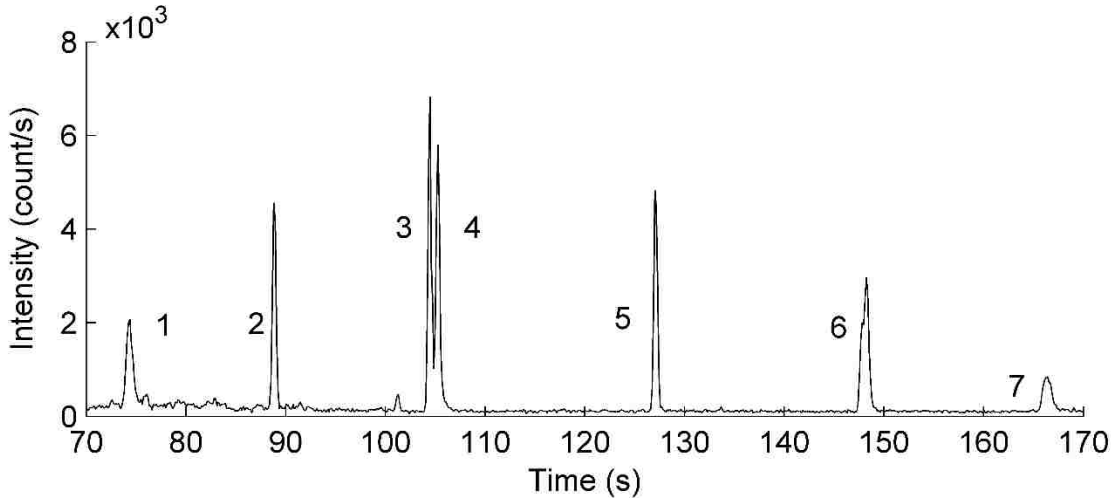

Figure 5.9 Polycyclic aromatic hydrocarbons (injection of 5 ng each). The column temperature began at 35 °C for 10 s and was then ramped at a rate of 1.5 °C/s, and the helium flow was kept at 1.0 mL/min. Peaks from left to right are: (1) acenaphthylene, (2) fluorene, (3) phenanthrene, (4) anthracene, (5) pyrene, (6) benz[a]anthracene, (6) chrysense, (7) benzo[b]fluoranthene, (7) benzo[k]fluoranthene.

5.4 Conclusions

A simple pre-concentration unit and miniaturized GC assembly has been developed and tested using atmospheric samples. This system can potentially be used for field GC, and GC-MS instrumentation. The simplicity of the system is demonstrated by the fact that all components of the PCC and GC were assembled in the laboratory without specialized equipment. The PCC unit and GC assembly were integrated into current portable GC-MS systems, such as the Torion Technologies Guardian-7, and can be used for in-field separation and detection of environmentally relevant organic compounds, such as PAHs, levoglucosan, and other organic acids. The PCC unit is particularly useful for enhanced fast separation of levoglucosan.

5.5 Acknowledgements

Funding for this project was provided by Sunset Laboratory Inc., 10180 Nimbus Avenue, Suite L/5, Tigard, OR 97223

We acknowledge the help of Torion Technologies for assistance with the mass spectrometer and the associated GC temperature control hardware and software. We also thank Dr. Lee Hansen for his support and suggestions regarding this study.

5.6 Chapter References

15. Lin, L.; Lee, M. L.; Eatough, D. J., Gas chromatographic analysis of organic marker compounds in fine particulate matter using solid-phase microextraction. *Journal of the Air & Waste Management Association* **2007,** *57* (1), 53-58.
26. Schauer, J. J.; Cass, G. R., Source apportionment of wintertime gas-phase and particle-phase air pollutants using organic compounds as tracers. *Environmental Science & Technology* **2000,** *34* (9), 1821-1832.
66. Williams, B. J.; Goldstein, A. H.; Kreisberg, N. M.; Hering, S. V., An in-situ instrument for speciated organic composition of atmospheric aerosols: Thermal Desorption Aerosol GC/MS-FID (TAG). *Aerosol Science and Technology* **2006,** *40* (8), 627-638.
68. Lin, L.; Lee, M. L.; Eatough, D. J., Review of Recent Advances in Detection of Organic Markers in Fine Particulate Matter and Their Use for Source Apportionment. *Journal of the Air & Waste Management Association* **2010,** *60* (1), 3-25.
70. Cropper, P. M.; Goates, S. R.; Hansen, J. C., A compact gas chromatograph and pre-column concentration system for enhanced in-field separation of levoglucosan and other polar organic compounds. *Journal of Chromatography A* **2015,** *1417*, 73-78.
74. Schkolnik, G.; Rudich, Y., Detection and quantification of levoglucosan in atmospheric aerosols: A review. *Analytical and Bioanalytical Chemistry* **2006,** *385* (1), 26-33.
77. Nolte, C. G.; Schauer, J. J.; Cass, G. R.; Simoneit, B. R. T., Highly polar organic compounds present in meat smoke. *Environmental Science & Technology* **1999,** *33* (19), 3313-3316.
78. Grall, A.; Leonard, C.; Sacks, R., Peak Capacity, Peak-Capacity Production Rate, and Boiling Point Resolution for Temperature-Programmed GC with Very High Programming Rates. *Analytical Chemistry* **1999,** *72* (3), 591-598.
79. PerkinElmer. The Evolution of Gas Chromatographic Instrumentation at PerkinElmer *The Evolution of Gas Chromatographic Instrumentation at PerkinElmer* [Online], 2005. http://www.perkinelmer.com/CMSResources/Images/44-74443BRO_GasChromaEvolution.pdf (accessed September 2015).
80. Sides, G. D.; Cates, M. Continuous air monitoring apparatus and method. US5014541 A, 1991.

81. Rounbehler, D. P.; Achter, E. K.; Fine, D. H.; Jarvis, G. B.; MacDonald, S. J.; Wheeler, D. B.; Wood, C. D. High speed gas chromatography. US5808178 A, 1998.
82. Maswadeh, W. M.; Snyder, A. P. Hand-held temperature programmable modular gas chromatograph. US5856616 A, 1999.
83. Stadermann, M.; McBrady, A. D.; Dick, B.; Reid, V. R.; Noy, A.; Synovec, R. E.; Bakajin, O., Ultrafast gas chromatography on single-wall carbon nanotube stationary phases in microfabricated channels. *Analytical Chemistry* **2006,** *78* (16), 5639-5644.
84. Collin, W. R.; Serrano, G.; Wright, L. K.; Chang, H. W.; Nunovero, N.; Zellers, E. T., Microfabricated Gas Chromatograph for Rapid, Trace-Level Determinations of Gas-Phase, Explosive Marker Compounds. *Analytical Chemistry* **2014,** *86* (1), 655-663.
85. Serrano, G.; Paul, D.; Kim, S. J.; Kurabayashi, K.; Zellers, E. T., Comprehensive Two-Dimensional Gas Chromatographic Separations with a Microfabricated Thermal Modulator. *Analytical Chemistry* **2012,** *84* (16), 6973-6980.
86. Zampolli, S.; Elmi, I.; Mancarella, F.; Betti, P.; Dalcanale, E.; Cardinali, G. C.; Severi, M., Real-time monitoring of sub-ppb concentrations of aromatic volatiles with a MEMS-enabled miniaturized gas-chromatograph. *Sensors and Actuators B: Chemical* **2009,** *141* (1), 322-328.
87. Ochiai, N.; Takino, M.; Daishima, S.; Cardin, D. B., Analysis of volatile sulphur compounds in breath by gas chromatography–mass spectrometry using a three-stage cryogenic trapping preconcentration system. *Journal of Chromatography B: Biomedical Sciences and Applications* **2001,** *762* (1), 67-75.
88. Pillonel, L.; Bossett, J. O.; Tabacchi, R., Rapid preconcentration and enrichment techniques for the analysis of food volatile. A review. *Lebensmittel-Wissenschaft Und-Technologie-Food Science and Technology* **2002,** *35* (1), 1-14.
89. Contreras, J. A.; Murray, J. A.; Tolley, S. E.; Oliphant, J. L.; Tolley, H. D.; Lammert, S. A.; Lee, E. D.; Later, D. W.; Lee, M. L., Hand-Portable Gas Chromatograph-Toroidal Ion Trap Mass Spectrometer (GC-TMS) for Detection of Hazardous Compounds. *Journal of the American Society for Mass Spectrometry* **2008,** *19* (10), 1425-1434.
90. Ettre, L. S., Nomenclature for Chromatography. *Pure and Applied Chemistry* **1993,** *65* (4), 819-872.
91. Luong, J.; Gras, R.; Mustacich, R.; Cortes, H., Low thermal mass gas chromatography: Principles and applications. *Journal of Chromatographic Science* **2006,** *44* (5), 253-261.
92. Wang, A.; Tolley, H. D.; Lee, M. L., Gas chromatography using resistive heating technology. *Journal of Chromatography A* **2012,** *1261* (0), 46-57.
93. Schkolnik, G.; Falkovich, A. H.; Rudich, Y.; Maenhaut, W.; Artaxo, P., New analytical method for the determination of levoglucosan, polyhydroxy compounds, and 2-methylerythritol and its application to smoke and rainwater samples. *Environmental Science & Technology* **2005,** *39* (8), 2744-2752.

6 CONCENTRATION, COMPOSITION AND SOURCE APPORTIONMENT OF $PM_{2.5}$ ADJACENT TO THE I-710 FREEWAY IN LONG BEACH, CA

Chapter 6 of this dissertation is in preparation for submission to the Journal of Air and Waste Management. The primary contribution of the author was collection of data in Long Beach, CA, along with preparation of the data for source apportionment.

6.1 Introduction

Under the National Ambient Air Quality Standards put in place as a result of the Clean Air Amendments of 1990, many regions in the state of California, especially the South Coast Air Basin, which includes Los Angeles County, are in violation of the 24-h National Ambient Air Quality Standard (NAAQS) for both $PM_{2.5}$ and ozone. The metropolitan nature of the area (Los Angeles population of 4 million, South Coast Air Basin population of 21 million), coupled with its valley basin geography, makes the Basin susceptible to elevated pollution concentrations. These elevated pollution concentrations have contributed to increased instances of adverse health effects, including decreased lung function, cancer, respiratory symptoms, asthma and mortality.[94-98] In general, fine particulate matter and anthropogenic pollutant gases are dominated by local emissions and not by transport from other regions. These local emissions are mainly composed of diesel emissions and gasoline emissions.[99] Westerdahl et al. demonstrated a correlation between diesel truck traffic and high concentrations of black carbon (BC) and ultrafine particles (UFP).[100] They also demonstrated a correlation between gasoline emissions and UFP, CO and NO. Studies have shown that concentrations of UFP, BC, particle bound-

PAHs, CO and NO_x in Los Angeles appeared to range from 18,000-33,000 particles/cm^3, 0.2-24.8 μg/m^3, 18-36 ng/m^3, 1.7-2.6 ppm and 35 ppb, respectively.[101-104] In areas near the Los Angeles freeways and roadways there is a two to five times increased concentration of particles as far as 150 m downwind of the roadways.[105-106] To combat the high pollution levels, many air control measures have been implemented, but the improvements have not been sufficient to put these regions into attainment.

The I-710 sampling site (AQS Station Code) located in Long Beach, CA, is run jointly by Southern California Edison (SCE) and the South Coast Air Quality Management District (SCAQMD), and is located 10 m east of the freeway and just south of the Long Beach Avenue exit. During August and September, 2012, a study was conducted to determine the sources of $PM_{2.5}$ adjacent to the I-710 Long Beach Freeway (Long Beach, CA). The site is of interest because Long Beach, CA, has been designated as one of 55 urban, long-term, nationwide multipollutant NCore sites by the U.S. Environmental Protection Agency (EPA). The NCore network is designed to enhance existing monitoring capabilities in an effort to produce an integrated multi-pollutant approach to air quality monitoring. In addition to collecting information on criteria pollutants, NO_X, O_3, CO, and PM, emphasis has been placed on measuring noncriteria pollutants, specifically NH_3 and HNO_3 because of their importance in secondary PM formation. These species are measured in an effort to improve emission control strategies as well as to obtain more complete information for scientific, public health, and ecosystem assessments. However, new methods are needed to help identify the anthropogenic pollutants from their various sources.

This study aims to provide concentration, composition and apportionment of pollutants along the Long Beach area, and introduces a new GC-MS instrument that is able to monitor

particle phase organic compounds which aid in identifying pollutant sources. This especially pertains to particulate matter (PM). PM is chemically complex and its sources are highly variable. PM complexity is largely due to the organic fraction, which ranges from 10-90% of its total mass. However, the organic compounds in PM are usually only manually monitored due to limitations in current field analysis techniques. This instrument is capable of autonomously monitoring semi and non-volatile organic compounds of PM on an hourly averaged basis. This chapter describes the sampling program and results of positive matrix factorization (PMF) analysis.

6.2 Experimental

Data were collected at the Long Beach Boulevard sampling site shown in Figures 6.1 and 6.2 from Aug 1, 2012 through Sep 2, 1012. All data were obtained on a 1-hr averaged time basis. The following species were measured:

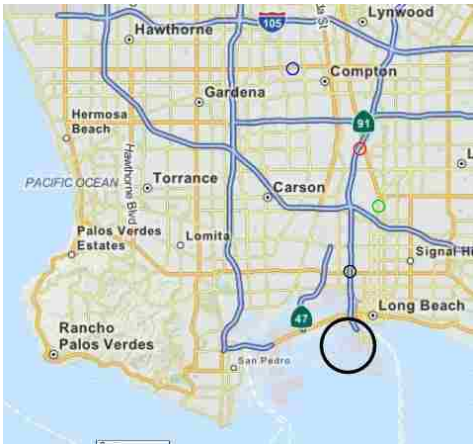

Figure 6.1 Location of the I-710 sampling site (small black circle).The red and green circles mark the location of the Compton and Long Beach sampling sites, respectively. The Large black circle marks the location of the port.

6.2.1 Fine Particulate Mass

Total fine particulate mass, including the semi-volatile species, was measured with an R&P model 8500 tapered element oscillating microbalance (TEOM) with a filter dynamics measurement system (FDMS). One-hour averaged concentrations of PM_{10}, $PM_{2.5}$, NO_x (NO and NO_2), O_3, CO, and NH_3 were measured. Particle-phase nitrate, nitrite, and sulfate and gas-phase HONO, HNO_3, and SO_2 were also measured on a 1-h average basis. Speciation data were collected for $PM_{2.5}$, as it is the focus of this paper. PM_{10} data was collected; however, no speciation data are available on the coarse particle fraction. One-hour averaged PM_{10} and $PM_{2.5}$ masses were measured using two FDMS TEOM units, with PM_{10} and $PM_{2.5}$ cyclone cut-off filters. The sampler used firmware version 1.22. The size distribution of particulate matter was measured with a California Measurements PC-2HX impactor with measurements of PM mass collected on oscillating crystals with size cuts of 0.10, 0.15, 0.25, 0.4, 0.7, 1.0, 2.5, 4, 7 and 10 microns.

6.2.2 Fine Particulate Composition

An URG model 9000D Ambient Ion Monitor (AIM) was used to measure both particulate and gas phase cations and anions. The instrument draws in air at a rate of 3 L/min through a $PM_{2.5}$ sharp-cut cyclone filter. The air is passed through a liquid diffusion denuder, where gases are removed by reaction with a dilute aqueous solution of H_2O_2 (0.3% in water). The oxidant solution in the denuder is used to convert SO_2 to sulfate. Particles are subsequently collected as the air stream after the denuder enters an aerosol supersaturation chamber. Both the gas and particle phases are collected for 1 h and then analyzed with ion chromatography (IC; Dionex ICS-1000). The lower limit of detection for both particle- and gas-phase ions is species dependent and approximately 0.05 mg/m^3. The AIM instrument was calibrated according to the

user manual instructions every 2 weeks with a seven-anion standard and a six-cation standard purchased from Dionex (P/N 56933). The denuder membrane was changed every 4 weeks. Measured species specifically included in the PMF analysis were ammonium nitrate, ammonium sulfate, and sodium chloride in the particles. However, all AIM data are presented and discussed in this manuscript. Gas phase NH_3, and HNO_3 are compared to particulate ammonium nitrate. Gas phase SO_2 was also measured and used in the PMF analysis. Fine particulate carbonaceous material was measured with a Sunset Laboratory Dual Oven Carbon Monitor.[107] This instrument gives nonvolatile organic material (NVOC, corrected to NVOM with a factor of 1.6), black carbon (BC) and semi-volatile organic carbon. However, the second oven to measure the semi-volatile organic material (SVOM) was not functioning well during the study and SVOM was estimated as $PM_{2.5}$ mass minus all other measured fine particulate components. An Andersen Instruments (model RTAA-900) aethalometer was used for the determination of aerosol BC. In addition, 1-h UV absorption data were obtained, which is believed to be a good indicator of fresh diesel emissions. Continuous 1-h averaged data were obtained for all species.

6.2.3 PMF Species

Measured species specifically included in the PMF analysis were ammonium nitrate, ammonium sulfate, and chloride in the particles. Gas phase SO_2 was also measured and used in the PMF analysis.

Comparisons of the sum of all measured species and the FDMS TEOM $PM_{2.5}$ measurements were generally in agreement, except for periods when high concentrations of ammonium sulfate or chloride were measured. Comparison of the FDMS TEOM and the CM impactor data indicated that for these samples a significant fraction of the particulate material

was found in the 1.0 to 4.0 micron size region. The 2.5 micron cut points of the FDMS TOEM and the URG AIM are not identical. The cut off curve of the AIM introduces a bias towards somewhat larger particles such that ammonium sulfate and chloride were not sampled the same. The majority of these species were sampled by the AIM, but not by the FDMS TEOM. To avoid the effect of this difference in the PMF analysis, the $PM_{2.5}$ fit in the PMF analysis was calculated as the sum of all measured fine particulate components except for ammonium sulfate and chloride, see Figure 6.3. The AIM measured ammonium sulfate and chloride (assumed to be NaCl) were, however, used in the PMF analysis.

6.2.4 Other Components Used in the PMF Analysis

In addition to the particulate components listed above, other measurements were included in the PMF analysis. These included all measurements related to either $PM_{2.5}$ emissions or to the formation of secondary $PM_{2.5}$. Measurements made at the sampling site by BYU provided concentrations of SO_2 as a precursor to sulfate. Measurements made by the South Coast Air Quality Management District (SCAQMD) related to primary emissions or secondary aerosol formation included gas phase NO_X, NO_2, and the traffic count on the freeway. This latter number included all vehicles (both gasoline and diesel powered) going either direction. Two other species which have been shown to be useful in distinguishing between gasoline and diesel powered vehicular traffic or to secondary pollutant formation are CO and O_3, respectively (Eatough 2008, Grover 2008a). These species were intended to be measured, but for technical reasons were not. However, ozone was measured by the SCAQMD at their Long Beach and Compton sites (see Figure 6.1). In addition, CO, NO_X and BC were also measured at the Long Beach site. Ozone is expected to be somewhat regional in nature. Concentrations of ozone at the Long Beach and Compton sites were in good agreement, and the average of these two

measurements was assumed to represent ozone at the near-freeway sampling site. The Long Beach sampling site, but not the Compton site, is close to the intersection of two freeways, including the harbor freeway. The principal useful components in a PMF analysis for distinguishing between diesel and gasoline powered vehicles are CO, NO_X and BC.[27, 108] Regression analysis of the data from the SCAQMD Long Beach site gave:

$$CO = 0.23 \pm 0.11 + (0.0445 \pm 0.0027)\ NO_X + (0.0161 \pm 0.0096)\ BC \qquad (6\text{-}1)$$

For equation 6-1, n = 684 and R = 0.59. PMF analysis of the data set without CO did not allow the separation of factors related to gasoline and diesel emissions. Therefore, equation 6-1 was used to estimate CO at the I-710 sampling site, giving the results shown in Figure 6.2. These CO concentrations were used in the analysis reported here.

6.3 Meteorological Analysis

Interpretation of the PMF analysis was aided using streamlines to identify probable origins of air masses influencing the sampling site for each data point. The LA Basin is populated by approximately 18 million residents. It is bounded on the west and south by the Pacific Ocean. Mountains define the Basin to the north and east. The north mountains rise from west to east from about 1000 m to nearly 3500 m. The east mountains decrease from north to south from about 3300 m to 1500 m. The LA Basin is geographically large, averaging 70 km in width and about 110 km in length from west to east.

The LA Basin enjoys a Mediterranean climate. The summers are characterized by various high pressure systems. There is little to no precipitation. The boundary or mixed layer experiences daily late morning through early evening sea breezes. Because the average summer ocean temperatures are 20 °C, these sea breezes are thermally driven and provide natural air

conditioning to the Basin. The southern deserts to the east of the Basin heat to 40-45 °C during the summer, drawing in the marine air from west to east. A combination of topography and meteorological regimes leads to a stably stratified environment. The average summer mixing height is just 450 m. It increases little during the day because of sea breeze divergence which maintains and strengthens the inversion during the day. On many days, there is stratus along the coast extending inland about 30 miles during the night. While there is a typical 5-8 m/s diurnal sea breeze, the nights are close to calm. Average summer maximum temperatures at the coast are 24 °C, downtown LA, 28 °C, and in the inland valleys, 35 °C. Night minimums are typically 17 °C. August 2012 was a hotter than normal month.

From Aug 1 – Sep 3, a total of 34 days, 24 days were above average maximum temperatures and 25 days were above average minimums. There were long spells where the marine/mix layer was under 300 m. There were only 6 days when the air mass was cooler than normal. There were only 7 days when the stratus emanating from the ocean moved into the Basin overnight. Most days, there was little stratus even along the coast. From Aug 1-5 there was a weak upper level trough along the west coast. This led to ML heights from 275-730 m and surface temperatures below normal. The only other trough period was Aug 22-26 when ML heights ranged from 600-700 m and surface temperatures were below normal. Nearly all other days were dominated by high pressure centered to the east of CA over the "Four Corners" area. Since circulation around a high pressure is clockwise, this southeast flow advected monsoonal moisture from the Gulf of Mexico. This led to high clouds at times, disruption of the marine layer, warm nights, high relative humidity and warmer than normal days. The only other pattern was a dry high pressure ridge from Sept 1-3. This flow was southwest or from the Pacific Ocean. This pattern resulted in warmer days, but normal night temperatures, and a shallow marine layer.

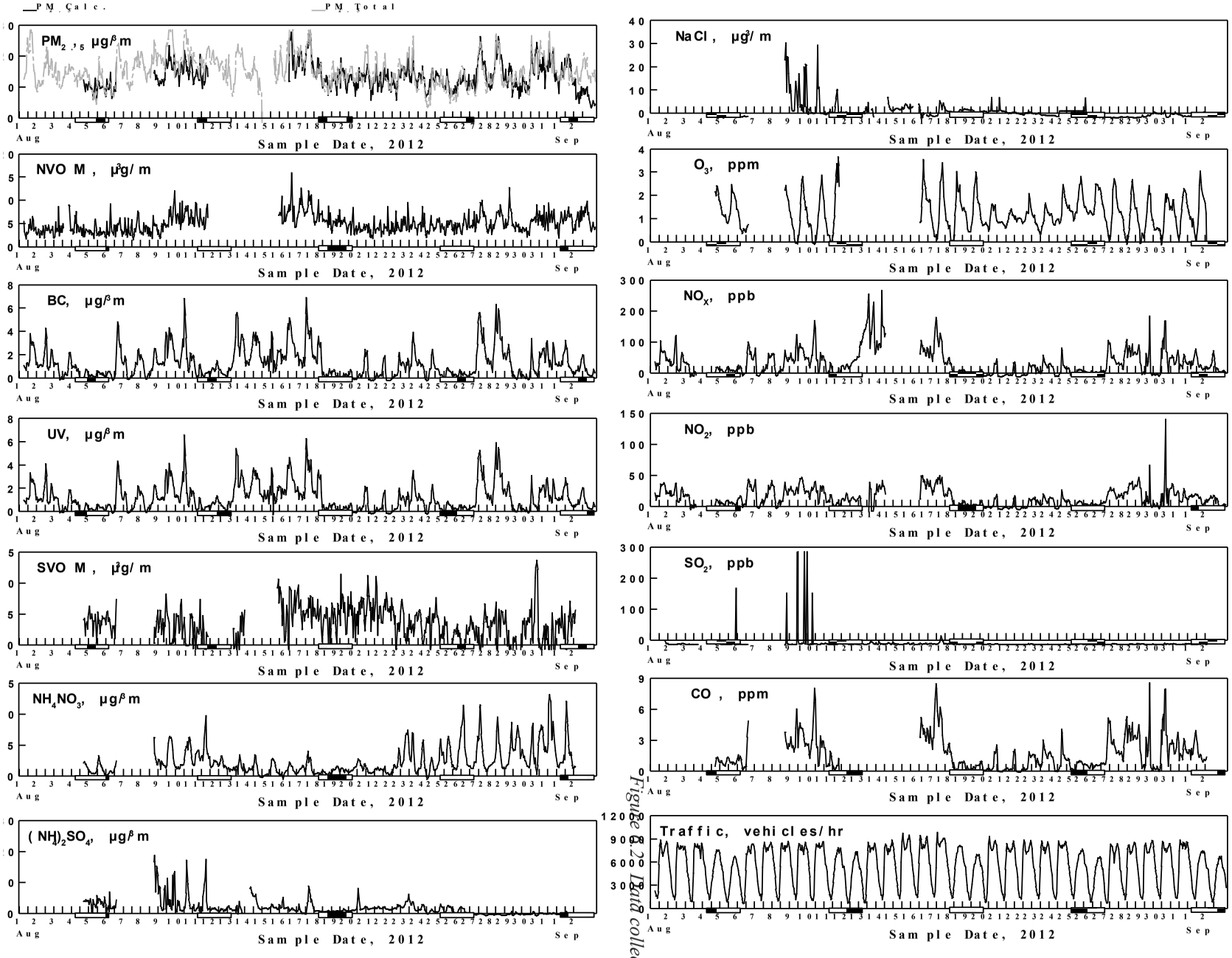

Figure 2.2: Data collected at the I-710 S

The meteorology associated with the sampling site is pertinent to this study. It is in the downwind path of the Palo Verde convergence zone. Winds come from Santa Monica Bay to the north of the PV peninsula and from the south in the direction of the Long Beach Port activities. At times, they come from both directions.

Greatly aiding in the meteorological analyses were continuous hourly streamline plots in the boundary layer. AWS TruePower exercised the Weather Research and Forecasting (WRF) model Advanced Research version 3.6. In simulated domain, the parent domain was 297 x 250 grid points, 50 vertical levels, 6-km horizontal resolution, 1782 km x 1500 km. The inner nested domain (two-way interactive with parent domain) was 250 x 250 grid points, 50 vertical levels, 2-km resolution, 500 x 500 km and centered on the Long Beach sampling site. The initialization data was GFS grib2 data: 0.5-degree resolution. GFW forecast hour 0 was used for initial and lateral boundary conditions as well as spectral nudging throughout the entire period, updated every six hours. The spectral nudging technique is after Waldron et al.[109] The run time is hourly forecasted from one continuous model run. The simulation period began 0Z on July 30, 2012 and ended at 06Z on Sep 30, 2012 with the first 48 h used as spin-up. The displayed output included PBL height, surface parameters including sea level pressure (mb), 2-m temperature (ºC) and 10-m wind (m/s), 10-m streamlines with speed (m/s) shaded, 50-m streamlines with speed (m/s) shaded and 80-m streamlines with speed (m/s). Where possible, the modeled results were compared to observations and found to be quite accurate.

6.4 PMF Analysis

PMF2 and the algorithm used in the analysis has been previously described.[110] With PMF2, the results are constrained so that factor contributions cannot be negative for any species.

One of the advantages to PMF2 is the ability to account for missing and below detection limit data. The uncertainty in each measurement can be adjusted to account for aberrations in the data set. In this study, error uncertainty estimates were chosen similar to those previously outlined by Grover et al.[27] For what were determined to be reliable data, the concentration values were directly used and the error estimates were assigned as the measurement error plus one third the limit of detection (LOD). In a few instances when the measurement was below the LOD, the error was estimated as 5/6 the LOD. Missing values in the data set were accounted for by taking the geometric mean of the hour preceding and following the missing data point. In this study, SVOM concentrations were obtained as the difference between the FDMS TEOM and the sum of the other measured components of $PM_{2.5}$. Therefore, the error estimate was performed as mentioned above using the highest LOD of the various measurement techniques. The uncertainty of the fitted parameter, FDMS TEOM measured $PM_{2.5}$ mass, was taken to be four times the measured value.[111]

6.4.1 PMF2 Analysis of Mass and Composition Data

One-hour semi-continuous measurements were made throughout the study period with instruments to measure both $PM_{2.5}$ mass, $PM_{2.5}$ chemical species, and gas phase species with concentrations as summarized above and shown in Figure 6.2. In performing PMF2, the number of factors to be identified is defined by the user. However, a higher order solution does not necessarily contain all the same factors as a lower order solution. Experimentation with the number of factors is performed until the most reasonable results are obtained (i.e. until the results describe the data and are meaningful). In this study, the robust mode [110] was used in which data were down weighted if the standard deviation was greater than four times the error estimate.

Fourteen species for 520 1-h averaged data sets were used in this PMF2 analysis and ten factors were identified. Rotational ambiguity, which can plague this type of factor analysis, can be restrained by applying an FPEAK value. In this case, an FPEAK value of zero resulted in the most meaningful results. An evaluation of the quality of the fitted data can be obtained by comparing the degrees of freedom (i.e. the number of data points) with the calculated value of *Q*. If a reasonable fit is obtained, the calculated value of *Q* should be equal to or less than the degrees of freedom. Deviation from the theoretical value suggests that the errors in the model are not well defined. For this study, the degrees of freedom was 7280 and the resultant *Q* value was 459. This solution was further evaluated using the "key" feature of PMF2 and the resulting Q value was 484. Residuals were small and gaussian in nature. Examination of G-Space edges[112] indicated all factors were independent of each other. A second check on the fit of the solution can be made by comparing the sum of the factor contributions to the measured mass, to verify that the measured mass is well defined by the calculated sources. In this case, the sum of the factor contributions were in good agreement with the measured $PM_{2.5}$ mass. Linear regression analysis resulted in a zero intercept slope of 0.970 ± 0.006 (R^2 = 0.76, n = 520) and a regression calculated slope of 0.922 ± 0.022 (R^2 = 0.76 and intercept = 0.8 ± 2.2 μg/m^3). As indicated in Figure 6.3, the comparison of the FDMS mass and the PMF estimated mass in the PMF2 analysis was random and the average deviation was 1.7 μg/m^3 (average $PM_{2.5}$ = 15.2 μg/m^3).. Likewise, all fitted parameters were well accounted for in the analysis (see Figure 6.4). The factor profiles and concentrations for the ten identified factors are shown in Figure 6.5.

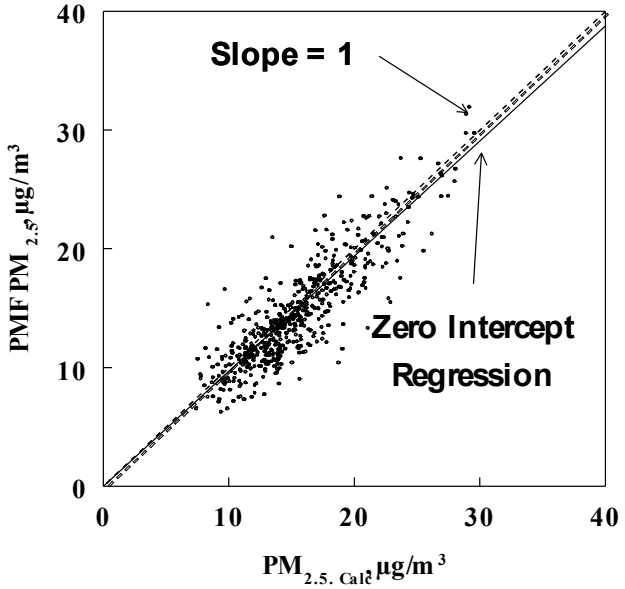

Figure 6.3 Comparison of the sum of the factors to the measured mass.

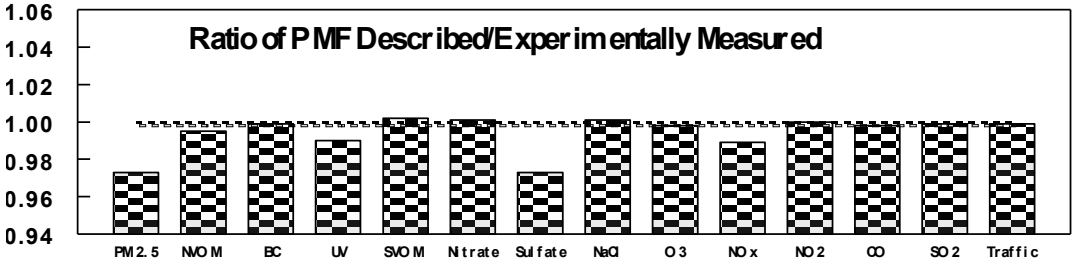

Figure 6.4 The parameters used to fit the PMF model vs the measured values.

In source apportionment, a prior knowledge of chemical markers that can be attributed to a particular source is needed to identify sources most likely associated with each factor. Relevant time patterns and meteorological stream lines were also used in this study to aid in the identification of the sources associated with each factor. This analysis was greatly aided by the hourly averaged nature of the results.

Because of the location of the sampling site, mobile sources provided a higher than usual contribution to the $PM_{2.5}$. Mobile sources which impacted the site include gasoline combustion

emission from automobiles, diesel trucks from the port and diesel emission from both heavy and light duty diesel vehicles which do not originate from the port. It is believed that BC is more associated with diesel emissions. It is also anticipated that a marked weekday – weekend difference exists in diesel emissions. A total of four factors were associated with characteristics of mobile sources. These characteristics are summarized in Table 6.1.

Table 6.1 Characteristics of the four factors associated with mobile sources.

#	Factor Name	Avg. $\mu g/m^3$	Weekend Reduced	BC/ $PM_{2.5}$	$NO_x/PM_{2.5}$	$CO/PM_{2.5}$	%Traffic
1	Port 1	1.5	Yes	0.75	1.1	46	13.1
2	Port 2	0.4	Yes	0.23	45	2020	1.1
3	Diesel	0.7	Yes	0.17	29	1375	1.8
4	Auto	1.1	No	0.001	0.8	36	84.9

Results of the G-Space edge analysis[110] comparing the three diesel related factors (1-3) are shown in Figure 6.6. Factors 1, 2 and 3 were assumed to be associated with diesel emissions because of the high fraction of the $PM_{2.5}$ present as BC (Table 6.1), and because of the significant reduction in concentration of the factors on weekends (see Figure 6.5). The lack of well-defined edges along the X and Y axis for the three comparisons in Figure 6.6 indicates the 3 diesel factors are independent of each other. Factor 4 was assumed to be associated with emission from automobiles because of the absence of BC in the profile and strong correlation with traffic (see Figure 6.5). This included morning and evening rush hour peaks during the week days, and the lack of these peaks on the weekend. To better delineate the differences in the four sources, the average of the diurnal pattern for each factor on those days with maximum concentrations from Factor 1 and Factor 2 (Thursday and Friday) were compared (see Figure

6.7). Factors 1 and 2 had similar diurnal time patterns (Figure 6.5), in that both began to increase early in the morning.

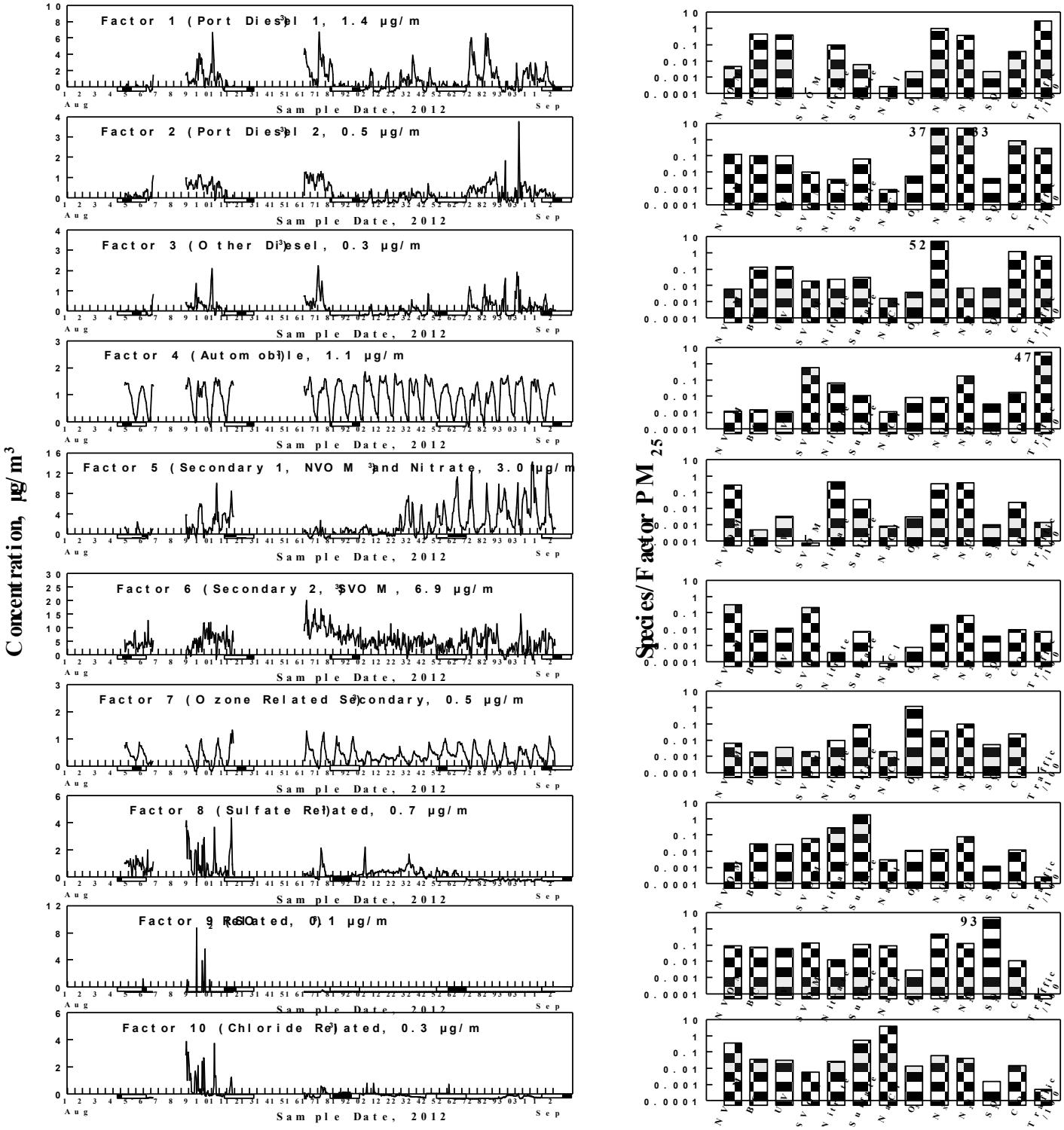

Figure 6.5 The factor profiles and concentrations for the ten identified factors.

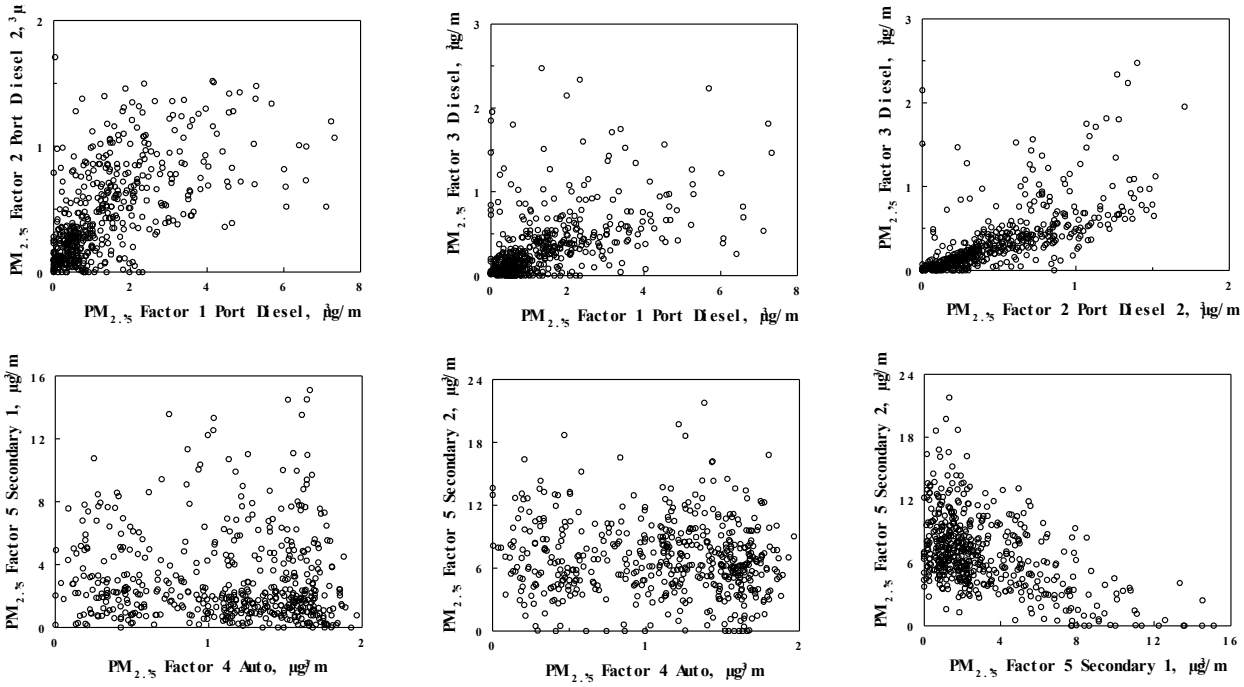

Figure 6.6 G-Space edge analysis of 3 diesel related factors.

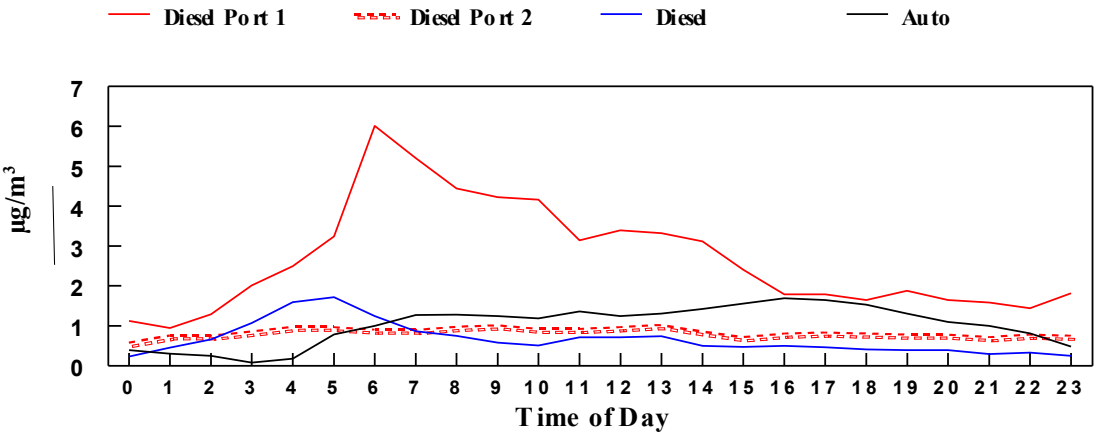

Figure 6.7 Compatrison of average concentrations for diesel and auto factors. Factors 1,2,3 and 4 are marked as diesel port 1, diesel port 2, diesel, and auto, respectively.

Factor 4 is associated with emissions from gasoline burning automobiles. The BC in this factor is very low and the factor is strongly associated with traffic (see Table 6.1 and Figure 6.8). A comparison between the $PM_{2.5}$ in Factor 4 for all hourly samples where the PMF analysis was done and total traffic count for all hourly samples is shown in Figure 6.10. The weekday

morning and afternoon rush hour events are clearly seen in both data sets. In addition, these rush hour peaks are absent during the weekend in both data sets.

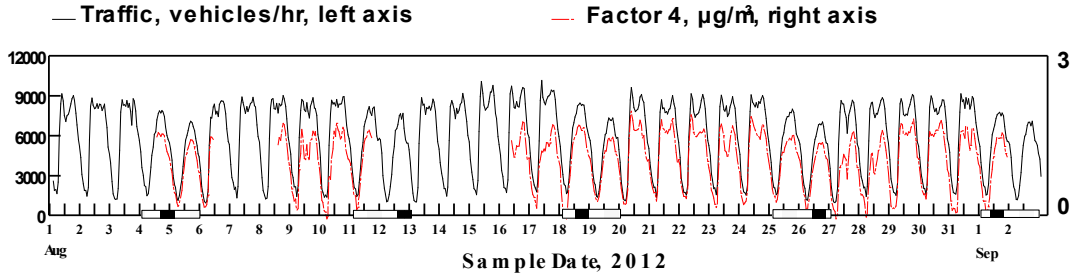

Figure 6.8 Comparison of traffic count with Factor 4 concentration.

Factors 5, 6 and 7 are identified in Figure 6.5 as being associated with the formation of secondary $PM_{2.5}$, rather than associated with primary emissions. This is because the factor profiles are generally associated with components expected to be important in secondary processes, e.g., NVOM, ammonium nitrate, SVOM and (to a lesser extent) ammonium sulfate. The concentrations of the $PM_{2.5}$ associated with these factors also do not have time patterns similar to the patterns associated with the first four traffic-related factors. The G-Space edge analysis plots also indicated that the two major secondary factors 5 and 6 are not related to each other or to the auto factor 4 (Figure 6.6). The characteristics of these three factors with respect to the potential secondary material is given in Table 6.2, along with the name with which they are associated in Figure 6.7.

Factor 5 is dominated by the presence of NVOM (52% of the factor mass) and ammonium nitrate (85% of the factor mass) and only minor contribution from other particulate species (Figure 6.5 and Table 2). As indicated, the ratio of factor species to factor mass is 1.45, and poor closure is seen between these two species mass and factor mass. Mass closure was reasonable for all other factors.

Table 6.2 Characteristics of the three factors associated with formation of secondary $PM_{2.5}$.

#	Factor Name	Avg. µg/m³	NVOM/$PM_{2.5}$ (%NVOM)	Nitrate/$PM_{2.5}$ (% Nit.)	SVOM/$PM_{2.5}$ (%SVOM)	Sulfate/$PM_{2.5}$ (% Sul.)	% Traffic
5	NVOM & Nitrate	3.2	0.52 (27%)	0.85 (80%)	0.00 (0%)	0.07 (7%)	0.0[a]
6	SVOM	6.8	0.59 (65%)	0.001 (0%)	0.41 (68%)	0.01 (2%)	0.1
7	Ozone Related[b]	0.6	0.02 (0%)	0.10 (2%)	0.003 (0%)	0.19 (4%)	0.0
	% Species In Other Factors		8% (In diesel factors)	17% (In diesel & auto)	32% (In auto)	87% (Sulfate)	

Factors 5 and 6 can be considered in relation to the meteorology. Generally, the nitrate in Factor 5 was high when the organic material in Factor 6 was low and vice versa. The nitrate was high from Aug 26-Sep 2 while the organics were high from Aug 16-21. In both periods, ambient temperatures in the LA Basin were 3-6 °C warmer than normal. In the Aug 16-21 period, the night minimums were 21 to 24 °C, warm for the LA Basin. The relative humidity was higher due to a combination of SE monsoonal flow and variable high clouds in the area. There was no stratus in the basin and the mixing heights were low, ranging from 120 to 200 m increasing to 400 m at the end of the period. The afternoon sea breeze was weak particularly at the beginning of the period when organic concentrations were highest.

There were subtle differences between the two periods. From Aug 26-Sep 2, the ambient maximum surface temperatures were comparable. However, the minimums were lower, closer to normal, ranging from 12 to 20.5 °C. The air mass was drier with mostly a southwestly flow off the Pacific. The mixing heights were comparable. However, the sea breeze was stronger. The lower dew points in the deserts led to hotter day time temperatures.

The relative importance of Factor 5 (the nitrate and NVOM containing secondary factor) is much higher from Aug 26 through the end of the study, and less significant on Aug 9, 10, 24 and 25, and minimal on all other days. These patterns are consistent with the presence of stratus cloud moisture as summarized in the meteorological section above. Thus the conversion of precursors to the factor secondary material may be directly related to atmospheric water content. The formation of this factor is also enhanced during the day, as compared to the night (Figure 6.5).

In contrast, Factor 6 contains both NVOM and SVOM; however, none of the other secondary factors have significant amount of SVOM. The formation of this factor does not show a significant day-night variation and the concentrations of the factor are highest on days when stratus clouds, and the accompanying moisture, is not present (see Figure 6.5 and the meteorological section).

Finally the diurnal pattern for Factor 8 is consistent with changes in ozone concentrations, and 93% of the ozone contribution to the PMF solution is contained in this factor. The PMF solution did not describe the composition of this factor well, with only 34% of the factor mass being accounted for, ammonium nitrate and sulfate being the most important contributors to the factor mass (see Figure 6.5 and Table 6.2).

For the species which might be formed by secondary processes, all but 8% of the NVOM, 13% of the ammonium nitrate and 32% of the SVOM were associated with the secondary factors. The remainder of the mass was either associated with primary diesel or diesel and automotive factors (see Table 6.2). None of the secondary factors were strongly associated with the meteorological transport vectors.

The final three factors are very irregular in the factor time pattern and are either dominated by the influence of sulfate, SO_2 or chloride and are so named (Figure 6.5). Possible sources of either the sulfate or SO_2 (Factors 8 and 9, respectively), are ship traffic emissions (incoming or at port), or nearby refinery emissions, possible during flare upsets. The meteorological data eliminates the importance of the port or ships at sea as important contributors to these two factors. Generally, when episodes of these two factors were present transport was either from the east, northeast or west of the sampling site and the transport winds were weak. The SCAQMD keeps logs of locations and significance of refinery upsets. Under normal operations, the refinery downwind ambient AQ signal was small/negligible for both SO_2 and sulfate. However, during upset and flare periods at a nearby 3.5 km upwind refinery, from PMF analysis, the SO_2, sulfate and chloride related factor concentrations (8-10) were significant (see Figure 6.5). The suggested impact by emissions from the refinery appears to be corroborated by the WRF streamline analyses.

An excellent example of this impact occurred Aug 8-11, when high concentrations of the three factors were correlated with the Palo Verde convergence zone lee side stagnation. Figure 9 illustrates this condition. The Palo Verde peninsula and hills are about 500 m high, rising next to the Pacific Ocean. Winds can go around both sides of these hills as shown in Figure 6.9. A convergence/stagnation zone then forms on the lee side of these hills. This is in the general area of the BP/Arco refinery. Later this same day, the afternoon westerlies took over, essentially removing the convergence zone (Figure 6.9). This pattern was repeated several times during Aug 8-11. There was a good correlation between these two wind patterns and the pollutant levels. When stagnation conditions prevailed, the pollutant concentrations increased and vice versa when the westerlies took over.

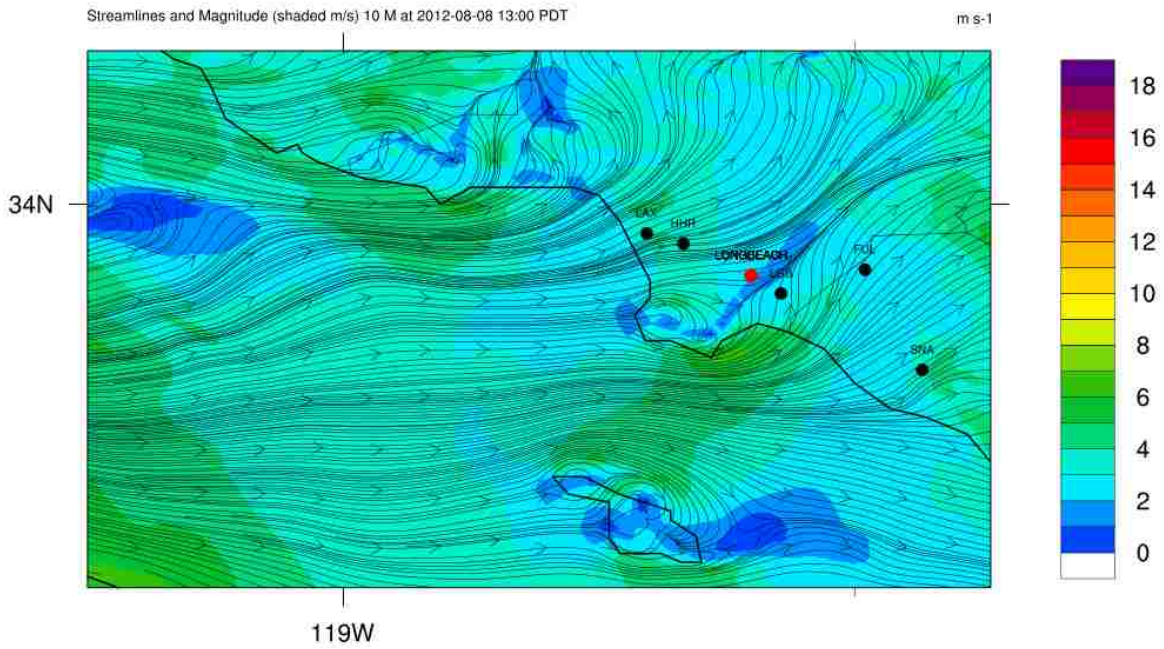

Figure 6.9 Streamlines and magnitudes in the Long Beach area resulting in a stagnation zone.

Factors 8 and 10 are dominated by sulfate and chloride, respectively. The data in Figure 6.10 indicate an excellent correlation between these two factors, indicating both are emitted from the refinery under similar conditions. Sulfur oxides can be emitted from several oil refinery processes including catalytic cracking, sulfur recovery plant, steam boiler, process furnace or process heater. Chloride is emitted (as HCl) during catalytic reforming. Emissions of chloride and sulfur oxides are comparable (refinery emissions). Conversion of emitted SO_2 to sulfate in a steam vent can be expected to be rapid. These refinery emission conditions are consistent with the data in Figure 6.10.

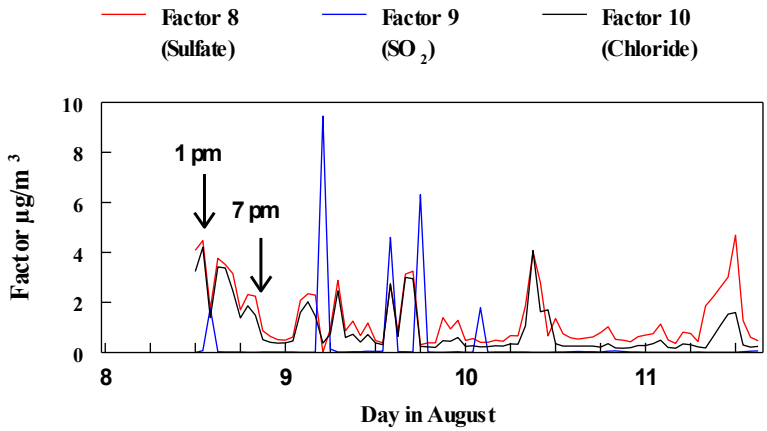

Figure 6.10 Comparison of 3 refinery related factors.

6.5 Conclusions

PMF2 analysis of sources of $PM_{2.5}$ during the I-710 2012 study were greatly aided by the use of hourly average data. Three different diesel sources were identified, 2 of which are associated with port activity. Both SO_2 and a SO_4 related sources were seen, possibly due to local refinery emissions. Meteorological data greatly aided in the interpretation of the results, and excluded the possibility of at-sea port associated traffic. Increases in pollution were seen when meteorological conditions created a stagnation zone near the sampling site.

6.6 Chapter References

27. Grover, B. D.; Eatough, D. J., Source apportionment of one-hour semi-continuous data using positive matrix factorization with total mass (nonvolatile plus semi-volatile) measured by the R&P FDMS monitor. *Aerosol Science and Technology* **2008,** *42* (1), 28-39.
94. Venn, A. J.; Lewis, S. A.; Cooper, M.; Hubbard, R.; Britton, J., Living near a main road and the risk of wheezing illness in children. *American Journal of Respiratory and Critical Care Medicine* **2001,** *164* (12), 2177-2180.
95. Brunekreef, B.; Janssen, N. A. H.; deHartog, J.; Harssema, H.; Knape, M.; vanVliet, P., Air pollution from truck traffic and lung function in children living near motorways. *Epidemiology* **1997,** *8* (3), 298-303.
96. Perez, L.; Lurmann, F.; Wilson, J.; Pastor, M.; Brandt, S. J.; Kunzli, N.; McConnell, R., Near-Roadway Pollution and Childhood Asthma: Implications for Developing "Win-Win" Compact Urban Development and Clean Vehicle Strategies. *Environmental Health Perspectives* **2012,** *120* (11), 1619-1626.

97. Lin, S.; Munsie, J. P.; Hwang, S. A.; Fitzgerald, E.; Cayo, M. R., Childhood asthma hospitalization and residential exposure to state route traffic. *Environmental Research* **2002,** *88* (2), 73-81.
98. Institute, H. E., Traffic-Related Air Pollution: A Critical Review of the Literature on Emissions, Exposure, and Health Effects. In *HEI Special Report*, Institute, H. E., Ed. 2010; Vol. 17.
99. Fruin, S.; Westerdahl, D.; Sax, T.; Sioutas, C.; Fine, P. M., Measurements and predictors of on-road ultrafine particle concentrations and associated pollutants in Los Angeles. *Atmospheric Environment* **2008,** *42* (2), 207-219.
100. Westerdahl, D.; Fruin, S.; Sax, T.; Fine, P. M.; Sioutas, C., Mobile platform measurements of ultrafine particles and associated pollutant concentrations on freeways and residential streets in Los Angeles. *Atmospheric Environment* **2005,** *39* (20), 3597-3610.
101. Westerdahl, D.; Fruin, S. A.; Fine, P. L.; Sioutas, C., The Los Angeles International Airport as a source of ultrafine particles and other pollutants to nearby communities. *Atmospheric Environment* **2008,** *42* (13), 3143-3155.
102. Hu, S. S.; Paulson, S. E.; Fruin, S.; Kozawa, K.; Mara, S.; Winer, A. M., Observation of elevated air pollutant concentrations in a residential neighborhood of Los Angeles California using a mobile platform. *Atmospheric Environment* **2012,** *51*, 311-319.
103. Zhu, Y. F.; Hinds, W. C.; Kim, S.; Shen, S.; Sioutas, C., Study of ultrafine particles near a major highway with heavy-duty diesel traffic. *Atmospheric Environment* **2002,** *36* (27), 4323-4335.
104. Zhu, Y. F.; Hinds, W. C.; Kim, S.; Sioutas, C., Concentration and size distribution of ultrafine particles near a major highway. *Journal of the Air & Waste Management Association* **2002,** *52* (9), 1032-1042.
105. Kozawa, K. H.; Winer, A. M.; Fruin, S. A., Ultrafine particle size distributions near freeways: Effects of differing wind directions on exposure. *Atmospheric Environment* **2012,** *63*, 250-260.
106. Kozawa, K. H.; Fruin, S. A.; Winer, A. M., Near-road air pollution impacts of goods movement in communities adjacent to the Ports of Los Angeles and Long Beach. *Atmospheric Environment* **2009,** *43* (18), 2960-2970.
107. Grover, B. D.; Kleinman, M.; Eatough, N. L.; Eatough, D. J.; Cary, R. A.; Hopke, P. K.; Wilson, W. E., Measurement of fine particulate matter nonvolatile and semi-volatile organic material with the Sunset Laboratory Carbon Aerosol Monitor. *Journal of the Air & Waste Management Association* **2008,** *58* (1), 72-77.
108. Eatough, D. J. *Semi-continuous Monitoring and the Source Apportionment of PM2.5 Mass and Its Constituents. Final Report on NSF ATM-0407695*; 2008.
109. Waldron, K. M.; Paegle, J.; Horel, J. D., Sensitivity of a spectrally filtered and nudged limited-area model to outer model options. *Monthly Weather Review* **1996,** *124* (3), 529-547.
110. Paatero, P., Least squares formulation of robust non-negative factor analysis. *Chemometrics and Intelligent Laboratory Systems* **1997,** *37* (1), 23-35.
111. Polissar, A. V.; Hopke, P. K.; Paatero, P., Atmospheric aerosol over Alaska - 2. Elemental composition and sources. *Journal of Geophysical Research-Atmospheres* **1998,** *103* (D15), 19045-19057.
112. Paatero, P.; Hopke, P. K.; Begum, B. A.; Biswas, S. K., A graphical diagnostic method for assessing the rotation in factor analytical models of atmospheric pollution. *Atmospheric Environment* **2005,** *39* (1), 193-201.

7 CONCLUSIONS AND FUTURE WORK

The collection of hourly averaged data in the Lindon, UT, 2012, and Roubidoux, CA, 2003, studies signifies the need for alternative instrumentation and the need for shorter averaging times if measured urban visibility is to be related to human perception. In areas where an FDMS TEOM is used to measure $PM_{2.5}$, high humidity causes an underestimation of light extinction due to PM bound water. This occurs because the particle-bound water has a sharp increase once the deliquescence point of NH_4NO_3 and $(NH_4)_2SO_4$ is reached. In areas where hourly speciation data is not available, the calculation of light scattering will be skewed, especially if a 24-h averaged value of NH_4NO_3 is used to calculate the MLEE, thus creating a bias for over-estimating light scattering during times when RH is high and NH_4NO_3 levels are actually low. This is especially the case at nighttime. More significantly, the EPA proposed standard will not account for diurnal variation of visibility degradation and, therefore, it will poorly relate to human visibility assessment. The correlations between particle mass and scattering reported here would be improved by the use of instruments akin to the GRIMM model 1100 monitor, which measures particle associated water. Furthermore, obtaining data using a nephelometer and a GRIMM model 1100 monitor together would show the accuracy of scattering measurements based on reliable mass measurement systems (such as the GRIMM). Such measurements are recommended.

During the Salt Lake Valley, UT, 2009 study, ammonium nitrate averaged 40% of the total $PM_{2.5}$ in the absence of inversions and 69% during strong inversions. Ammonium nitrate formation was nitric acid limited, with a large excess of ammonia present. Sulfates and nitrites together constitute 7% during inversion and 11% outside of inversion periods of the total $PM_{2.5}$ and are not as significant as ammonium nitrate. Ozone levels throughout the study remained well below EPA limits. Overall, the lower boundary layer in the Salt Lake Valley was found to be oxidant and VOC deficient with respect to ozone formation. Because ozone levels during the study remained well within EPA standards, the most effective way of reducing contributions of ammonium nitrate to secondary particle formation during the inversion periods is to decrease NOx emissions. However, a decrease in NOx will increase ozone concentrations. A complete ozone isopleth would further inform this decision.

The GC-MS Organic Aerosol Monitor provides invaluable information concerning air pollution and its sources by obtaining speciated data for individual organic compounds with time resolution of 1 h. Laboratory results indicate that the OAM performs well at overcoming matrix effects for the samples collected in this study. Field results show that daily peaks in levoglucosan and elemental carbon are highly correlated and confirm the presence of evening wood smoke for the region studied herein. By running autonomously in the field, the GC-MS OAM has the capability to monitor organic aerosol in depth and further characterize air pollution and its sources.

A simple pre-concentration unit and miniaturized GC assembly has been developed and tested using atmospheric samples. This system can potentially be used for field GC, and GC-MS instrumentation. The simplicity of the system is demonstrated by the fact that all components of the PCC and GC were assembled in the laboratory without specialized equipment. The PCC unit

and GC assembly were integrated into the GC-MS OAM, and have been used for in-field separation and detection of environmentally relevant organic compounds, such as PAHs, levoglucosan, and other organic acids. The PCC unit is particularly useful for enhanced fast separation of levoglucosan.

For future work it is intended to upgrade the GC-MS OAM platform. A 3-dimentional sketch of the future embodiment of the instrument is shown in Figure 7.1.

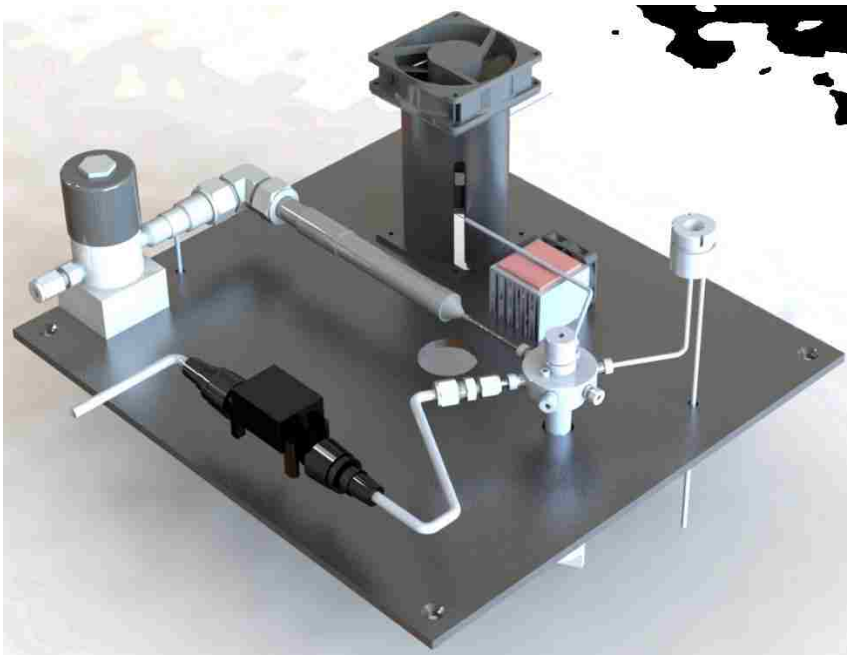

Figure 7.1 Three dimentional rendition of the instrument schematic. Compare Figure 4.1. Included in this image is the desorption chmber, 6 port valve, PCC, GC housing, injection port, and a sample flow meter. The mass spectrometer(not shown here) will sit on the back right side of the image.

Future work also includes integrating VOC sampling into the GC-MS OAM. This can be done by integrating a sorbent tube into the sampling stream following the filter as shown in Figure 7.2, or by splitting the sample flow as shown in Figure 7.3. This would provide a complete knowledge of the organic compounds that exist in air pollution. The addition of a sorbent trap would also greatly aid in characterizing the organics that are lost from the filter during sampling. This could be done by collecting a sample, or injecting standard onto the filter,

followed by passing clean air across the filter and trapping any organics that evaporate. A complete step by step explanation of Figures 7.2 and 7.3 is provided in the appendix.

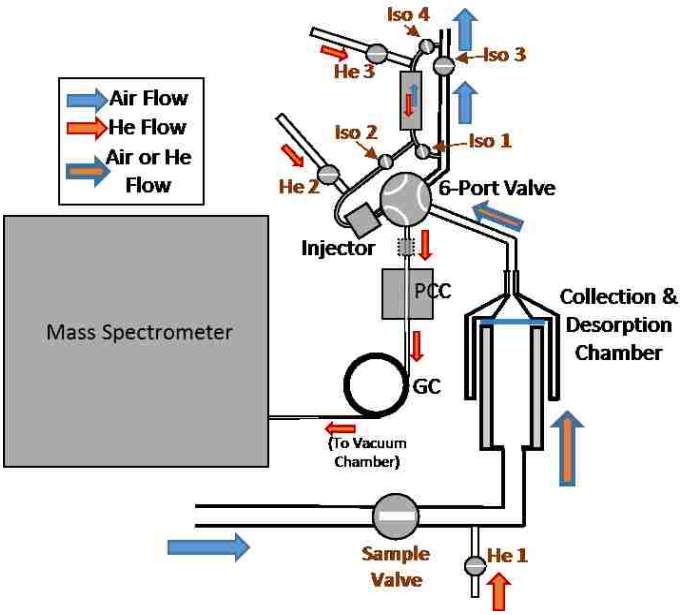

Figure 7.2 Detailed diagram showing structure of a second embodiment of the GC-MS OAMthat includes a sorption tube for collecting volatile organic compounds that are not collected by the filter in the thermal desorption chamber.

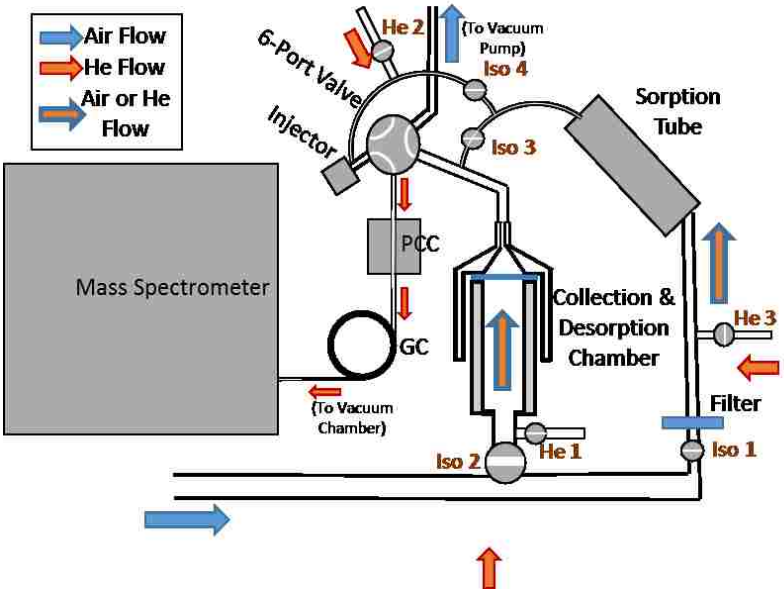

Figure 7.3 Detailed diagram showing structure of a third embodiment of the GC-MS OAM that includes a sorption tube for collecting volatile organic compounds that are not collected by the filter in the thermal desorption chamber.

Finally, further development of the GC-MS OAM also includes the need for further method validation. It is necessary to test how well the GC-MS OAM quantifies organic compounds by comparing results to other methods, such as traditional solvent extraction methods. The results here show that the GC-MS OAM works, but the quality of information provided must still be tested. This instrumentation represents important advances in air sampling technology at a time when the need to characterize organic aerosol is significant. The information provided by the instrument has the potential to improve source apportionment models, further general knowledge of organic aerosol chemistry, and further relate health effects to individual organic compounds.

8 APPENDIX-VOC SORBENT TRAP

This section contains text from the patent that describes integration of a sorbent trap, referring to Figures 7.2 and 7.3. See the full patent text for more information including claims and description of prior art. Patent application number 62058757; EFS ID 20309415.

8.1 Detailed Description of VOC Sampling

The first embodiment of the invention describes a GC-MS OAM that may autonomously monitor aerosol or particle phase organics. However, the present invention may also be modified to perform volatile organic compound (VOC) monitoring. This may be accomplished as shown in Figures 7.2 and 7.3.

The time utilization of the GC-MS OAM may be divided between collection and analysis. The majority of the time may be spent collecting a sample. The following description including time spent on tasks and on physical dimensions is for illustration purposes only and should not be considered as limiting the operation or structure of the second and third embodiments.

Suppose that the OAM may collect a sample over a period of 20 to 45 minutes. Then the OAM may spend 10 to 15 minutes performing the analysis of the aerosol sample that was collected. Therefore, a single cycle of collection, separation and detection may take up to an hour. It was determined that the OAM may be capable of performing analysis of volatile organic compounds (VOCs) in air at the same time as the OAM is performing collection of the aerosol

sample from air. Thus, if the OAM may only spend 10 minutes to perform separation and detection of the aerosol component of air, then the time spent collecting the sample for aerosol analysis may be used for separation and detection of the VOCs.

The second and third embodiments describe the addition of a sorption tube as shown in Figures 7.2 and 7.3. The sorption tube may be a tube approximately one half inch in diameter that is filled with a sorbent material. The sorbent material may be selected to have an affinity for VOCs, such as activated carbon. While the aerosol particles are caught by the filter in the thermal desorption chamber, the gas phase organics that are more volatile may pass through the filter and become trapped in the sorption tube. After the particle sample is collected in the thermal desorption chamber, the thermal desorption chamber is heated so that the aerosol sample is then swept into the GC and mass spectrometer for separation and detection. When this process is completed, the GC may be cooled so that the VOCs collected in the sorption tube may be analyzed. Accordingly, the sorption tube may be heated and the VOC sample may be swept into the GC and the mass spectrometer for separation and detection.

Figures 7.2 and 7.3 illustrate second and third embodiments of the invention having different placement of the sorption tube and various valves that enable the two different samples to be analyzed at different times. It should be understood that the second and third embodiments show only two of the possible designs of the OAM that may be constructed to enable a flow to and from the sorption tube to obtain quantitative measurements of the VOCs after particle phase analysis is complete.

In the second embodiment shown in Figure 7.2, the following timeline of events is provided to enable operation of the system to perform particle phase and VOC analysis. It should be understood that He1, He2 and He3 refer to the valves that provide helium to the

system. Furthermore, Iso1, Iso2, Iso3 and Iso4 refer to isolation valves that control sample and helium flow.

When the system is idle for routine injections and calibration: Iso2 is closed and He2 is open for regular injection in the GC-MS OAM system.

For Sampling: For collection of particles on the filter, and VOCs on the sorption tube, the entire sample flow may be collected through the sorption tube, or just a fraction. The sample valve is open and He1 is closed. The 6-port valve is open between vacuum pump and chamber. Iso1, Iso3 and Iso4 are all open, and the amount of flow split to the sorption tube is controlled. Iso2 is closed. He2 is open for continuous helium flow to the GC column assembly, and He3 is closed.

For Particle Desorption & Analysis: The Sample Valve is closed. He1 is open and the chamber is compressed and heated. The 6-port valve is open between the chamber and the PCC/GC. Iso1, Iso2, and Iso4 are closed as the sample in the sorption tube awaits analysis.

For VOC Desorption & Analysis: Helium is used to transfer the sample from the sorption tube to the GC-MS, while the sorption tube is heated to release the VOCs. The 6-Port valve is open between the Injector and the PCC/GC. Iso1 and Iso4 are closed, He3 is open, Iso2 is open and He2 is closed.

For the third embodiment shown in Figure 7.3, it should be noted that an extra filter may need to be disposed between Iso1 and the sorption tube as shown.

For idling when performing routine injections and calibration: Iso4 is closed, and He2 is open for regular injection into the GC-MS system.

For Sampling: For collection of particles on the filter, and VOCs on the sorption tube. The sample flow is split between the chamber and the sorption tube. Iso1, Iso2, Iso3 are open and the amount of flow split to the sorption tube is controlled. He1, and He3 and Iso4 are closed. The 6-port valve is open between the vacuum pump and the chamber.

For Particle Desorption & Analysis: The Sample Valve is closed. He1 is open and the chamber is compressed and heated. The 6-port valve is open between the chamber and the PCC/GC. Iso1, Iso3 and Iso4 are closed as the sample in sorption tube awaits analysis.

For VOC Desorption & Analysis: Helium may be used to transfer the sample from the sorption tube to the GC-MS, while the sorption tube is heated to release the VOCs. The 6-Port valve is open between the Injector and the PCC/GC. Iso1, Iso3 and He2 are closed. He3 is open and Iso4 is open.

It should be understood that all temperatures and dimensions cited in this document are for illustration purposes only for embodiments of the invention and should not be considered to be limiting of the temperatures and dimensions that may be used in other embodiments. Accordingly, modifications to the temperatures and dimensions should be considered to be within the scope of the embodiments of the invention.

9 REFERENCES

1. Heagle, A. S.; Body, D. E.; Neely, G. E., Injury and Yield Responses of Soybean to Chronic Doses of Ozone and Sulfur-Dioxide in Field. *Phytopathology* **1974,** *64* (1), 132-136.
2. Fuhrer, J.; Skarby, L.; Ashmore, M. R., Critical levels for ozone effects on vegetation in Europe. *Environmental Pollution* **1997,** *97* (1-2), 91-106.
3. Kampa, M.; Castanas, E., Human health effects of air pollution. *Environmental Pollution* **2008,** *151* (2), 362-367.
4. Comes, F. J., Recycling in the Earths Atmosphere - the Oh Radical - Its Importance for the Chemistry of the Atmosphere and the Determination of Its Concentration. *Angewandte Chemie-International Edition in English* **1994,** *33* (18), 1816-1826.
5. Sharma, M.; Kishore, S.; Tripathi, S. N.; Behera, S. N., Role of atmospheric ammonia in the formation of inorganic secondary particulate matter: A study at Kanpur, India. *Journal of Atmospheric Chemistry* **2007,** *58* (1), 1-17.
6. Hao, L. Q.; Wang, Z. Y.; Huang, M. Q.; Fang, L.; Zhang, W. J., Effects of seed aerosols on the growth of secondary organic aerosols from the photooxidation of toluene. *Journal of Environmental Sciences-China* **2007,** *19* (6), 704-708.
7. Pandis, S. N.; Harley, R. A.; Cass, G. R.; Seinfeld, J. H., Secondary Organic Aerosol Formation and Transport. *Atmospheric Environment Part a-General Topics* **1992,** *26* (13), 2269-2282.
8. Kroll, J. H.; Seinfeld, J. H., Chemistry of secondary organic aerosol: Formation and evolution of low-volatility organics in the atmosphere. *Atmospheric Environment* **2008,** *42* (16), 3593-3624.
9. Volkamer, R.; Jimenez, J. L.; San Martini, F.; Dzepina, K.; Zhang, Q.; Salcedo, D.; Molina, L. T.; Worsnop, D. R.; Molina, M. J., Secondary organic aerosol formation from anthropogenic air pollution: Rapid and higher than expected. *Geophysical Research Letters* **2006,** *33* (17).
10. Dockery, D. W.; Pope, C. A., Acute Respiratory Effects of Particulate Air-Pollution. *Annual Review of Public Health* **1994,** *15*, 107-132.
11. Smith, R. L.; Davis, J. M.; Sacks, J.; Speckman, P.; Styer, P., Regression models for air pollution and daily mortality: analysis of data from Birmingham, Alabama. *Environmetrics* **2000,** *11* (6), 719-743.
12. EPA National Ambient Air Quality Standards (NAAQS). http://www.epa.gov/air/criteria.html (accessed 08 February, 2013).
13. Elias, V. O.; Simoneit, B. R. T.; Cordeiro, R. C.; Turcq, B., Evaluating levoglucosan as an indicator of biomass burning in Carajas, Amazonia: A comparison to the charcoal record. *Geochimica et Cosmochimica Acta* **2001,** *65* (2), 267-272.
14. Simoneit, B. R. T.; Schauer, J. J.; Nolte, C. G.; Oros, D. R.; Elias, V. O.; Fraser, M. P.; Rogge, W. F.; Cass, G. R., Levoglucosan, a tracer for cellulose in biomass burning and atmospheric particles. *Atmospheric Environment* **1999,** *33* (2), 173-182.
15. Lin, L.; Lee, M. L.; Eatough, D. J., Gas chromatographic analysis of organic marker compounds in fine particulate matter using solid-phase microextraction. *Journal of the Air & Waste Management Association* **2007,** *57* (1), 53-58.

16. Schauer, J. J.; Kleeman, M. J.; Cass, G. R.; Simoneit, B. R. T., Measurement of emissions from air pollution sources. 2. C-1 through C-30 organic compounds from medium duty diesel trucks. *Environmental Science & Technology* **1999,** *33* (10), 1578-1587.
17. Chow, J. C.; Watson, J. G.; Lowenthal, D. H.; Chen, L. W. A.; Zielinska, B.; Mazzoleni, L. R.; Magliano, K. L., Evaluation of organic markers for chemical mass balance source apportionment at the Fresno Supersite. *Atmospheric Chemistry and Physics* **2007,** *7* (7), 1741-1754.
18. Elsasser, M.; Crippa, M.; Orasche, J.; DeCarlo, P. F.; Oster, M.; Pitz, M.; Cyrys, J.; Gustafson, T. L.; Pettersson, J. B. C.; Schnelle-Kreis, J.; Prevot, A. S. H.; Zimmermann, R., Organic molecular markers and signature from wood combustion particles in winter ambient aerosols: aerosol mass spectrometer (AMS) and high time-resolved GC-MS measurements in Augsburg, Germany. *Atmospheric Chemistry and Physics* **2012,** *12* (14), 6113-6128.
19. Schauer, J. J.; Rogge, W. F.; Hildemann, L. M.; Mazurek, M. A.; Cass, G. R.; Simoneit, B. R. T., Source apportionment of airborne particulate matter using organic compounds as tracers. *Atmospheric Environment* **1996,** *30* (22), 3837-3855.
20. Zheng, M.; Ke, L.; Edgerton, E. S.; Schauer, J. J.; Dong, M. Y.; Russell, A. G., Spatial distribution of carbonaceous aerosol in the southeastern United States using molecular markers and carbon isotope data. *Journal of Geophysical Research-Atmospheres* **2006,** *111* (D10).
21. Bruns, E. A.; Perraud, V.; Greaves, J.; Finlayson-Pitts, B. J., Atmospheric Solids Analysis Probe Mass Spectrometry: A New Approach for Airborne Particle Analysis. *Analytical Chemistry* **2010,** *82* (14), 5922-5927.
22. Jayne, J. T.; Leard, D. C.; Zhang, X. F.; Davidovits, P.; Smith, K. A.; Kolb, C. E.; Worsnop, D. R., Development of an aerosol mass spectrometer for size and composition analysis of submicron particles. *Aerosol Science and Technology* **2000,** *33* (1-2), 49-70.
23. Lee, S.; Liu, W.; Wang, Y. H.; Russell, A. G.; Edgerton, E. S., Source apportionment of PM2.5: Comparing PMF and CMB results for four ambient monitoriniz sites in the southeastern United States. *Atmospheric Environment* **2008,** *42* (18), 4126-4137.
24. Docherty, K. S.; Stone, E. A.; Ulbrich, I. M.; DeCarlo, P. F.; Snyder, D. C.; Schauer, J. J.; Peltier, R. E.; Weber, R. J.; Murphy, S. M.; Seinfeld, J. H.; Grover, B. D.; Eatough, D. J.; Jimenez, J. L., Apportionment of Primary and Secondary Organic Aerosols in Southern California during the 2005 Study of Organic Aerosols in Riverside (SOAR-1). *Environmental Science & Technology* **2008,** *42* (20), 7655-7662.
25. Martello, D. V.; Pekney, N. J.; Anderson, R. R.; Davidson, C. I.; Hopke, P. K.; Kim, E.; Christensen, W. F.; Mangelson, N. F.; Eatough, D. J., Apportionment of ambient primary and secondary fine particulate matter at the Pittsburgh National Energy Laboratory particulate matter characterization site using positive matrix factorization and a potential source contributions function analysis. *Journal of the Air & Waste Management Association* **2008,** *58* (3), 357-368.
26. Schauer, J. J.; Cass, G. R., Source apportionment of wintertime gas-phase and particle-phase air pollutants using organic compounds as tracers. *Environmental Science & Technology* **2000,** *34* (9), 1821-1832.
27. Grover, B. D.; Eatough, D. J., Source apportionment of one-hour semi-continuous data using positive matrix factorization with total mass (nonvolatile plus semi-volatile) measured by the R&P FDMS monitor. *Aerosol Science and Technology* **2008,** *42* (1), 28-39.
28. Cropper, P. M.; Hansen, J. C.; Eatough, D. J., Measurement of light scattering in an urban area with a nephelometer and PM2.5 FDMS TEOM monitor: Accounting for the effect of water. *Journal of the Air & Waste Management Association* **2013,** *63* (9), 1004-1011.

29. EPA, U. S. E. P. A. *National Ambient Air Quality Standards for Particulate Matter; Proposed Rule*; FRL-9682-9

EPA-HQ-OAR-2007-0492; Federal Register/ Vo. 77, No. 126, 2012; pp 38889-39055.
30. EPA, U. S. E. P. A., Policy Assessment for the Review of the Particulate Matter National Ambient Air Quality Standards. Agency, U. S. E. P., Ed. Federal Register: 2011; Vol. 77, pp 38889-39055.
31. DeBell, L. J.; Gebhart, K. A.; Hand, J.; Malm, W. C.; Pitchford, M.; Schichtel, B.; White, W. H. Interagency Monitoring of Protected Visual Environments (IMPROVE): Spatial and Seasonal Patterns and Temporal Variability of Haze and its Constituents in the United States: Report IV 2006. (accessed November 2006).
32. Hyslop, N. P., Impaired visibility: the air pollution people see. *Atmospheric Environment* **2009,** *43* (1).
33. Grover, B. D.; Eatough, N. L.; Woolwine, W. R.; Eatough, D. J.; Cary, R. A., Modifications to the Sunset Laboratory Carbon Aerosol Monitor for the Simultaneous Measurement of PM2.5 Nonvolatile and Semi-Volatile Carbonaceous Material. *Journal of the Air & Waste Management Association* **2009,** *59* (8).
34. Grover, B. D.; Eatough, N. L.; Woolwine, W. R.; Cannon, J. P.; Eatough, D. J.; Long, R. W., Semi-continuous mass closure of the major components of fine particulate matter in Riverside, CA. *Atmospheric Environment* **2008,** *42* (2).
35. Obeidi, F.; Eatough, N. L.; Eatough, D. J., Use of the RAMS to measure semivolatile fine particulate matter at Riverside and Bakersfield, California. *Aerosol Science and Technology* **2002,** *36* (2).
36. Ding, Y. M.; Pang, Y. B.; Eatough, D. J., High-volume diffusion denuder sampler for the routine monitoring of fine particulate matter: I. Design and optimization of the PC-BOSS. *Aerosol Science and Technology* **2002,** *36* (4).
37. Grimm, H.; Eatough, D. J., Aerosol Measurement: The Use of Optical Light Scattering for the Determination of Particulate Size Distribution, and Particulate Mass, Including the Semi-Volatile Fraction. *Journal of the Air & Waste Management Association* **2009,** *59* (1).
38. Finlayson-Pitts, B. J.; Pitts, J. N. J., *Chemistry of the upper and lower atmosphere : theory, experiments, and applications.* Academic Press: San Diego, 2000.
39. Pitchford, M.; Malm, W.; Schichtel, B.; Kumar, N.; Lowenthal, D.; Hand, J., Revised algorithm for estimating light extinction from IMPROVE particle speciation data. *Journal of the Air & Waste Management Association* **2007,** *57* (11).
40. Hansen, J. C.; Woolwine, W. R., III; Bates, B. L.; Clark, J. M.; Kuprov, R. Y.; Mukherjee, P.; Murray, J. A.; Simmons, M. A.; Waite, M. F.; Eatough, N. L.; Eatough, D. J.; Long, R.; Grover, B. D., Semicontinuous PM2.5 and PM10 Mass and Composition Measurements in Lindon, Utah, during Winter 2007. *Journal of the Air & Waste Management Association* **2010,** *60* (3).
41. Grover, B. D.; Kleinman, M.; Eatough, N. L.; Eatough, D. J.; Hopke, P. K.; Long, R. W.; Wilson, W. E.; Meyer, M. B.; Ambs, J. L., Measurement of total PM(2.)5 mass (nonvolatile plus semivolatile) with the Filter Dynamic Measurement System tapered element oscillating microbalance monitor. *Journal of Geophysical Research-Atmospheres* **2005,** *110* (D7).
42. Tang, I. N.; Wong, W. T.; Munkelwitz, H. R., The relative importance of atmospheric sulfates and nitrate in visibility reduction. *Atmospheric Environment* **1981,** *15* (12).

43. Malm, W. C.; Gebhart, K. A.; Molenar, J.; Cahill, T.; Eldred, R.; Huffman, D., Examining the relationship between atmospheric aerosol and light extinction at Mount-Rainier-National-Park and North-Cascades-National-Park. *Atmospheric Environment* **1994,** *28* (2).
44. Sisler, J. F.; Malm, W. C.; Gebhart, K. A.; Molenar, J.; Cahill, T. In *The effect of relative humidity on visibility - Continental distributions*, Annual AWMA Meeting, Air and Waste Management Association, Pittsburgh, Pittsburgh, 1992.
45. Long, R. W.; Modey, W. K.; Smith, P. S.; Smith, R.; Merrill, C.; Pratt, J.; Stubbs, A.; Eatough, N. L.; Eatough, D. J.; Malm, W. C.; Wilson, W. E., One- and three-hour PM2.5 characterization, speciation, and source apportionment using continuous and integrated samplers. *Aerosol Science and Technology* **2005,** *39* (3), 238-248.
46. Kuprov, R. Y.; Eatough, D. A.; Cruickshank, T.; Olson, N.; Cropper, P. M.; Hansen, J. C., Composition and Secondary Formation of Fine Particulare Matter in the Salt Lake Vally: Winter 2009. *Journal of the Air & Waste Management Association* **2014,** *64* (8), 957-969.
47. EPA NCore. http://www.epa.gov/ttnamti1/ncore/ (accessed August 18).
48. Long, R. W.; Eatough, N. L.; Mangelson, N. F.; Thompson, W.; Fiet, K.; Smith, S.; Smith, R.; Eatough, D. J.; Pope, C. A.; Wilson, W. E., The measurement of PM2.5, including semi-volatile components, in the EMPACT program: results from the Salt Lake City Study. *Atmospheric Environment* **2003,** *37* (31), 4407-4417.
49. Pope, C. A.; Hansen, M. L.; Long, R. W.; Nielsen, K. R.; Eatough, N. L.; Wilson, W. E.; Eatough, D. J., Ambient particulate air pollution, heart rate variability, and blood markers of inflammation in a panel of elderly subjects. *Environmental Health Perspectives* **2004,** *112* (3), 339-345.
50. Grover, B. D.; Eatough, N. L.; Woolwine, W. R.; Cannon, J. P.; Eatough, D. J.; Long, R. W., Semi-continuous mass closure of the major components of fine particulate matter in Riverside, CA. *Atmospheric Environment* **2008,** *42* (2), 250-260.
51. EPA, Quality Assurance Handbook for Air Pollution Measurement Systems Volume II. 2008. http://www.epa.gov/ttnamti1/files/ambient/pm25/qa/QA-Handbook-Vol-II.pdf.
52. Whiteman, C. D.; Bian, X. D.; Zhong, S. Y., Wintertime evolution of the temperature inversion in the Colorado Plateau basin. *Journal of Applied Meteorology* **1999,** *38* (8), 1103-1117.
53. Long, R. W.; Eatough, N. L.; Eatough, D. J.; Meyer, M. B.; Wilson, W. E., Continuous determination of fine particulate matter mass in the Salt Lake City Environmental Monitoring Project: A comparison of real-time and conventional TEOM monitor results. *Journal of the Air & Waste Management Association* **2005,** *55* (12), 1839-1846.
54. Finlayson-Pitts, B. J., *Chemistry of the upper and lower atmosphere : theory, experiments, and applications.* Academic Press: San Diego, 2000; p 969.
55. Clapp, L. J.; Jenkin, M. E., Analysis of the relationship between ambient levels Of O-3, NO2 and NO as a function of NO chi in the UK. *Atmospheric Environment* **2001,** *35* (36), 6391-6405.
56. Pio, C. A.; Harrison, R. M., The Equilibrium of Ammonium-Chloride Aerosol with Gaseous Hydrochloric-Acid and Ammonia under Tropospheric Conditions. *Atmospheric Environment* **1987,** *21* (5), 1243-1246.
57. Mozurkewich, M., The Dissociation-Constant of Ammonium-Nitrate and Its Dependence on Temperature, Relative-Humidity and Particle-Size. *Atmospheric Environment Part a-General Topics* **1993,** *27* (2), 261-270.

58. Eatough, D. J.; Caka, F. M.; Farber, R. J., The Conversion of So2 to Sulfate in the Atmosphere. *Israel Journal of Chemistry* **1994,** *34* (3-4), 301-314.
59. Mannucci, P. M.; Harari, S.; Martinelli, I.; Franchini, M., Effects on health of air pollution: a narrative review. *Internal and Emergency Medicine* **2015,** *10* (6), 657-662.
60. Fiore, A. M.; Naik, V.; Spracklen, D. V.; Steiner, A.; Unger, N.; Prather, M.; Bergmann, D.; Cameron-Smith, P. J.; Cionni, I.; Collins, W. J.; Dalsoren, S.; Eyring, V.; Folberth, G. A.; Ginoux, P.; Horowitz, L. W.; Josse, B.; Lamarque, J. F.; MacKenzie, I. A.; Nagashima, T.; O'Connor, F. M.; Righi, M.; Rumbold, S. T.; Shindell, D. T.; Skeie, R. B.; Sudo, K.; Szopa, S.; Takemura, T.; Zeng, G., Global air quality and climate. *Chemical Society Reviews* **2012,** *41* (19), 6663-6683.
61. Turpin, B. J.; Saxena, P.; Andrews, E., Measuring and simulating particulate organics in the atmosphere: problems and prospects. *Atmospheric Environment* **2000,** *34* (18), 2983-3013.
62. Lee, S. H.; Allen, H. C., Analytical Measurements of Atmospheric Urban Aerosol. *Analytical Chemistry* **2012,** *84* (3), 1196-1201.
63. Wilson, W. E.; Grover, B. D.; Long, R. W.; Eatough, N. L.; Eatough, D. J., The measurement of fine-particulate semivolatile material in urban aerosols. *Journal of the Air & Waste Management Association* **2006,** *56* (4), 384-397.
64. Williams, B. J.; Goldstein, A. H.; Kreisberg, N. M.; Hering, S. V., In situ measurements of gas/particle-phase transitions for atmospheric semivolatile organic compounds. *Proceedings of the National Academy of Sciences of the United States of America* **2010,** *107* (15), 6676-6681.
65. Falkovich, A. H.; Rudich, Y., Analysis of semivolatile organic compounds in atmospheric aerosols by direct sample introduction thermal desorption GC/MS. *Environmental Science & Technology* **2001,** *35* (11), 2326-2333.
66. Williams, B. J.; Goldstein, A. H.; Kreisberg, N. M.; Hering, S. V., An in-situ instrument for speciated organic composition of atmospheric aerosols: Thermal Desorption Aerosol GC/MS-FID (TAG). *Aerosol Science and Technology* **2006,** *40* (8), 627-638.
67. Williams, B. J.; Goldstein, A. H.; Kreisberg, N. M.; Hering, S. V.; Worsnop, D. R.; Ulbrich, I. M.; Docherty, K. S.; Jimenez, J. L., Major components of atmospheric organic aerosol in southern California as determined by hourly measurements of source marker compounds. *Atmospheric Chemistry and Physics* **2010,** *10* (23), 11577-11603.
68. Lin, L.; Lee, M. L.; Eatough, D. J., Review of Recent Advances in Detection of Organic Markers in Fine Particulate Matter and Their Use for Source Apportionment. *Journal of the Air & Waste Management Association* **2010,** *60* (1), 3-25.
69. Kong, R. C.; Woolley, C. L.; Fields, S. M.; Lee, M. L., Deactivation of Small-Diameter Fused-Silica Capillary Columns for Gas and Supercritical Fluid Chromatography. *Chromatographia* **1984,** *18* (7), 362-366.
70. Cropper, P. M.; Goates, S. R.; Hansen, J. C., A compact gas chromatograph and pre-column concentration system for enhanced in-field separation of levoglucosan and other polar organic compounds. *Journal of Chromatography A* **2015,** *1417*, 73-78.
71. Austin, D. E.; Wang, M.; Tolley, S. E.; Maas, J. D.; Hawkins, A. R.; Rockwood, A. L.; Tolley, H. D.; Lee, E. D.; Lee, M. L., Halo ion trap mass spectrometer. *Analytical Chemistry* **2007,** *79* (7), 2927-2932.
72. Lammert, S. A.; Rockwood, A. A.; Wang, M.; Lee, M. L.; Lee, E. D.; Tolley, S. E.; Oliphant, J. R.; Jones, J. L.; Waite, R. W., Miniature toroidal radio frequency ion trap mass analyzer. *Journal of the American Society for Mass Spectrometry* **2006,** *17* (7), 916-922.

73. Kuprov, R. Y.; Buck, D.; Pope, C. A.; Eatough, D. J.; Hansen, J. C., Design and Characterization of a Two-Stage Human Subject Exposure Chamber. *Journal of the Air & Waste Management Association* **2011,** *61* (8), 864-871.
74. Schkolnik, G.; Rudich, Y., Detection and quantification of levoglucosan in atmospheric aerosols: A review. *Analytical and Bioanalytical Chemistry* **2006,** *385* (1), 26-33.
75. Bari, M. A.; Baumbach, G.; Kuch, B.; Scheffknecht, G., Wood smoke as a source of particle-phase organic compounds in residential areas. *Atmospheric Environment* **2009,** *43* (31), 4722-4732.
76. Eatough, D. J.; Long, R. W.; Modey, W. K.; Eatough, N. L., Semi-volatile secondary organic aerosol in urban atmospheres: meeting a measurement challenge. *Atmospheric Environment* **2003,** *37* (9-10), 1277-1292.
77. Nolte, C. G.; Schauer, J. J.; Cass, G. R.; Simoneit, B. R. T., Highly polar organic compounds present in meat smoke. *Environmental Science & Technology* **1999,** *33* (19), 3313-3316.
78. Grall, A.; Leonard, C.; Sacks, R., Peak Capacity, Peak-Capacity Production Rate, and Boiling Point Resolution for Temperature-Programmed GC with Very High Programming Rates. *Analytical Chemistry* **1999,** *72* (3), 591-598.
79. PerkinElmer. The Evolution of Gas Chromatographic Instrumentation at PerkinElmer *The Evolution of Gas Chromatographic Instrumentation at PerkinElmer* [Online], 2005. http://www.perkinelmer.com/CMSResources/Images/44-74443BRO_GasChromaEvolution.pdf (accessed September 2015).
80. Sides, G. D.; Cates, M. Continuous air monitoring apparatus and method. US5014541 A, 1991.
81. Rounbehler, D. P.; Achter, E. K.; Fine, D. H.; Jarvis, G. B.; MacDonald, S. J.; Wheeler, D. B.; Wood, C. D. High speed gas chromatography. US5808178 A, 1998.
82. Maswadeh, W. M.; Snyder, A. P. Hand-held temperature programmable modular gas chromatograph. US5856616 A, 1999.
83. Stadermann, M.; McBrady, A. D.; Dick, B.; Reid, V. R.; Noy, A.; Synovec, R. E.; Bakajin, O., Ultrafast gas chromatography on single-wall carbon nanotube stationary phases in microfabricated channels. *Analytical Chemistry* **2006,** *78* (16), 5639-5644.
84. Collin, W. R.; Serrano, G.; Wright, L. K.; Chang, H. W.; Nunovero, N.; Zellers, E. T., Microfabricated Gas Chromatograph for Rapid, Trace-Level Determinations of Gas-Phase, Explosive Marker Compounds. *Analytical Chemistry* **2014,** *86* (1), 655-663.
85. Serrano, G.; Paul, D.; Kim, S. J.; Kurabayashi, K.; Zellers, E. T., Comprehensive Two-Dimensional Gas Chromatographic Separations with a Microfabricated Thermal Modulator. *Analytical Chemistry* **2012,** *84* (16), 6973-6980.
86. Zampolli, S.; Elmi, I.; Mancarella, F.; Betti, P.; Dalcanale, E.; Cardinali, G. C.; Severi, M., Real-time monitoring of sub-ppb concentrations of aromatic volatiles with a MEMS-enabled miniaturized gas-chromatograph. *Sensors and Actuators B: Chemical* **2009,** *141* (1), 322-328.
87. Ochiai, N.; Takino, M.; Daishima, S.; Cardin, D. B., Analysis of volatile sulphur compounds in breath by gas chromatography–mass spectrometry using a three-stage cryogenic trapping preconcentration system. *Journal of Chromatography B: Biomedical Sciences and Applications* **2001,** *762* (1), 67-75.
88. Pillonel, L.; Bossett, J. O.; Tabacchi, R., Rapid preconcentration and enrichment techniques for the analysis of food volatile. A review. *Lebensmittel-Wissenschaft Und-Technologie-Food Science and Technology* **2002,** *35* (1), 1-14.

89. Contreras, J. A.; Murray, J. A.; Tolley, S. E.; Oliphant, J. L.; Tolley, H. D.; Lammert, S. A.; Lee, E. D.; Later, D. W.; Lee, M. L., Hand-Portable Gas Chromatograph-Toroidal Ion Trap Mass Spectrometer (GC-TMS) for Detection of Hazardous Compounds. *Journal of the American Society for Mass Spectrometry* **2008,** *19* (10), 1425-1434.
90. Ettre, L. S., Nomenclature for Chromatography. *Pure and Applied Chemistry* **1993,** *65* (4), 819-872.
91. Luong, J.; Gras, R.; Mustacich, R.; Cortes, H., Low thermal mass gas chromatography: Principles and applications. *Journal of Chromatographic Science* **2006,** *44* (5), 253-261.
92. Wang, A.; Tolley, H. D.; Lee, M. L., Gas chromatography using resistive heating technology. *Journal of Chromatography A* **2012,** *1261* (0), 46-57.
93. Schkolnik, G.; Falkovich, A. H.; Rudich, Y.; Maenhaut, W.; Artaxo, P., New analytical method for the determination of levoglucosan, polyhydroxy compounds, and 2-methylerythritol and its application to smoke and rainwater samples. *Environmental Science & Technology* **2005,** *39* (8), 2744-2752.
94. Venn, A. J.; Lewis, S. A.; Cooper, M.; Hubbard, R.; Britton, J., Living near a main road and the risk of wheezing illness in children. *American Journal of Respiratory and Critical Care Medicine* **2001,** *164* (12), 2177-2180.
95. Brunekreef, B.; Janssen, N. A. H.; deHartog, J.; Harssema, H.; Knape, M.; vanVliet, P., Air pollution from truck traffic and lung function in children living near motorways. *Epidemiology* **1997,** *8* (3), 298-303.
96. Perez, L.; Lurmann, F.; Wilson, J.; Pastor, M.; Brandt, S. J.; Kunzli, N.; McConnell, R., Near-Roadway Pollution and Childhood Asthma: Implications for Developing "Win-Win" Compact Urban Development and Clean Vehicle Strategies. *Environmental Health Perspectives* **2012,** *120* (11), 1619-1626.
97. Lin, S.; Munsie, J. P.; Hwang, S. A.; Fitzgerald, E.; Cayo, M. R., Childhood asthma hospitalization and residential exposure to state route traffic. *Environmental Research* **2002,** *88* (2), 73-81.
98. Institute, H. E., Traffic-Related Air Pollution: A Critical Review of the Literature on Emissions, Exposure, and Health Effects. In *HEI Special Report*, Institute, H. E., Ed. 2010; Vol. 17.
99. Fruin, S.; Westerdahl, D.; Sax, T.; Sioutas, C.; Fine, P. M., Measurements and predictors of on-road ultrafine particle concentrations and associated pollutants in Los Angeles. *Atmospheric Environment* **2008,** *42* (2), 207-219.
100. Westerdahl, D.; Fruin, S.; Sax, T.; Fine, P. M.; Sioutas, C., Mobile platform measurements of ultrafine particles and associated pollutant concentrations on freeways and residential streets in Los Angeles. *Atmospheric Environment* **2005,** *39* (20), 3597-3610.
101. Westerdahl, D.; Fruin, S. A.; Fine, P. L.; Sioutas, C., The Los Angeles International Airport as a source of ultrafine particles and other pollutants to nearby communities. *Atmospheric Environment* **2008,** *42* (13), 3143-3155.
102. Hu, S. S.; Paulson, S. E.; Fruin, S.; Kozawa, K.; Mara, S.; Winer, A. M., Observation of elevated air pollutant concentrations in a residential neighborhood of Los Angeles California using a mobile platform. *Atmospheric Environment* **2012,** *51*, 311-319.
103. Zhu, Y. F.; Hinds, W. C.; Kim, S.; Shen, S.; Sioutas, C., Study of ultrafine particles near a major highway with heavy-duty diesel traffic. *Atmospheric Environment* **2002,** *36* (27), 4323-4335.

104. Zhu, Y. F.; Hinds, W. C.; Kim, S.; Sioutas, C., Concentration and size distribution of ultrafine particles near a major highway. *Journal of the Air & Waste Management Association* **2002,** *52* (9), 1032-1042.
105. Kozawa, K. H.; Winer, A. M.; Fruin, S. A., Ultrafine particle size distributions near freeways: Effects of differing wind directions on exposure. *Atmospheric Environment* **2012,** *63*, 250-260.
106. Kozawa, K. H.; Fruin, S. A.; Winer, A. M., Near-road air pollution impacts of goods movement in communities adjacent to the Ports of Los Angeles and Long Beach. *Atmospheric Environment* **2009,** *43* (18), 2960-2970.
107. Grover, B. D.; Kleinman, M.; Eatough, N. L.; Eatough, D. J.; Cary, R. A.; Hopke, P. K.; Wilson, W. E., Measurement of fine particulate matter nonvolatile and semi-volatile organic material with the Sunset Laboratory Carbon Aerosol Monitor. *Journal of the Air & Waste Management Association* **2008,** *58* (1), 72-77.
108. Eatough, D. J. *Semi-continuous Monitoring and the Source Apportionment of PM2.5 Mass and Its Constituents. Final Report on NSF ATM-0407695*; 2008.
109. Waldron, K. M.; Paegle, J.; Horel, J. D., Sensitivity of a spectrally filtered and nudged limited-area model to outer model options. *Monthly Weather Review* **1996,** *124* (3), 529-547.
110. Paatero, P., Least squares formulation of robust non-negative factor analysis. *Chemometrics and Intelligent Laboratory Systems* **1997,** *37* (1), 23-35.
111. Polissar, A. V.; Hopke, P. K.; Paatero, P., Atmospheric aerosol over Alaska - 2. Elemental composition and sources. *Journal of Geophysical Research-Atmospheres* **1998,** *103* (D15), 19045-19057.
112. Paatero, P.; Hopke, P. K.; Begum, B. A.; Biswas, S. K., A graphical diagnostic method for assessing the rotation in factor analytical models of atmospheric pollution. *Atmospheric Environment* **2005,** *39* (1), 193-201.